Scholars' Mine

Spring 2017

Entropy-based performance analysis of jet engines; Methodology and application to a generic single-spool turbojet

Mohammad Abbas

Recommended Citation

ENTROPY-BASED PERFORMANCE ANALYSIS OF JET ENGINES;

METHODOLOGY AND APPLICATION TO A GENERIC SINGLE-SPOOL

TURBOJET

by

MOHAMMAD ABBAS

A THESIS

Presented to the Faculty of the Graduate School of the

MISSOURI UNIVERSITY OF SCIENCE AND TECHNOLOGY

In Partial Fulfillment of the Requirements for the Degree

MASTER OF SCIENCE IN AEROSPACE ENGINEERING

2017

Approved by

David Riggins, Advisor
Kelly Homan
Serhat Hosder
Henry Pernicka

ABSTRACT

Recently developed methodology that provides the direct assessment of traditional thrust-based performance of aerospace vehicles in terms of entropy generation (i.e., exergy destruction) is modified for stand-alone jet engines. This methodology is applied to a specific single-spool turbojet engine configuration. A generic compressor performance map along with modeled engine component performance characterizations are utilized in order to provide comprehensive traditional engine performance results (engine thrust, mass capture, and RPM), for on and off-design engine operation. Details of exergy losses in engine components, across the entire engine, and in the engine wake are provided and the engine performance losses associated with their losses are discussed. Results are provided across the engine operating envelope as defined by operational ranges of flight Mach number, altitude, and fuel throttle setting. The exergy destruction that occurs in the engine wake is shown to be dominant with respect to other losses, including all exergy losses that occur inside the engine. Specifically, the ratio of the exergy destruction rate in the wake to the exergy destruction rate inside the engine itself ranges from 1 to 2.5 across the operational envelope of the modeled engine.

ACKNOWLEDGMENTS

TABLE OF CONTENTS

LIST OF ILLUSTRATIONS

LIST OF TABLES

NOMENCLATURE

Symbol	Description
A	cross-sectional area
C_f	skin friction coefficient
c	perimeter
c_p	specific heat at constant pressure
c_v	specific heat at constant volume
D	circular cross-sectional diameter
$\dot{E}$	net energy input rate
$F_{uninstalled}$	engine uninstalled thrust
F_x	net axial force on a streamtube
$F_{x(flight)}$	net force on the engine/vehicle in the direction of flight
f	fuel-to-air ratio
$\dot{H}$	enthalpy flow rate
$\dot{H}_t$	total enthalpy flow rate
h	enthalpy per unit mass
h_t	total enthalpy per unit mass
h_{fuel}	lower heating value of the fuel
M	Mach number
$\dot{m}$	mass flow rate
$\dot{m}_{corr}$	corrected mass flow rate
N	shaft speed (RPM)
P	static pressure
P_t	total pressure
$\dot{Q}$	net heat input rate
q	heat interaction per unit mass
R	gas constant
$\dot{S}$	entropy change rate
ST	stream thrust

s	entropy per unit mass
T	static temperature
T_t	total temperature
u	flow (axial) velocity
$\dot{W}$	net work input rate
w	work interaction per unit mass
X	mole fraction
α	mass fraction
γ	ratio of specific heats
δ	scaled pressure
η	efficiency
θ	scaled temperature
π	total pressure ratio
ρ	fluid density
τ	total temperature ratio
τ_w	wall shear stress

Subscript	Description
b	burner
c	compressor
$conv$	convection
d	diffuser (inlet)
e	exit
ext	external
gen	generation
i	inlet/component i/species i
in	input
irr	irreversibility
n	nozzle
rad	radiation
STP	standard reference temperature and pressure

s	exit of side bounding sub-control volume
t	turbine
w	wake exit
0	freestream condition
$0s$	inlet of side bounding sub-control volume
0,1,…,9	different spatial locations
∞	freestream condition

1. INTRODUCTION

1.1. STUDY OBJECTIVES

Aerospace vehicles are complex systems consisting of multiple subsystems (propulsion, aerodynamic, and structural subsystems). Optimization has usually been pursued at the level of the individual subsystem rather than for the entire vehicle, especially in initial stages of the design process. This has been primarily due to the practicality-driven segregation of design responsibilities between various subsystem teams. The final design of the vehicle is eventually achieved through the top-down imposition of system level requirements and the resulting iteratively-balanced trades between subsystem performances. This approach necessarily mandates the use of many highly reliable and time-tested subsystem based efficiency and effectiveness parameters. These metrics have widely differing measures of 'goodness', as they are driven by sub-system-specific performance objectives. For example, the propulsion subsystem main figures of merit are commonly the specific thrust and thrust specific fuel consumption; the aerodynamic subsystem has main figures of merit such as lift-to-drag ratio and other aerodynamic performance-specific metrics; the structural subsystem design and optimization process are primarily driven by weights, etc. The engineers working on various individual subsystems generally and understandably view these sub-system-specific metrics as their highest priority in driving their 'piece' of the design process. Furthermore, each subsystem is, in turn, made up of several to many sub-components, each with its own unique performance/optimization measures. For instance, in a conventional gas turbine engine, the compressor performance is described in terms of the work-based compressor efficiency, while the burner performance is characterized in terms of total pressure drop and combustion efficiency. Traditionally, therefore, within the design process for a vehicle, these various efficiencies and measures of effectiveness for sub-systems and sub-system components are optimized to the extent possible. The overall vehicle requirements and integration requirements then iteratively institute compromises and trades that filter down through the sub-system designs until a suitably 'optimized' overall vehicle design is finalized. Note that the impact of costs often/usually drives the details of this final design as well, although cost concerns are not considered in this work. However, this subsystem-

based approach is necessarily tedious and time-consuming even when automated using optimization methodologies. Furthermore, it utilizes a large and complex underlying array of subsystem and component metrics and efficiencies that are often fundamentally unrelated to one another and functionally unrelated to actual overall aerospace vehicle performance. It also does not, in general, yield (or guarantee) a truly optimized overall system (i.e., vehicle).

The focus of the current work is upon a more fundamental approach to loss characterization and optimization in design and analysis. In this approach, a single performance/loss metric (or measure) is used as the 'common currency' for assessing all subsystem and individual component losses. This metric is entropy generation (or correspondingly, exergy destruction). Entropy generation is the most fundamental measure of loss for all physical processes and mechanisms, regardless of type or nature. Recent analytical work has provided the quantitative relationships describing conventional (overall) vehicle performance in terms of entropy generation; this work has generally focused on hypersonic flight vehicles, (see [1] and [2]). However, these methodologies and techniques for vehicle analysis, design, and optimization can also be directly and easily applied to general aerospace vehicles and systems across their operational range. Those applications include stand-alone (non-airframe mounted or integrated) conventional gas turbine (jet) engines.

For jet engines, entropy generation can be assessed to the level of detail enabled by the given level of modeling, simulation, or analysis; this assessment can be made for individual engine components as well as at the level of the overall system. Using the methodology noted, the details of the entropy generation can then be directly related to force-based engine performance. Ultimately, this technique (utilizing the single metric of entropy generation), should be useful in future engine design and optimization efforts. It should have particular utility for efforts that properly rely on multi-disciplinary methods and optimization processes.

The main objective of the work presented in this paper is therefore to develop the required methodology and to assess the conventional flight performance of a single-spool turbojet engine in terms of the details of the entropy generation associated with that engine (at both component and overall levels). This conventional flight performance and the

related entropic behavior of the engine is characterized for a specific engine across all possible ranges of flight Mach number, altitude, and throttle setting. The off-design analysis is based on component matching, in which individual components such as the compressor are characterized by individual performance maps and traditionally characterized loss information but are then appropriately linked together into an integrated engine. This work is an extension of the work of Abbas and Riggins [3] that was presented at the 52nd AIAA/SAE/ASEE Joint Propulsion Conference and is believed to represent the first systematic study of gas turbine engine performance across the operating envelope in terms of the entropy generation – flight performance relationships developed in recent years.

1.2. STUDY APPROACH

This work first describes in detail the methodology used to characterize turbojet engine performance in terms of integrated component-level performance information. This is followed by the development of the overall exergy-performance relationship for such an engine, in which engine performance is directly related to entropy generation and energy usage. Finally, the methodologies are applied in a case study of a specific turbojet engine.

The modeling of a turbojet engine requires the selection of the individual components that make up the engine: the inlet, compressor, burner, turbine, and nozzle, and the appropriate combination of these components in order to ensure adequate engine performance in the desired operational range. The individual components are defined in terms of their own individual performance metrics and parameters, some of which are nearly constant for all meaningful operating conditions while others are variable and can be strong functions of flow conditions, etc. For example, the stand-alone performance of the compressor is highly variable with operating condition and hence tends to be the most important component in the engine in terms of the necessity for adequately providing detailed component-specific information. This is in contrast to the performance metrics for the turbine in a simple turbojet, which tend to be relatively insensitive to operating conditions. In the most general sense, however, each component is usually defined by a 'map' or an equivalent digital database that provides the behavior of key performance parameters (e.g., efficiency) as the operating conditions for that component are varied.

Once all of the components are suitably defined in terms of performance maps or modeling information required, the overall engine must be analyzed in terms of performance. This requires the appropriate integration of the components and the determination of the overall system (engine) performance. This is done mathematically in a process known as component matching in which required component-to-component matching criteria are systematically applied. It should be noted that the engine must also be 'sized ' in terms of computing required cross-sectional areas; however, this is usually done early in the design process by requiring suitable constraints on internal flow characteristics for a single (demanded) on-design point.

The end result of the component matching process is that the capability is developed for enabling the complete fluid dynamic and thermodynamic description of flow through the engine for any operating condition (specifically for any allowed combination of altitude, flight Mach number, and fuel throttle setting). Along with the fluids through the engine, the conventional performance of the engine is also obtained. Here, conventional performance is defined as thrust, captured air mass flow rate, and engine RPM.

The main objective of this work is to directly relate conventional gas turbine (specifically turbojet) engine performance to the exergy/exergy destruction (availability analysis) characteristics of the engine. Specifically, recently developed methodology for correctly assessing the exergy losses and energy usage for high-speed air-breathing and rocket vehicles is applied to the stand-alone gas turbine engine in flight. The entropic analysis, as will be described in detail in this work, is then carried out in order to complement the base traditional performance analysis. It provides information regarding losses, loss distribution, etc., as well as demonstrating capability for determining engine performance such as thrust based solely on energy and entropy considerations.

The component matching, performance predictions, and exergy analysis is therefore applied to a defined turbojet at a specific level of modeling, with performance and exergy characteristics then examined for the entire range of possible engine operating conditions. This allows the observation of performance and loss trends for the engine as a whole and for the individual components across the entire envelope of operability. As a consequence, observations and conclusions can be deduced from such results, which, in turn, can be compared and contrasted to well-known observations from traditional

momentum-based analysis of gas turbine engines. In addition, the exergy analysis provides additional loss-related information and diagnosis that are not obtained from traditional engine performance analysis.

1.3. REVIEW OF THESIS ORGANIZATION

The work begins with a brief review of previous investigations related to second-law considerations of aerospace applications and entropy-based methodologies. The next section contains the description of the methodology for developing performance characteristics of a turbojet engine. This includes a thorough presentation of component matching procedures, including operating line development and the approach used to describe engine performance over the entire envelope of operability. The next section presents the derivation of the entropy-based method of analysis as well as the application of the method in terms of various levels of modeling used in preliminary engine design. This is followed by a description of the application of the methodologies and analysis techniques to a selected turbojet engine (a specific case study). This engine is analyzed in detail: Component matching results are shown in order to describe engine component characterization for the integrated engine. Engine performance is described in terms of both conventional performance and entropic behavior/exergy destruction characteristics. This is done for five distinct operating conditions, including the on-design condition and four selected off-design conditions. A comprehensive set of trends are then developed for all important performance parameters and losses for the turbojet engine defined in this study. Selected results are shown for important entropic and performance characteristics in order to illustrate engine performance and entropic behavior across the operating range of fuel throttle setting, flight Mach number, and altitude. Finally, conclusions resulting from this study are discussed and proposed future work related to this study (and for further entropy-based analysis of aerospace systems) is outlined.

2. LITERATURE SURVEY

The earliest work in the area of performance assessment of jet engines includes that of Foa [4], Builder [5], and Lewis [6]: The latter reference provides an energy utilization analysis which can be viewed in some sense as a precursor to exergy-based work. A significant amount of earlier work also attempted to directly apply traditional exergy analysis (frequently – and particularly in earlier work - termed availability analysis) to jet engines; an example can be found in Clarke and Horlock [7]. Interest in applying exergy methodology to aerospace vehicles, particularly hypersonic air-breathing vehicles, led to work including that of Czysz and Murthy [8], Murthy [9], and Brilliant [10]. A parallel effort (again with initial emphasis on high-speed systems) focused on analysis and optimization based on the minimization of engine thrust losses. This engineering performance-based approach was pioneered by Curran and Craig [11] who provided the basis of the thrust-potential methodology developed by Riggins, et al. (see, for example references [12], [13], and [14]). In these and related investigations, the thrust for a high-speed engine was explicitly linked to entropy production occurring inside the engine; this work, however, forced the realization that engine thrust performance was definitively not optimized when exergy loss inside the engine flow-field itself was minimized. Specifically, losses in an engine, and the balance of the losses in the engine as contributing to actual engine performance losses, were found to be explicitly dependent on the degree of expansion at engine exhaust as well as the sequence and spatial positioning of the losses occurring inside the engine. Due to the success obtained using thrust-based methodology in terms of providing engine-level thrust-based optimization, further work was done in terms of assessing engines (and entire vehicles) in terms of thrust potential and work potential (see, for example, Roth [15] and [16]). The fundamental and analytical relationships that directly link exergy methodology to traditionally used force-based performance assessment of aerospace systems has been rigorously developed and defined in more recent work by Riggins, et al. (for example, see [1] and [2]). Emphasis in terms of application in these works has been high-speed scramjet-powered and rocket-powered vehicles. The methodology developed in this recent work unifies thrust (and work) potential with the analysis of exergy losses for aerospace systems of all types. This

development is also complemented by work performed by Giles and Cumming [17]. The present work is also related to previous investigations ([18] and [19]) that sought to characterize gas turbine (turbojet and ramjet) transient behavior and performance utilizing entropic methods. Moorhouse [20] proposed a system-level interdisciplinary analysis based on the exergetic methodology. This would utilize exergy as the parameter of interest in analyzing and optimizing the conventional performance of a vehicle, such as range and other mission requirements. A similar exergy-based methodology formulation for the analysis of aircraft performance was developed by Arntz, et al. [21]. This work analyzed the propulsive system individually as well and included the formulation of traditional performance parameters (e.g. range) in terms of exergy.

The following cited works, though using exergy in their analyses, differ from the works mentioned above in that they do not generally relate the exergy (or availability) to the force-based power delivered to the vehicle, nor do they consider the wake mixing zone in the analysis. Turan ([22], [23], and [24]) studied the exergetic aspects of selected gas turbine engines. His work combines traditional cycle analysis with the evaluation of entropy generation and wasted energy to assess the performance of the engines. In a similar fashion, Ehyaei, et al. [25] and Bastani, et al. [26] evaluated the performance and losses of a turbojet engine and its components from the standpoint of exergy destruction. These studies examined the exergetic efficiencies of the components and the overall engine and the variance of the parameters at several different engine operating conditions. Balli [27] also studied a turbojet by assessing exergy destruction in the components. He categorized the exergy destruction into two categories: unavoidable/avoidable exergy destruction and endogenous/exogenous exergy destruction and attempted to characterize potential for improvement based on these categorizations. Balogun, et al. [28] compared the performance of a gas turbine-burner combination with a conventional turbine using exergy. Berg, et al. [29] developed a method of exergy mapping for an aircraft system, including developing software tools that enables the tracking of time-varying energy flows for the entire aircraft and its many subsystems over the entirety of time of operation (flight). Such tools enable the accounting of the time integrated energy usage and energy waste. Some work was done to include exergy in optimization schemes such as the work done by Tai, et al. [30] who implement genetic algorithms to optimize the performance of a turbofan

engine using exergetic parameters. Ekici, et al. [31] conducted a sustainability analysis for a turbojet that studied several different exergy-based parameters like exergy efficiency, waste exergy ratio, recoverable exergy ratio, environmental effect factor, and exergy destruction factor, etc.. Coban, et al. [32] studied the environmental impact (i.e., emissions) of a turbojet engine utilizing exergetic models. All these works, though not necessarily adopting the same methodology, have one thing in common: they all recognize that exergy destruction (or entropy generation) is the most fundamental measure of losses in an aerospace system.

3. DEVELOPMENT OF TURBOJET PERFORMANCE CHARACTERISTICS

In this section, the standard methodology for determining the performance characteristics of a turbojet is described in detail. This methodology is called component matching and is foundational to gas turbine engine design and analysis, and can be found in the aerospace propulsion literature (References [33] and [34]). It is documented in this section because it provides the basis for the subsequent detailed second-law analysis of a simple turbojet engine.

Component matching utilizes the measured or estimated stand-alone performance characteristics of each engine component and then combines the components together to form the integrated engine. This is accomplished by using physically required matching criteria such that the overall performance of a given engine can be predicted at any given operating condition of the engine. Engine performance is defined here in terms of three characteristics: 1) uninstalled thrust produced by the engine, 2) mass flow rate of air captured or processed by the engine, and 3) engine RPM. The operating envelope (or performance envelope) of a specified engine (with given components) is described by the quantification of engine performance (thrust, mass flow rate, and RPM) across all possible flight Mach numbers, fuel throttle settings, and altitudes at which the engine can operate. This envelope (made up of contours of thrust, mass flow rate, and RPM) lies within the operational 'three-space' of flight Mach number, fuel throttle setting, and altitude (see Figure 3.1). Limits on the engine performance envelope obviously exist in this three-space of engine operation due to lack of component map data and especially due to engine control system (ECS) limits.

In a turbojet, the gas turbine core components are the compressor, burner, and turbine. These components are distinct and are generally first characterized in terms of their own separate stand-alone performance. Component performance (e.g., a compressor performance map or the digitized data-base that represents the map) is developed by the manufacturer or designer of the specific component. The performance map or database then provides a complete description of the stand-alone performance of the individual component in terms of its own functionality (i.e., its own mapped or digitized performance, not related to engine performance). This stand-alone component performance is

experimentally obtained from actual test-stand measurements of the component by itself, or is obtained prior to manufacture by using predictive tools that generate models of the performance map, or maps, representing component stand-alone performance.
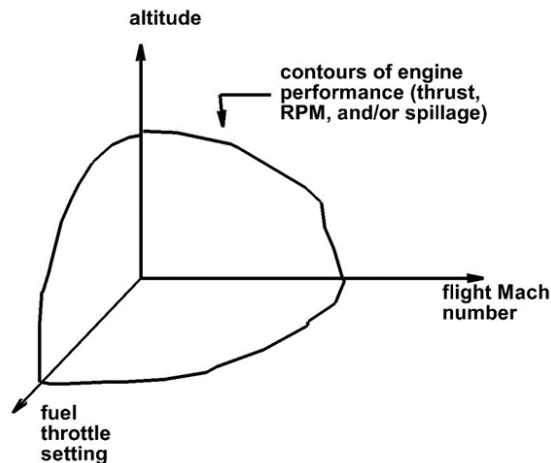
Figure 3.1. Operational 'three-space' of flight Mach number, fuel throttle setting, and altitude.

An essential outcome of the subsequent integration and matching of the gas turbine core components (along with an inlet and nozzle in order to form a complete operational turbojet flow-path) is the development of the steady-state operating line on the individual component performance maps. The engine-integrated performance of the individual component effectively becomes constrained (reduced in scope and specifically localized into a distinct operating line) on the individual component performance map.

This section is organized as follows: First, a brief overview of the turbojet engine, its components, and their respective roles are given. A discussion of total temperature and pressure relationships to engine losses and thermodynamic parameters is then provided. This discussion clarifies the linkage between classic engine loss metrics as used in typical engine analysis (generally based on total temperature and total pressure) and second-law and energetic considerations for engine performance as developed in later sections. This is followed by a section describing the method of component matching, including the matching criteria used, in developing the engine operating line on the focal compressor performance map. Finally, the procedure used to establish the engine performance across all possible fuel throttle settings, flight Mach numbers, and altitudes is described.

3.1. BRIEF OVERVIEW OF THE TURBOJET ENGINE

A turbojet is an air-breathing single-stream gas turbine engine whose purpose is to provide propulsive thrust to atmospheric aerospace vehicles. This is accomplished by processing inducted air and energizing it via fuel/air combustion in order to increase its momentum from inlet to exit of the engine, hence producing a net force in the flight direction on the structure of the engine. Mechanical compression and expansion take place upstream and downstream, respectively, of the combustion chamber, or burner. Figure 3.2 provides numerical designations for the different stations in the engine; this station numbering scheme is generally an AIAA-standard designation and is used in this work. The compressor-burner-turbine is known as the gas turbine core.

The first in-line component of a turbojet engine is the inlet (also known as a diffuser) between stations 1 and 2 on the schematic. The inlet is responsible for efficiently capturing the inducted air and preparing it to enter the compressor. In high speed flight inlets often provide partial compression (deceleration) through aerodynamic means. The compressor, the upstream gas turbine core component (located between stations 2 and 3) is responsible for raising the pressure and temperature of the flow by mechanical compression (energy addition as a work interaction) prior to fuel-air combustion. The burner, located between stations 3 and 4, energizes the flow by means of exothermic combustion of injected fuel with the oxygen in the airstream exiting the compressor. The downstream gas turbine core component is the turbine which is located between stations 4 and 5. It extracts energy from the flow as a work interaction in order to power the compressor and to provide other possible power needs to the engine and/or vehicle. Downstream of the gas turbine core (station 5 to 9) is the nozzle. The nozzle is nominally responsible for expanding (accelerating) the flow. For afterburning engines, the afterburner is located between stations 6 and 7 within the nozzle; its purpose is to energize the flow further by means of addition fuel injection and combustion. Station 8 is the physical throat of the nozzle, while station 9 is the exit of the engine (station 8 and station 9 coincide for a converging-only nozzle, such as examined in the results section of this study).
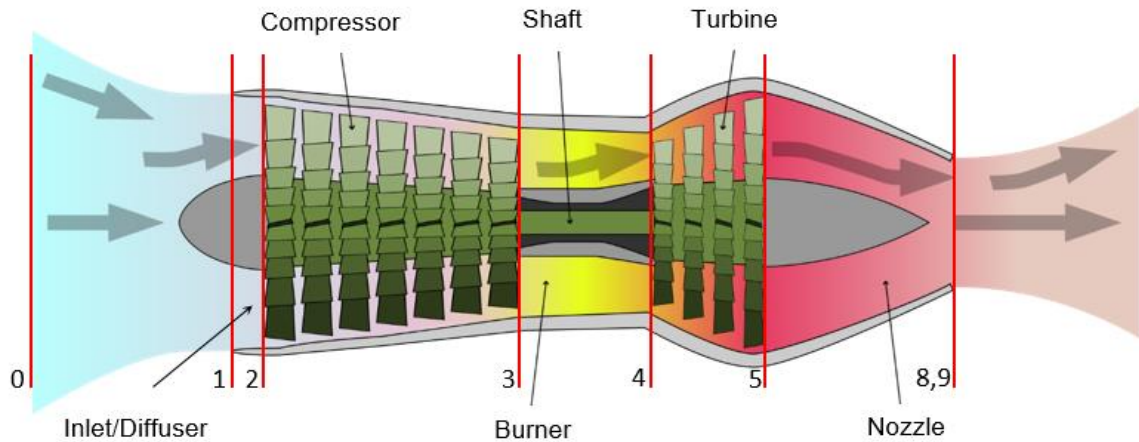
Figure 3.2. Turbojet schematic with station numbering (source: Wikipedia).

3.2. GENERAL DISCUSSION OF LOSSES AND THERMODYNAMIC METRICS (TOTAL PRESSURE AND TOTAL TEMPERATURE RATIOS) IN COMPONENTS

Jet engine analysis for cycle performance predictions and for preliminary (and even advanced) design and evaluation universally relies upon being able to quantify the evolution and distribution of total temperature and total pressure throughout the engine. A total (or stagnation) property is defined in fluid dynamics as the property obtained if a flow is isentropically decelerated to zero velocity. For a flowing system, this means that total properties are generally reference properties rather than actual physical flow properties. The direct use of the property of entropy in developing performance estimations in engine analysis is generally not observed, since traditional engine performance analysis can be suitably (adequately and fully) described and developed without explicit entropic considerations. This is reflective of the fact that total pressure and total temperature changes in an engine flowpath are driven only by external energy interactions and internal irreversibilities and hence serve as very useful (and generally well-understood) thermodynamic handles for evaluating engine flow-fields. However, because this study necessarily involves both traditional engine and component performance descriptions (via total temperature and total pressure-based metrics) as well as the fundamental description of performance in terms of entropy generation (the focus/contribution of the present study), it is instructive to fundamentally describe the thermodynamic and fluid dynamic drivers that effect changes in total pressure and total temperature.

3.2.1. Total Pressure, Energy, and Entropy. The total pressure ratio, $\boldsymbol{\pi}$, of a component is defined in Eq. (1).

$$\pi_{1 \to 2} = \frac{P_{t2}}{P_{t1}} \tag{1}$$

Reductions in the total pressure ratio for a component from what would be observed for that component with completely ideal processes are in fact directly caused by entropy generation due to internal irreversibility and (for non-adiabatic components) non-ideal heat transfer. Therefore, losses in component performance are universally - but not uniquely - described by examination of losses in the total pressure through the component. Specifically, due to their function, compressors and turbines must utilize more general efficiency definitions than π to adequately define component losses. For example, in a compressor the realized compressor total pressure ratio is itself the main function-specific performance metric; i.e. the function of the compressor is to raise the total pressure via energy addition as a work interaction to the fluid. Hence the total pressure ratio across a compressor cannot uniquely be used as a measure of losses/non-ideal effects since that ratio is also inherently dependent upon the amount of supplied work interaction, as well as the losses occurring in the compressor. However, reductions in that ratio for given work interaction amounts do adequately represent losses in compressor performance. This effect is then reflected within the general compressor efficiency definition. On the other hand, the total pressure ratios (losses from unity) in inlet and nozzle components do directly and uniquely reflect the degree of irreversibility and hence are by themselves complete measures of the performance loss in those components. The total pressure in a gas turbine burner decreases due to the combined effects of irreversibilities and non-ideal heat addition at non-zero Mach number (where total temperature differs from static temperature).

The following derivation yields a relationship that defines the total pressure ratio between two stations (station 1 to station 2) in a streamtube (for instance as processed through a given engine component, or even across the entire engine). Assumptions for producing this relationship include constant gas constant and specific heats (i.e. fuel-lean engine operation; a common and valid assumption for most gas turbine engines). Using the

differential energy equation for an open system in terms of total properties and dividing through by the total temperature:

$$\frac{dh_t}{T_t} = c_p \frac{dT_t}{T_t} = \frac{\delta q}{T_t} + \frac{\delta w}{T_t} \tag{2}$$

Also, a different form of the first law is:

$$ds = c_p \frac{dT_t}{T_t} - R \frac{dP_t}{P_t} \tag{3}$$

Combining Eq. (2) with Eq. (3) yields,

$$ds = \frac{\delta q}{T_t} + \frac{\delta w}{T_t} - R \frac{dP_t}{P_t} \tag{4}$$

The second law also gives an expression for a differential change in entropy:

$$ds = \frac{\delta q}{T} + ds_{irr} \tag{5}$$

Modifying the expression,

$$ds = \frac{\delta q}{T_t} + \delta q \left(\frac{1}{T} - \frac{1}{T_t} \right) + ds_{irr} \tag{6}$$

The second term on the right hand side is known as the 'Rayleigh loss' and represents the non-ideal heat transfer contribution to entropy change. It is represented as such because heat addition to fluids at finite flow speeds occurs at lower static temperatures than the total temperature thus results in greater entropy change in the fluid. The lowest entropy increase possible is achieved when heat is added at the maximum temperature possible (i.e., the total temperature). This occurs at zero velocity; hence the first term on the right side of Eq. (6) is known as the ideal heat transfer entropy contribution. Thus, Eq. (6) can be rewritten as:

$$ds = \frac{\delta q}{T_t} + ds_{non-ideal\ heat} + ds_{irr} \tag{7}$$

Combining Eq. (4) and Eq. (7), rearranging, and integrating yields:

$$\frac{P_{t2}}{P_{t1}} = e^{\int_1^2 \left\{\frac{\delta w}{RT_t}\right\} - \frac{\Delta s_{irr+non-ideal\ heat\ transfer}}{R}} \tag{8}$$

This very useful formulation clarifies the fundamental drivers that effect total pressure changes – specifically 1) energy as a work interaction (positive or negative, e.g. a compressor or a turbine), 2) entropy generation due to irreversibilities, and 3) entropy associated with non-ideal heat transfer (when heat is transferred to the flow at finite Mach number). Note that the work term is left in integral form since the total temperature is itself dependent on work interaction via the energy equation.

3.2.2. Total Temperature, Energy, and Entropy. The total temperature ratio across a component, τ, is defined in Eq. (9). A change in the total temperature (for perfect gases proportional to a change in specific total enthalpy) from station to station in a flow is purely a measure of how much energy has been added in the form of either heat or work interactions. Specifically, Eq. (10) defines the total temperature ratio between two stations in an engine component. This relationship is in fact just the energy equation for fluid flow with constant specific heats and specific gas constant; Eq. (2) integrated between stations 1 and 2.

$$\tau_{1\rightarrow2} = \frac{T_{t2}}{T_{t1}} \tag{9}$$

$$\frac{T_{t2}}{T_{t1}} = 1 + \frac{(q_{1\rightarrow2} + w_{1\rightarrow2})}{c_P T_{t1}} \tag{10}$$

This change in total temperature (or the ratio as defined across a segment of the flow as given above) is independent of whether or not 1) the energy interaction per mass occurs as heat $q_{1\rightarrow2}$ or as work $w_{1\rightarrow2}$ or 2) internal irreversibilities occur. Hence in an adiabatic non-work component (inlet, internal ducts, and nozzle), total temperature does not change and the ratio is unity, even though irreversibilities may occur.

Basic cycle analysis of jet engine combustors generally relies on modeling the heat-release associated with exothermic chemical reactions as a non-adiabatic interaction that raises the total enthalpy. This is even done in an adiabatic combustor (thermally insulated

with respect to the surroundings); this standard approximation is generally considered acceptable for fuel-lean (small fuel-to-air ratio) situations and is the approach taken in this work. It is noted that the burner efficiency is usually defined separately from the total pressure drop experienced by the burner. It is reflective of the completeness of combustion (incomplete mixing, etc.) and the presence of possible non-adiabatic effects. The burner efficiency is thus itself inherently related to the total temperature change across the burner.

3.3. COMPONENT MATCHING AND OPERATING LINE DESCRIPTION, DEVELOPMENT METHODOLOGY, AND APPROACH

Historically, component performance is represented visually on what is termed a component performance map (a single graph or sometimes multiple graphs). A component performance map is composed of overlaid carpet plots and contours that adequately quantify the main performance parameters and efficiencies defining stand-alone component performance. For example, the compressor map (see Figure 3.3) is visually represented by a detailed plot of measured (or predicted) compressor total pressure ratios along with contours of compressor general efficiencies. This data is provided for various (scaled) blade speeds and corrected mass flow rates (defined subsequently) and is comprehensive for the stand-alone compressor at all possible isolated component operating points. The engine operating line that is shown on Figure 3.3 is relevant to integrated engine compressor performance and will be discussed later.

3.3.1. Component Matching Criteria. Gas turbine component performance maps are traditionally/usually based on the entrance corrected mass flow rate. The corrected mass flow rate is defined in Eq. (11) where 'i' designates the entrance station for a component; it can be shown to scale directly with flow Mach number for a fixed cross-sectional area.

$$\dot{m}_{corr,i} = \dot{m}_i \frac{\sqrt{\theta_i}}{\delta_i} \tag{11}$$

Here, $\theta_i = \frac{T_{ti}}{T_{STP}}$: $T_{STP} = 288 \ K$, and $\delta_i = \frac{P_{ti}}{P_{STP}}$: $P_{STP} = 101325 \ Pa$

When examining the performance map of a general component, all points on the map represent possible operating points of the component when the component is in

operation in a steady flow, stand-alone mode (i.e., not integrated with other gas turbine components). However, when the component is integrated into the engine, the component is necessarily restricted to operate at only certain points on its performance map. This is due to the fact that the fluid dynamics and the heat and work interactions between the different components are interlinked and influence one another. By mandating matching criteria such as mass flow rates, RPM, and power balances across all components in an integrated engine, discrete steady-state operating lines (as sketched in Figure 3.3 on the compressor map) describing these permissible points are then developed on the individual component maps.
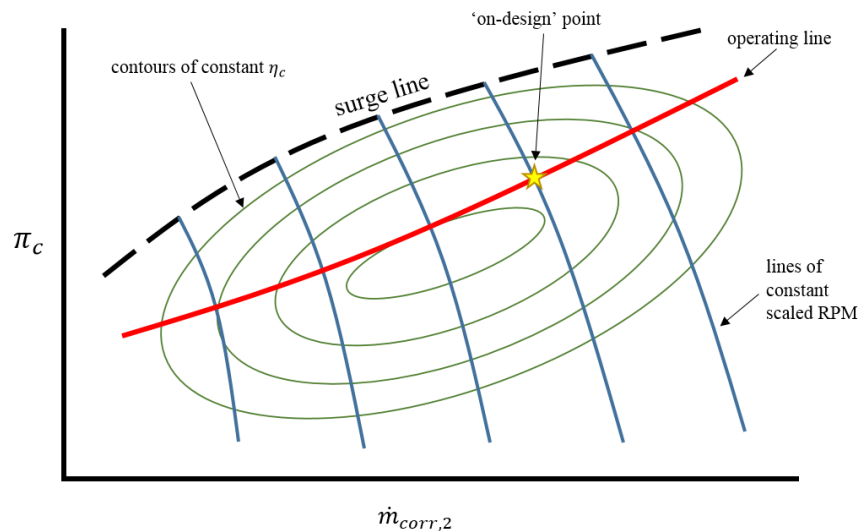
Figure 3.3. Generic sketch of a compressor performance map (with engine operating line shown).

3.3.2. On-Design Point of Engine Operation; Definition. Before describing the required component-to-component matching criteria in more detail, it is beneficial to clarify what the single on-design operating point is, as opposed to the 'universe' of off-design operating points that define comprehensive engine operation. For component matching, the on-design point is simply considered to be a known or specified (reference) single point of operation for the engine (i.e., at some design-demanded single value of fuel flow rate, altitude, and flight Mach number). At this point, all information and performance parameters are known or calculable. The definition of the on-design point predicates that the engine has been designed (components correctly chosen or designed and appropriately

integrated) in order to produce specific 'on-design' performance at that specific combination of fuel flow rate, flight Mach, and altitude. This on-design operating point then serves as a starting point for the development of the engine-integrated component 'operating line' as will be discussed subsequently. Hence, all other operating points (all other possible fuel flow rates, altitudes, and flight Mach numbers other than the specific design values) are considered 'off-design', including operational points that may be represented by the same point on the operating line of a component.

3.3.3. Engine Matching Criteria.

3.3.3. Engine Matching Criteria. The matching criteria utilized in the component matching methodology are now described. For steady operation of the engine and with the assumption of small fuel-to-air ratio, the actual mass flow rate at all stations of the engine has to be identical (from conservation of mass considerations), such that:

$$\dot{m}_0 = \dot{m}_2 = \dot{m}_3 = \dot{m}_4 = \dot{m}_5 = \dot{m}_8 = \dot{m}_9 \tag{12}$$

Also, for a single-spool shaft with no gearbox, the actual blade speeds for both the compressor and turbine have to match,

$$N_c = N_t \tag{13}$$

When the simple situation is mandated that all the power extracted from the turbine is supplied to the compressor (or there is a known mechanical efficiency describing the percentage of turbine work supplied to the compressor), the power balance between compressor and turbine then serves as another required matching criteria. The relationship is more useful when cast in terms of standard engine analysis parameters, described below:

$$|w_{turbine}| = |w_{compressor}| \tag{14}$$

$$h_{t4} - h_{t5} = h_{t3} - h_{t2} \tag{15}$$

$$c_p T_{t4} - c_p T_{t5} = c_p T_{t3} - c_p T_{t2} \tag{16}$$

Applying a calorically perfect gas assumption, i.e. constant c_p,

$$T_{t4} - T_{t5} = T_{t3} - T_{t2} \tag{17}$$

Dividing through by T_{t2},

$$\frac{T_{t4}}{T_{t2}} - \frac{T_{t5}}{T_{t2}} = \tau_c - 1 \tag{18}$$

Multiplying the second term on the left hand side by T_{t4}/T_{t4} and rearranging,

$$\frac{T_{t4}}{T_{t2}}(1 - \tau_t) = \tau_c - 1 \tag{19}$$

Another matching criterion links the nozzle with the gas turbine core (comprising the compressor-burner-turbine trio). Specifically, the corrected mass flows at stations 8 and 2 are cast in terms of a ratio:

$$\frac{\dot{m}_{corr,8}}{\dot{m}_{corr,2}} = \frac{\dot{m}_8 \dfrac{\sqrt{\dfrac{T_{t8}}{T_{STP}}}}{\dfrac{P_{t8}}{P_{STP}}}}{\dot{m}_2 \dfrac{\sqrt{\dfrac{T_{t2}}{T_{STP}}}}{\dfrac{P_{t2}}{P_{STP}}}} \tag{20}$$

Assuming that $\dot{m}_8 = \dot{m}_2$ and that there is no afterburner (i.e., $T_{t8} = T_{t5}$) this then simplifies to:

$$\frac{\dot{m}_{corr,8}}{\dot{m}_{corr,2}} = \frac{1}{P_{t8}/P_{t2}}\sqrt{\frac{T_{t5}}{T_{t2}}} \tag{21}$$

Rewriting the expression in terms of more useful parameters, the following required matching criterion is then written:

$$\frac{\dot{m}_{corr,8}}{\dot{m}_{corr,2}} = \frac{1}{\pi_c \pi_b \pi_t \pi_n}\sqrt{\tau_t \frac{T_{t4}}{T_{t2}}} \tag{22}$$

Furthermore, if the flow at station 8 is choked (i.e. $M_8 = 1.0$), and the area at station 8 (nozzle throat) is constant, $\dot{m}_{corr,8}$ is then fixed for all on and off-design operating conditions.

3.3.4. Compressor Operating Line Development. As discussed earlier, the operating line on a component performance map defines the performance of a component when it is actually integrated into the engine. When the engine is operating at a specific flight Mach number, altitude, and fuel throttle setting, the performance of each component is then uniquely defined utilizing these component operating lines. The operating line is then defined and located using the matching criteria outlined above.

In this work, the compressor operating map is the focus; the turbine and burner maps are of secondary importance for the purposes of this investigation and do not factor in the analysis under simplifying assumptions used here. As noted earlier, the operating line on the compressor map as sketched in Figure 3.3 forms the locus of all possible (steady-state) operating points for the compressor when integrated with the burner, turbine, and nozzle (including any requisite inlet or diffuser information). Also, as mentioned previously, each individual point defining the operating line on the compressor map completely defines compressor performance for a large space of possible fuel throttle positions, flight Mach numbers, and altitudes. Hence, the 'on-design' point as indicated in the figure provides compressor performance in terms of compressor pressure ratio, compressor efficiency, scaled blade speed, and corrected mass flow rate for the single on-design fuel throttle, flight Mach, altitude operating point as discussed earlier. However, it (the same point shown on the compressor map) also reflects the same information as applicable for an entire field of other possible fuel throttle settings, Mach number, and altitudes. In other words, any single point on the operating line is not associated with only a single unique combination of these three-space parameters, rather, each point corresponds with many combinations of these parameters. The development of the operating line and associated information then provides the information that will enable the compressor performance to be described at all possible fuel flow rates, Mach numbers, and altitudes. This information will then enable the prediction of overall engine performance in the space of possible fuel flow rates, flight Mach numbers, and altitudes.

The iterative procedure used in this work to develop the operating line on the compressor map and associated information (note that the on-design point is known) is now described. Assumptions made in this procedure include choked flow at stations 4 and 8. These assumptions are used across all possible operating points of the engine. The

iterative procedure begins by selecting a new value of the corrected compressor speed, $N_c/\sqrt{\theta_2}$, different than that associated with the on-design point. Somewhere on that new corrected speed line, a point may (and generally does) exist for which all engine matching criteria as described above are met, i.e., that point will then, by definition, lie on the operating line itself. The step-by-step iterative procedure to determine this operating point on the new speed line is outlined as follows:

1) Choose a π_c value on the selected speed line as an initial guess. This will yield corresponding values for $\dot{m}_{corr,2}$, η_c, and τ_c.

2) Calculate $\dot{m}_{corr,4}\frac{N_t}{\sqrt{\theta_4}}$, which for $\dot{m}_2 = \dot{m}_4$ and $N_t = N_c$ would be equivalent to $\dot{m}_{corr,2}\frac{1}{\pi_c\pi_b}\frac{N_c}{\sqrt{\theta_2}}$.

3) The value of $\dot{m}_{corr,4}\frac{N_t}{\sqrt{\theta_4}}$ then yields the value of $N_t/\sqrt{\theta_4}$ as long as the flow is choked (M = 1.0) at station 4 (which is a valid assumption for a wide range of operating conditions for a turbojet). Recall that the corrected mass flow rate at station 4 is known from the on-design point analysis.

4) A value of T_{t4}/T_{t2} is then obtained from the following relation:

$$\sqrt{\frac{T_{t4}}{T_{t2}}} = \frac{\left(\dfrac{N_c}{\sqrt{\theta_2}}\right)}{\left(\dfrac{N_t}{\sqrt{\theta_4}}\right)} \tag{23}$$

5) Find τ_t from the compressor-turbine power balance, i.e. Eq. (19).

6) If the turbine efficiency, η_t, is assumed constant across the operating envelope of a turbojet (a good assumption for most turbojets and hence used in this work), the turbine component map is formally unnecessary. With this approximation, the definition of the turbine efficiency is directly used to calculate π_t:

$$\eta_t = \frac{1 - \tau_t}{1 - \pi_t^{\frac{\gamma-1}{\gamma}}} \tag{24}$$

Here $\gamma = c_p/c_v$ (the ratio of specific heats for air).

7) Finally, the nozzle matching criterion given in Eq. (22) is checked.

8) If the matching criterion in the last step (7) is not satisfied within a chosen tolerance, modify the original guess for π_c and repeat steps 1 through 7 until the convergence criterion is met (i.e. the matching criterion is satisfied).

This process is then repeated for all other available speed lines on the compressor map (in this work there are eight speed lines in the generic map used, including the speed line corresponding to the on-design engine operational point). Each operating point has associated with it a unique T_{t4}/T_{t2} ratio, compressor pressure ratio, compressor efficiency, scaled blade speed, corrected mass flow rate, etc. The information embedded in the operating line development can then be tabulated or graphically represented. Graphical/digital representations were done in the present work using a cubic-spline curve fitting technique. As noted earlier, due to assumptions of constant turbine efficiency, only the compressor operating line is developed in this work. For a typical turbojet, there is in fact very little movement on the turbine performance map across the operational performance envelope, due to nearly constant turbine efficiency.

3.4. OPERATING ENVELOPE PERFORMANCE ANALYSIS

As a result of the development of the operating line, every point on the steady-state operating line corresponds to a unique (monotonically changing) value of the ratio of total temperature at burner exit to the total temperature at compressor entrance. This ratio, designated here as T_{t4}/T_{t2}, can then be viewed as the driving parameter as the engine is operated across all possible fuel throttle, altitude, and flight Mach number ranges (the three-space of the engine operating envelope). This can be easily seen since the altitude (ambient conditions) and flight Mach number together define a T_{t2} value (total temperature at compressor inlet face), and the throttle setting at a given flight Mach number and altitude defines the T_{t4} value (total temperature at the burner's exit). Each point on the operating line (and its associated T_{t4}/T_{t2} value) therefore defines an entire 'surface' of possible fuel throttle settings, flight Mach numbers, and altitudes in the general operational envelope for the engine. In other words, there exists many combinations of fuel throttle setting, flight Mach number, and altitude that will yield a certain value of T_{t4}/T_{t2}, hence defining an engine operating condition with its corresponding component performance parameters.

When the operating line is developed, the performance of the individual components as integrated into the engine is then available; so, for instance, compressor pressure ratio, corrected RPM, and compressor efficiency are known for any given value of corrected mass flow rate at the compressor entrance. This then allows the engine performance to be obtained in terms of thrust, mass capture (or spillage), and engine RPM for any possible set of fuel throttle, flight Mach number, and altitude conditions (the ranges of which collectively define the engine's operating envelope).

3.4.1. Engine Performance (Thrust, RPM, and Mass Capture/Spillage). The uninstalled thrust is defined as the net force developed on the engine. Uninstalled thrust mandates the assumption of constant ambient pressure on the outer envelope of the engine structure and does not account for upstream acceleration/deceleration of the captured air stream. It is the net force exerted by the fluid on all wetted surfaces of the engine (side walls, blades, etc.) through the two mechanisms of pressure and shear (friction). Thrust is the most important performance metric for any aerospace engine. RPM is also considered as a metric of fundamental engine performance since it describes the rotational speed of the spool and is a main driver for turbomachinery aerodynamics within the compressor and turbine.

In addition to thrust and RPM, air mass capture (and the related mass spillage that occurs upstream of the engine) is another critical performance parameter for a jet engine. Spillage is defined here as the difference between the actual mass flow rate demanded by the engine at some given fuel throttle, flight Mach number, and altitude, and the mass flow rate that would be processed if there was full mass capture at the same flight Mach number and altitude. Full mass capture corresponds to the situation where the engine ingests upstream air with no curvature of the sides of the captured streamtube of air between freestream and inlet face, i.e. the cross-sectional area in the free-stream of the captured streamtube is equal to the engine's inlet area; $A_0 = A_1$. Hence, for full mass capture, the captured streamtube is neither accelerated nor decelerated upstream of the inlet face (from 0 to 1). Spillage (deviation, positive or negative) from that (usually reference) full mass capture value then arises because the engine always inducts the amount of air it requires at a given operating condition, hence mandating upstream acceleration or deceleration of the captured streamtube of air, as necessary. Figure 3.4 provides a sketch of the three basic

engine spillage conditions. In this figure, for case (a), the engine requires a higher mass flow rate than can be provided by full mass capture, so the upstream air is necessarily accelerated; the spillage in such a case is by definition negative. This situation typically occurs at low speed, high throttle (fast spooling) operation. Case (b) illustrates an engine at full mass capture. In case (c), the engine cannot process the mass flow rate of air associated with full mass capture, hence some of the flow is 'spilled' around the cowl/nacelle. In such a case the flow experiences external deceleration; this is a case of positive spillage and is characteristic of high speed (high flight Mach number) operation. An engine operating with spillage or negative spillage has deleterious effects including additive drag associated with the upstream streamtube as well as possible undesirable fluid dynamic effects. These fluid dynamic effects are due to the upstream curvature of the captured streamtube; separation in the inlet can result.

a) Static operation (or insufficient air for engine)

b) Low-speed operation (correct engine air)

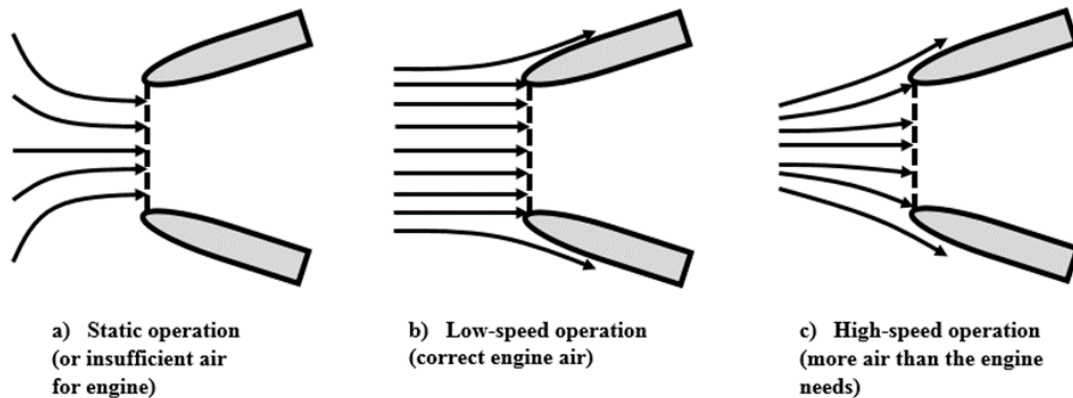c) High-speed operation (more air than the engine needs)

Figure 3.4. Typical streamline patterns for a subsonic inlet.

Supersonic flight necessarily gives rise to further complications and the degree and efficiency of compression and spillage is highly dependent on the shape of the inlet/diffuser system. This will in turn define oblique and normal shock systems developing in and around the inlet, hence allowing engine-mandated spillage of mass. In this work, the performance of the inlet/diffuser is summarized by a representative performance metric in order to approximate the effects of the different associated phenomena without delving too deep into the details. Specifically, an inlet total pressure loss (diffuser total pressure drop) model is developed through curve fitting a wide representation of data found in [33]. The results of this curve fit, in terms of the ratio of total pressure at inlet exit (station 2) to total

pressure of free-stream (station 0), spanning both subsonic and supersonic flight regimes, is presented in the engine description section later.

To summarize the preceding discussion and lead into the next section, once the operating lines on the individual component maps are developed, the performance of the individual components as integrated into the engine is then available. So, in this study (which focuses on the compressor map as the critical component map for a simple turbojet), the compressor pressure ratio, corrected RPM, and compressor efficiency are then known for any given value of corrected mass flow rate at the compressor entrance. This will then allow the engine performance to be determined in terms of thrust, mass capture (or spillage), and engine RPM for any possible set of fuel throttle, flight Mach number, and altitude conditions (the possible ranges of which collectively define the engine's operating envelope). This is the focus of the following section.

3.4.2. Engine Performance Analysis Procedure. In this section, the analytical procedure for producing engine performance at a given fuel throttle setting, flight Mach number, and altitude is described. Nominally, as noted, the three independent variables (inputs) to be provided are the altitude, fuel throttle setting, and the flight Mach number. In order to define a single point in the operating envelope and to determine the associated performance (thrust/RPM/mass capture) at that point, the approach used in this investigation is to assume an altitude (hence fixing the ambient temperature and pressure, T_0 and P_0). A corrected mass flow rate at the compressor inlet (station 2) is then chosen. Corrected mass flow rate was defined in Eq. (11); it scales directly with Mach number for a fixed cross-sectional area. The chosen corrected mass flow rate (via the associated point on the operating line as previously developed) corresponds to a given T_{t4}/T_{t2} ratio along with a specific compressor pressure ratio, compressor efficiency, and compressor (scaled) RPM. The flight Mach number associated with this unique operating line point along with a specified fuel flow rate can then be readily backed out from the burner energy balance (given in expanded form for this analysis in Eq. (25)). The reason why the corrected mass flow rate at the compressor's inlet is chosen as an independent variable instead of the flight Mach number is because the compressor performance maps (and the corresponding operating lines) are developed with $\dot{m}_{corr,2}$ as the independent variable; this then greatly simplifies the approach, eliminating the need for interpolation on the maps. In calculating

the flight Mach number associated with a point on the operating line and a specified fuel flow rate in this fashion, it can also be determined if the engine can actually physically operate at that point (i.e., if no real solution exists to Eq. (25), the engine cannot operate - in steady state- at that point). The engine control system (ECS) may also limit or prohibit performance via the imposition of criteria such as maximum temperature allowed at turbine entrance, maximum RPM allowed, etc. The engine (air) mass flow rate is directly calculated from Eq. (11).

$$M_0 = \sqrt{\frac{2}{\gamma - 1} \left[\left(\frac{\dot{m}_{fuel} \, h_{fuel} \, P_{STP}}{\pi_d P_0 \dot{m}_{corr,2} c_p \sqrt{T_0 T_{STP}} \left(\frac{T_{t4}}{T_{t2}} - \tau_c \right)} \right)^{\frac{2\gamma - 2}{3\gamma - 1}} - 1 \right]^{1/2}} \qquad (25)$$

To reiterate, the procedure to fully determine engine performance at any off-design point begins with defining the operating point/condition through the selection of an altitude, a given fuel throttle setting, and an $\dot{m}_{corr,2}$. The altitude will directly determine the freestream (ambient) conditions (ambient temperature, pressure, and density determined from atmospheric models [35]). Once a value for $\dot{m}_{corr,2}$ is selected, the compressor pressure ratio, π_c, engine RPM (corrected), and compressor efficiency, η_c are all determined from the information provided by the operating line associated with the compressor map. The compressor total temperature ratio follows:

$$\tau_c = 1 + \frac{\pi_c^{\frac{\gamma - 1}{\gamma}} - 1}{\eta_c} \qquad (26)$$

Utilizing the assumption that the flow is choked at both the turbine entrance and the nozzle throat, it follows that: $\dot{m}_{corr,4} = \dot{m}_{corr,4 \, (on-design)}$ and $\dot{m}_{corr,8} = \dot{m}_{corr,8 \, (on-design)}$ The matching criteria described earlier are then used to determine engine parameters such as the scaled turbine speed:

$$\frac{N_t}{\sqrt{\theta_4}} = \frac{\dot{m}_{corr,2}}{\dot{m}_{corr,4}} \frac{1}{\pi_c \pi_b} \frac{N_c}{\sqrt{\theta_2}} \qquad (27)$$

Similarly (following the matching criteria development),

$$\frac{T_{t4}}{T_{t2}} = \frac{\left[\left(\frac{N_c}{\sqrt{\theta_2}}\right)\right]^2}{\left[\left(\frac{N_t}{\sqrt{\theta_4}}\right)\right]} \tag{28}$$

The turbine total temperature ratio can then be calculated:

$$\tau_t = 1 - \frac{\tau_c - 1}{T_{t4}/T_{t2}} \tag{29}$$

The turbine total pressure ratio follows:

$$\pi_t = \left[1 - \frac{1 - \tau_t}{\eta_t}\right]^{\frac{\gamma}{\gamma-1}} \tag{30}$$

Note that the turbine efficiency in this work is taken to be invariant for all engine operating conditions, per earlier discussion.

At this point, the flight Mach number is still undetermined. Recall that an inlet diffuser loss model is used such that $\pi_d = \pi_d(M_0)$. Equation (25) can then be solved numerically for the flight Mach number, M_0, corresponding to the given altitude, fuel throttle setting and corrected mass flow rate at compressor entrance. Then, since the flow is adiabatic through the inlet/diffuser:

$$T_{t2} = T_{t0} = T_0(1 + \frac{\gamma - 1}{2}M_0^2) \tag{31}$$

By definition,

$$T_{t4} = T_{t2}\frac{T_{t4}}{T_{t2}} \tag{32}$$

If the total temperature at the burner exit exceeds an assigned limit (for specific results to be presented in this work taken as $1600K$) then the operating point is not obtainable; the engine control system will prevent throttling the engine to that point. However if the values of M_0 and T_{t4} are such that the engine is operable without ECS limits being reached at the given flight Mach, fuel throttle setting, and altitude, engine uninstalled

thrust, spool RPM, and spillage are then calculated. The spool RPM (actual or raw RPM) can be calculated from the scaled/corrected compressor speed:

$$N_c = \left(\frac{N_c}{\sqrt{\theta_2}}\right)\sqrt{\theta_2} = \left(\frac{N_c}{\sqrt{\theta_2}}\right)\sqrt{\frac{T_{t2}}{T_{STP}}} \tag{33}$$

Spillage can be determined as follows:

$$Spillage = \dot{m}_{full\ mass\ capture} - \dot{m}_{actual} \tag{34}$$

Here,

$$\dot{m}_{full\ mass\ capture} = \rho_0 u_0 A_1 \tag{35}$$

The freestream velocity (flight velocity of the engine) is easily obtained from the definition of the Mach number:

$$u_0 = M_0\sqrt{\gamma R T_0} \tag{36}$$

The actual mass flow rate inducted through the engine is determined from the definition of $\dot{m}_{corr,2}$:

$$\dot{m}_{actual} = \dot{m}_{engine} = \dot{m}_{corr,2}\frac{P_{t2}/P_{STP}}{\sqrt{T_{t2}/T_{STP}}} \tag{37}$$

Here,

$$P_{t2} = \pi_d P_0 \left(1 + \frac{\gamma-1}{2}M_0^2\right)^{\frac{\gamma}{\gamma-1}} \tag{38}$$

The engine's uninstalled thrust is determined from the conditions at nozzle exit (station 8 in this work).

$$P_8 = \pi_n \pi_t \pi_n \pi_c \pi_d P_0 \left(1 + \frac{\gamma-1}{2}M_0^2\right)^{\frac{\gamma}{\gamma-1}} \tag{39}$$

$$T_8 = \tau_n \tau_t T_{t4} \frac{2}{\gamma + 1} \tag{40}$$

$$u_8 = \sqrt{\gamma R T_8} \tag{41}$$

The uninstalled thrust is:

$$F_{uninstalled} = \dot{m}_{engine}(u_8 - u_0) + A_8(P_8 - P_0) \tag{42}$$

This methodology then allows the complete description of the flow through the engine and the corresponding description of engine performance (in terms of thrust, spillage, and RPM) across the operating range of all possible fuel throttle settings, flight Mach numbers, and altitudes.

4. LOSSES, ENTROPY GENERATION, AND THE PERFORMANCE OF JET ENGINES

This section develops the methodology for exergy analysis of aerospace gas turbine engines. This methodology relates exergy directly to the conventionally defined performance of these engines. The first part of this section discusses the general approach as applied to an aerospace vehicle in flight and is a summary of work reported in references [1] and [2]. The method is based on a global control volume encompassing the vehicle and extending to far-field boundaries at sides and downstream of the vehicle wake. The second part of this section extends the method to a stand-alone gas turbine engine and its components and discusses tools by which losses are quantified. Different levels of modeling are discussed. Methods for determining the entropy change and generation in the various engine components are described, as well as the method for analyzing the entropy generation in the wake region.

4.1. GLOBAL CONTROL VOLUME AND EXERGY BALANCE FOR AN AEROSPACE VEHICLE IN FLIGHT

Exergy destruction (or work availability loss) and entropy generation (entropy change associated with irreversible processes in which work potential is destroyed) describe the universal construct that underlays the second law of thermodynamics. Specifically, entropy generation provides the most fundamental measure possible for describing losses of any type and due to any mechanism. The rate of exergy destruction (destruction of available work potential) is then directly proportional to the rate of entropy generation of the system where the proportionality factor is the equilibrium temperature (i.e., for an aerospace system, the equilibrium temperature is ultimately the ambient temperature of the surroundings). Note that the exergy loss rate has units of power.

A simplified exergy balance for an aerospace vehicle in flight can be obtained by combining conservation of mass, momentum, and the first and second laws of thermodynamics. These laws are applied to a global fluid control volume enveloping the solid structure of the vehicle and hence properly include internal propulsive and fluid flow-paths. The global control volume has constant cross-sectional area (see Figure 4.1 for a two-dimensional sketch of the global control volume). This control volume has the vehicle

'embedded' within it (from free-stream plane '0' to vehicle exit plane 'e') and includes the wake region (defined by the wake equilibration process which stretches axially from vehicle exit plane 'e' to an equilibrated wake exit plane 'w'). The global control volume cross sectional area should be sufficiently large to ensure analytic convergence (theoretically infinitely large in cross-sectional extent but practically finite for meaningful calculations). The axial dimension of the global stream tube (from 'e' to 'w') is formerly immaterial to global control volume analysis; the assumption is that the wake exit plane has reached a uniform (totally equilibrated) plane. Assumptions used in the following derivation of the aerospace vehicle exergy balance include steady flow and a simple calorically perfect gas (air). Additionally, any exothermic heat release associated with fuel-air combustion is modeled as an equivalent heat received by the fluid in the control volume (from the vehicle). This heating-value model is foundational in much of gas turbine engine analysis.
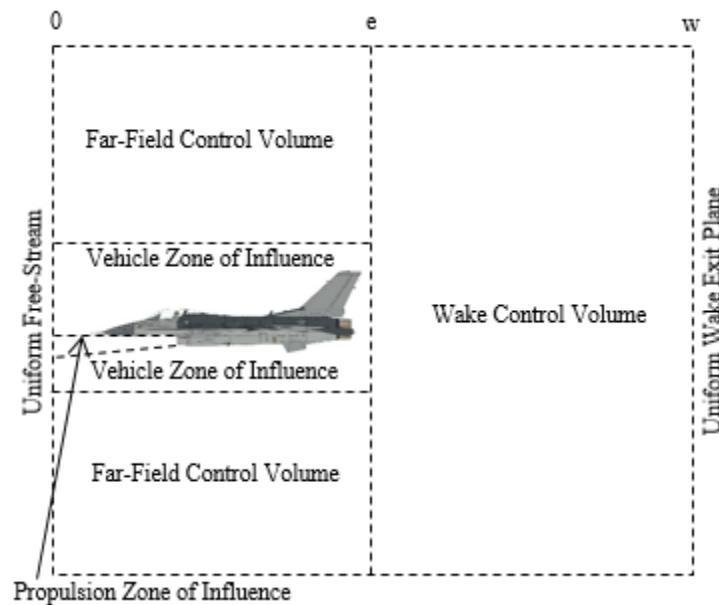
Figure 4.1. Global control volume for vehicle exergy analysis.

In order to develop the governing equation that relates on-board energy and entropy generation and losses to the realized (productive) force power associated with vehicle flight, the energy equation is first applied to the global control volume. Specifically, the change in total enthalpy flow rate from inflow plane '0' to wake exit plane 'w' equals the

net energy rate received by the fluid in the control volume as heat and/or work interactions from the vehicle. This is represented as:

$$\dot{Q} + \dot{W} = \dot{H}_{t,w} - \dot{H}_{t,0} \tag{43}$$

Here $\dot{H}_t$ is the flow rate of total enthalpy defined as:

$$\dot{H}_t = \dot{m}\left(h + \frac{u^2}{2}\right) = \dot{m}\left(c_p T + \frac{u^2}{2}\right) \tag{44}$$

Eq. (43) then can be written as:

$$\dot{Q} + \dot{W} = \dot{m}c_p T_w - \dot{m}c_p T_0 + \dot{m}\frac{u_w^2}{2} - \dot{m}\frac{u_0^2}{2} \tag{45}$$

In order to introduce the productive work done on the vehicle, it is necessary to manipulate the energy equation to include the magnitude of the net axial force due to all fluid pressures and shear stresses that act on the solid wetted surfaces of the vehicle. This includes both internal (propulsion system) and external (aerodynamic) wetted surfaces (all vehicle surfaces adjacent to the fluid). Here, the axial direction refers to the instantaneous flight direction of the vehicle (the direction of instantaneous velocity). Let this force magnitude be given as $F_{x(flight)}$. Note that for a vehicle that is not accelerating or decelerating, $F_{x(flight)}$ is, by definition, zero. In an approximate sense, this force can therefore be thought of as the conventional 'thrust – drag' operating on the vehicle as a whole. The axial momentum equation applied to the global stream tube yields the result that this force is the change in stream thrust between the exit and inlet of the stream tube:

$$F_x = (ST)_w - (ST)_0 = (P_w A_w + \dot{m}u_w) - (P_0 A_0 + \dot{m}u_0) \tag{46}$$

The vehicle force power associated with $F_{x(flight)}$ is by definition simply $F_{x(flight)}$ multiplied by flight velocity. Incorporating the vehicle force power into the energy equation, Eq. (45), the following is obtained:

$$\dot{Q} + \dot{W} = \dot{m}c_p T_w - \dot{m}c_p T_0 + \dot{m}\frac{u_w^2}{2} - \dot{m}\frac{u_0^2}{2} + u_0 F_x - u_0 P_w A_w - \dot{m}u_0 u_w$$
$$+ u_0 P_0 A_0 + \dot{m}u_0^2 \tag{47}$$

In this equation, all cross-sectional areas are equal. Combining like terms and simplifying:

$$\dot{Q} + \dot{W} = \dot{m}c_p(T_w - T_0) - u_0 A_0(P_w - P_0) + \frac{\dot{m}}{2}(u_w^2 - 2u_0 u_w + u_0^2) + u_0 F_x \tag{48}$$

This is then rewritten as:

$$\dot{Q} + \dot{W} = \dot{m}c_p \Delta T - \dot{m}\frac{\Delta P}{\rho_0} + \dot{m}\frac{(\Delta u)^2}{2} + u_0 F_x \tag{49}$$

Here, ΔP, ΔT, and Δu are the change in pressure, temperature, and velocity from free-stream plane to wake exit plane. For very large cross-sectional areas of the global stream tube, the conditions (flow properties) at the equilibrated wake exit plane are only infinitesimally (differentially) displaced from conditions at the (upstream) free-stream plane, i.e.,

$$u_w = u_0 + du \tag{50}$$

$$T_w = T_0 + dT \tag{51}$$

$$P_w = P_0 + dP \tag{52}$$

The combined first and second laws of thermodynamics for a differential process can be written as:

$$dh = Tds + \frac{dP}{\rho} \tag{53}$$

This can be recast in rate terms as follows:

$$Td\dot{S} = d\dot{H} - \dot{m}\frac{dP}{\rho} = \dot{m}c_p dT - \dot{m}\frac{dP}{\rho} \tag{54}$$

Rewriting Eq. (49) in terms of the differential changes,

$$\dot{Q} + \dot{W} = \dot{m}c_p dT - \dot{m}\frac{dP}{\rho_0} + \dot{m}\frac{(du)^2}{2} + u_0 F_x \tag{55}$$

Substituting Eq. (54) into Eq. (55) and discarding higher order terms, namely the $(du)^2$ term, yields,

$$\dot{Q} + \dot{W} = T_0\dot{S} + u_0 F_x \tag{56}$$

The fundamental entropy-force (exergy balance) relationship is then obtained by rearranging this relationship, and combining the heat and work terms as a single net power input term. This exergy or availability balance is then written as:

$$u_0 F_{x(flight)} = \dot{E} - T_0\dot{S}_{total} \tag{57}$$

In Eq. (57), u_0 is the vehicle flight velocity, $F_{x(flight)}$ is the net resultant force in the direction of flight (effectively or traditionally the 'thrust – drag' or net accelerative force), $\dot{E}$ is the sum of $\dot{Q}$, the net rate of energy as heat interaction to the fluid, and $\dot{W}$, the net rate of energy as work addition to the fluid, T_0 is the free-stream ambient temperature, and $\dot{S}_{total}$ is the net rate of entropy change inside the global control volume (between the undisturbed far-field upstream and the exit of the wake mixing zone). Specifically,

$$\dot{S}_{total} = \dot{S}_{vehicle} + \dot{S}_{wake} = \dot{S}_{irr(vehicle)} + \dot{S}_{heat(vehicle)} + \dot{S}_{wake} \tag{58}$$

The total entropy change is due to 1) all irreversibilities occurring in the global fluid control volume between free-stream and vehicle exit plane 'e'; this includes both external (aerodynamic) and internal (propulsive) flow paths, 2) entropy change due to heat interactions between vehicle and fluids, and 3) entropy generation due to irreversibilities occurring in the wake mixing zone ('e' to 'w').

The global control volume described here can usefully be divided into three main portions (as in Figure 4.1): 1) the vehicle zone of influence (i.e. the volume surrounding the vehicle and impacted or influenced by the vehicle, extending from '0' to 'e', and

including the propulsion flow path or zone of influence), 2) the side-bounding far-field control volume that (nominally) is at free-stream conditions (especially relevant for very high-speed systems). This portion theoretically extends to infinity in the lateral plane and axially from '0' to 'e', and 3) the wake mixing volume or zone that is downstream of the vehicle exit plane (extending from station 'e' to station 'w'). Again, the total entropy change rate has two main sources, 1) entropy generated and entropy transferred to the fluid due to processes associated with the fluid inside and around the vehicle within the vehicle zone of influence, and 2) entropy generated in the wake mixing zone. The entropy generated in the wake equilibration process which has often been neglected in prior work, is of vital importance and cannot be omitted. It often significantly exceeds the total entropy generated in the vehicle zone of influence, including within the propulsive system.

Entropy generation due to irreversibilities has many sources throughout the flow external to the vehicle including friction, shock waves, heat transfer, etc. Similarly, for fluid associated with the propulsive flowpath, entropy generation is due to friction, shock waves, heat transfer, species mixing, non-equilibrium chemical reactions, non-isentropic work interactions, etc. Also, entropy generation due to irreversibilities and non-ideal effects in on-board (non-propulsive and non-aerodynamic) subsystems most generally result in the transfer of rejected heat and associated entropy to the fluid within the control volume and hence are also included in the exergy balance described in Eq. (57) and Eq. (58).

If the total entropy generation rate can be quantified, the net resultant force acting on the vehicle in the direction of flight can be determined using Eq. (57). Furthermore, in principle, by utilizing the single universal currency of entropy, the complete quantification and breakdown ('auditing') of force and performance losses due to the individual entropy generation details (in terms of individual loss mechanisms and sub-systems) can also be realized. These performance losses can then be related back to classic vehicle performance such as range, endurance, ceiling, maximum flight speed, etc.

Finally, note that (fundamentally) energy transferred as a heat interaction is exergetically less useful than an equal amount of energy transferred as a work interaction; this reduction in realized exergy is inherently due to the entropy increase associated with the (positive) heat interaction since heat, as opposed to work, is the 'disorganized' form of

energy transfer. Hence from the standpoint of the entropy-power relation for a vehicle (Eq. (57)), exergy losses are measured with respect to the total amount of energy (heat or work equivalent) supplied to the vehicle initially. Therefore, any given entropy change, whether due to irreversibilities (internal generation of heat) or whether due to energy transfer as a heat interaction, is equally associated with an exergy loss in terms of the flight-based force-power of the vehicle. Thus, although the entropy associated with a (positive) heat interaction is thermodynamically different than the entropy increase associated with exergy destruction due to internal irreversibilities (internal generation of heat from energy originally available as work), it nevertheless is measurable as an equivalent loss in terms of aerospace system performance.

4.2. APPLICATION OF ENTROPY-FORCE RELATIONSHIP TO A STAND-ALONE GAS TURBINE ENGINE

The exergy performance analysis for aerospace vehicles as discussed previously can be readily adapted to a stand-alone gas turbine engine operating in either subsonic or supersonic conditions. Here the term 'stand-alone' refers to an engine in flight without considerations of airframe mounting or integration. In such an application and reflective of the approach described in the last section, the global control volume, as seen in Figure 4.2, is again divided into three main parts: 1) the 'outer' or side-bounding stream tube
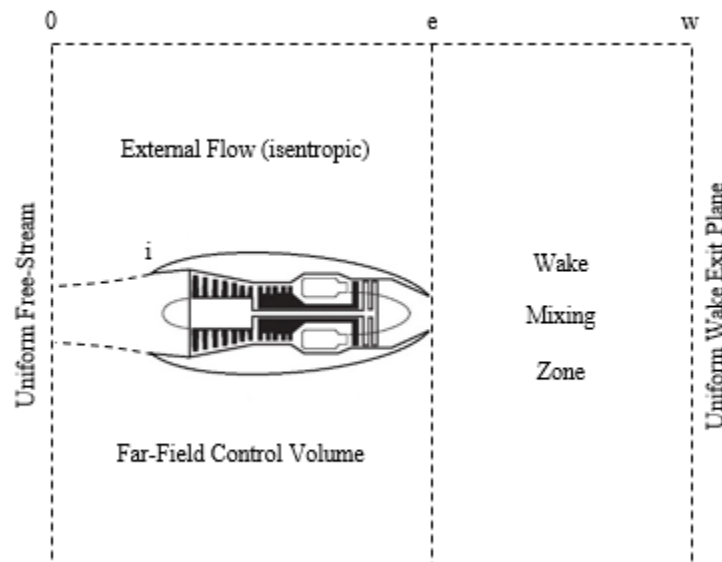
Figure 4.2. Global control volume for stand-alone gas turbine exergy analysis.

surrounding the engine, 2) the stream tube associated with the air that is actually inducted into the engine i.e., the propulsive flow path, and 3) the downstream wake mixing control volume. For the stand-alone engine analysis, which is the focus of the results in this thesis, the fluid dynamics in the side-bounding stream tube is isentropically compressed (or expanded) as determined by the area ratio between engine exit and freestream capture point.

As done for a complete aerospace vehicle in the previous section, the global control volume for the gas turbine engine theoretically extends to infinity in the lateral directions. Upstream external acceleration or deceleration of the captured airflow (for subsonic or subcritical engine operation) is allowed such that the propulsive flow path extends forward of the inlet to the free-stream or far-field (plane '0'). In the case of the stand-alone engine under the given conditions, the net axial force given in Eq. (57) becomes, by definition, the engine uninstalled thrust:

$$F_{uninstalled} = \frac{1}{u_0}\left(\dot{E} - T_0 \dot{S}_{total}\right) \tag{59}$$

The uninstalled thrust is also defined from momentum considerations (representing the traditional formulation for engine thrust) as follows:

$$F_{uninstalled} = (\dot{m}_9 u_9 - \dot{m}_0 u_0) + (P_9 - P_0)A_9 \tag{60}$$

For simplicity, if all power extracted by the turbine is assumed to power the compressor such that the net work rate across the entire engine is zero (compressor-turbine power match with no auxiliary power draw from the turbine) and the net heat rate input is simply modeled as the product of the fuel mass flow rate and the heating value of the fuel (energy content per unit mass of fuel), the uninstalled thrust of the stand-alone jet engine in terms of heating value of the fuel and total entropy generation is then written as:

$$F_{uninstalled} = \frac{1}{u_0}\left[\dot{m}_{fuel} h_{fuel} - T_0\left(\dot{S}_{irr(engine)} + \dot{S}_{heat(engine)} + \dot{S}_{wake}\right)\right] \tag{61}$$

4.3. ENGINE COMPONENT LOSSES AND THEIR ENTROPY CHANGE GENERATION MODELING

This section provides a discussion of the quantification methodology necessary for assessing entropy terms in the stand-alone engine exergy relationship. First, the method for simple computation of overall entropy rate in a lumped individual component is developed. Lumped component analysis is defined here as simple analysis describing fluid/thermodynamic mandated changes from inlet to exit of the component. This is then followed by a more detailed description of methodology for parsing entropy in terms of loss mechanism and spatial location in a component when using a differential quasi-one-dimensional solver.

4.3.1. Overall Entropy Change Rate in a Lumped Individual Component. In order to quantify losses across a given engine component with exit conditions denoted using the subscript 'e' and entrance conditions denoted using the subscript 'i', the entropy change between the exit and inlet of that component must be calculated. The differential entropy change from the combined first and second laws for a calorically perfect gas is given by

$$ds = c_p \frac{dT}{T} - R \frac{dP}{P} \tag{62}$$

Integrating from component inlet to exit plane and multiplying by the mass flow rate, the following expression is obtained for the rate of entropy change in the component from inlet to exit:

$$\dot{S}_{component} = \dot{m} \left[c_p \ln \left(\frac{T_e}{T_i} \right) - R \ln \left(\frac{P_e}{P_i} \right) \right] \tag{63}$$

The static temperature and pressure ratios can be conveniently replaced by the total/stagnation conditions at the same stations, or

$$\dot{S}_{component} = \dot{m} \left[c_p \ln \left(\frac{T_{te}}{T_{ti}} \right) - R \ln \left(\frac{P_{te}}{P_{ti}} \right) \right] \tag{64}$$

For each component, the total temperature and total pressure ratios across a component, $\tau_{component}$ and $\pi_{component}$, respectively, have been previously defined such that

$$\dot{S}_{component} = \dot{m}\left[c_p \ln\left(\tau_{component}\right) - R\ln\left(\pi_{component}\right)\right] \qquad (65)$$

As these parameters are known from the engine analysis methodology as previously described in an earlier section, the rate of entropy generation/change for each component can then be readily quantified. The overall entropy rate of change across the entire engine is then:

$$\dot{S}_{engine} = \sum \dot{S}_{component} \qquad (66)$$

This method of quantifying entropy is simple to implement but does not allow for the division of the entropy generation in terms of the various loss mechanism contributions (i.e. amount of entropy generated due to friction, species mixing, non-ideal heat transfer, etc.). In order to have this level of detail in the quantification of losses, a more sophisticated analysis must be performed.

4.3.2. Determination of Entropy Change Rates in Terms of Loss Mechanism and Spatial Location for Differential Quasi-One-Dimensional Modeling. Although the lumped component approach is very useful (and is in fact used in this work when numerical results are given), it is also useful to formulate the approach for the next highest level of analysis. This level of analysis corresponds to a differential quasi-1D solver within the component or the engine as a whole. This method generally allows the calculation of entropy change/generation at each step due to friction, heat (ideal and non-ideal contributions), external work interactions with irreversibilities, species mixing, and chemical reactions. That is because the flow-field is being modeled across differential spatial steps using consistent formulations of the governing equations that inherently include loss models. The methodology enables (but does not require) removing the single species, calorically perfect gas assumption for the flow and applying a more realistic treatment of the flow using multiple species, chemical reactions, etc. This method nominally requires prior knowledge of models for the cross-sectional area distribution, skin friction coefficient, C_f, axial distribution, wall temperature distribution, the work and heat interaction distributions, work interaction mechanical efficiencies, chemical reaction distributions, and mixing distributions. Approximate or simplified models for these input

parameters or their axial distributions may be employed. Further details of modeling techniques as described in this section can be found in Ref. [2].

For each axial step, a system of nonlinear differential equations is obtained from the governing equations of a control volume, namely continuity (conservation of mass), momentum, energy, and gas equation of state:

Continuity
$$\frac{d\rho}{\rho} + \frac{du}{u} + \frac{dA}{A} = 0 \tag{67}$$

Momentum
$$\frac{dP}{\rho} + udu = -\frac{\tau_w c}{\rho A} dx + \eta \, \delta w_{ext} \tag{68}$$

Energy
$$dh + udu = \delta q_{ext} + \delta w_{ext} \tag{69}$$

Equation of State
$$\frac{dP}{P} = \frac{d\rho}{\rho} + \frac{dT}{T} + \frac{dR}{R} \tag{70}$$

The four unknown parameters to be solved are either ρ, u, P, T at the next station or $d\rho, du, dT, dP$ depending on the numerical technique utilized for solving the system. Note that,

$$dh = c_p(T)dT = \sum_{i=1}^{N} \left[\alpha_i c_{p_i}(T)dT + h_i(T)d\alpha_i \right] \tag{71}$$

Here, α_i is the mass fraction of species i defined as $\alpha_i \equiv \dot{m}_i / \sum \dot{m}_i$. In the case of a general model of reacting mixtures where the gas constant changes, $dR = \sum R_i d\alpha_i$, where R_i is the gas constant of species i.

The momentum equation includes the skin (wall) friction, where c is the perimeter (circumference for circular cross-sections), and τ_w is the wall shear stress, usually modeled using a skin friction coefficient:

$$\tau_w = \frac{1}{2}\rho u^2 C_f \tag{72}$$

In the relations above, δw_{ext} is the amount of differential work supplied across the boundary (positive into the flow and negative when extracted from the flow) while the effective amount realized as an actual change in momentum is determined by using an (input) second law effectiveness parameter, η. For positive work interaction, η varies between 0 and 1; for negative work interaction η is greater than 1 (note that $\eta = 1$ corresponds to isentropic work interaction). The lost work potential due to irreversibilities in a work interaction is then realized (internally) as entropy generation (see Ref. [36]). The change/generation of entropy per mass across a given differential (spatial) step in a differential solver is given by the following relationship:

$$ds = \frac{\delta q_{ext}}{T} + ds_{gen} \tag{73}$$

The differential entropy generation term here is due to all internal irreversibilities.

The first term on the right hand side in Eq. (73), the heat transfer entropy change, can be divided into two contributions: ideal heat addition, corresponding to the minimum possible entropy change associated with an amount of heat δq_{ext}. This would be the case if the heat is transferred at zero velocity (where $T = T_t$). The second contribution would be associated with additional entropy change due to heat transfer at finite velocity (where $T < T_t$); the so-called 'Rayleigh' loss in propulsion analysis. This can be written as:

$$ds_{heat} = \frac{\delta q_{ext}}{T} = \frac{1}{T_t}\delta q_{ext} + \left(\frac{1}{T} - \frac{1}{T_t}\right)\delta q_{ext} = ds_{ideal\ heat} + ds_{non-ideal\ heat} \tag{74}$$

This division might seem trivial but note that it is only the $ds_{non-ideal\ heat}$ that contributes to total pressure loss in a heat transfer event; the ideal portion of the entropy change associated with heat transfer has no impact on total pressure (see Section 3). The heat transfer itself can be further divided into two contributions due to the different heat transfer mechanisms: convection and radiation; this in turn allows the further subdivision of entropy increments in terms of mechanism. Specifically,

$$\delta q_{ext} = \delta q_{conv} + \delta q_{rad} \tag{75}$$

For quasi-one-dimensional flows, modeling of the convective heat transfer between the engine walls and the fluid requires knowledge of the axial distribution of the wall temperature. Using the Reynolds analogy, the convective differential heat transfer can be separately defined as (see [34] for details of this standard development):

$$\delta q_{conv} = \frac{1}{2} c_p C_f (T_w - T_t) \left(\frac{c}{A}\right) dx \tag{76}$$

Here, T_w is the wall temperature.

No model of radiative heat transfer is shown here. Nonetheless, the combustion in a gas turbine burner can be (and often is in engine analysis) simulated as a heat transfer by using effectively a 'radiation like' term where the total heat addition rate is simply related to the heating value of the fuel injected. For instance, for a linear progressive combustion heat release schedule using the δq_{rad} term as a construct for modeling exothermic heat release, the combustion equivalence heat rate would be divided equally over the axial steps in the burner:

$$\delta q_{rad} = \frac{\dot{Q}_{fuel}}{number\ of\ axial\ steps\ in\ burner} \tag{77}$$

Here,

$$\dot{Q}_{fuel} = f \dot{m}_{engine} h_{fuel} \tag{78}$$

f is the fuel-to-air ratio and h_{fuel} is the heating value (content) of the fuel.

The entropy generation due to internal irreversibilities in Eq. (73) can be decomposed into the contributions from the different (modeled) loss mechanisms:

$$ds_{gen} = ds_{viscous} + ds_{lost\ external\ work} + ds_{chemical\ reaction} + ds_{species\ mixing} \tag{79}$$

The first term in Eq. (79) is the entropy generation due to viscous effects (friction) and is quantified as follows:

$$ds_{viscous} = \frac{\tau_w c}{\rho T A} dx \tag{80}$$

The second term in Eq. (79) is the entropy generation due to all internal irreversibilities associated with (externally supplied) shaft work interaction (the development of this is found in References [36] and [37]). It can be calculated as follows:

$$ds_{lost\ external\ work} = \frac{\delta w_{lost\ external}}{T} = \frac{\delta w_{ext} - \delta w_{effective}}{T} = \frac{1-\eta}{T} \delta w_{ext} \tag{81}$$

The third term in Eq. (79) is the entropy generation due to chemical reactions (as found in Ref. [2]) and is quantified as follows:

$$ds_{chemical\ reaction} = -\sum_{i=1}^{N} \left(\frac{h_i}{T} - s_i\right) d\alpha_i \tag{82}$$

Here, h_i and s_i are the enthalpy and entropy, respectively, of species i at that axial step. The last term in Eq. (79) is the entropy generation due to species mixing (mass diffusion). It can be modeled (see Ref. [2]) as follows:

$$ds_{species\ mixing} = -\sum_{i=1}^{N} \alpha_i R_i \frac{dX_i}{X_i} \tag{83}$$

X_i is the mole fraction of species i.

In summary, the differential change in entropy per mass across an axial step can be rewritten in terms of all the individual entropy increments developed here as:

$$ds = \frac{\delta q_{ext}}{T_t} + \left(\frac{1}{T} - \frac{1}{T_t}\right)\delta q_{ext} + \frac{\tau_w c dx}{\rho T A} + \frac{1-\eta}{T}\delta w_{ext} - \sum_{i=1}^{N}\left(\frac{h_i}{T} - s_i\right)d\alpha_i$$
$$- \sum_{i=1}^{N} \alpha_i R_i \frac{dX_i}{X_i} \tag{84}$$

The analysis method described above can provide significant detail regarding the mechanisms responsible and spatial location of losses in the engine and in engine

components. It should be emphasized that this type of analysis (differential quasi-one-dimensional methodology) was not used for the case study presented in the body of this thesis but was successfully implemented in a related investigation. Loss results for that investigation are presented in Appendix B. A more sophisticated loss analysis can be done in conjunction with a multi-dimensional CFD analysis.

4.3.3. Entropy Generation in the Wake Region. In order to calculate the overall entropy generation rate in the wake mixing zone, the wake mixing region can be readily treated analytically from basic flow-rate and conservation considerations. In application, instead of an infinitely large global control volume in terms of cross-sectional or lateral extent, a control volume that is sufficiently large to ensure asymptotic convergence for the exergy relationship is used. In this study, the ratio of cross sectional area of the global control volume to the inlet entrance cross-sectional area is therefore taken to be 10^9; this value is significantly larger than necessary but ensures asymptotic convergence for all cases analyzed. A check for convergence using the thrust obtained from the exergy balance against the thrust value obtained from traditional momentum considerations is always done in order to ensure correct implementation of both physics and modeling. For a base-line case to be discussed in the results section, such a validation is shown in Figure 4.3, which shows thrust calculated using Eq. (61) for increasing global control volume cross-sectional area. The net force value for overall engine asymptotes to the conventional thrust magnitude as the lateral extent of the wake control volume is increased.

In order to compute the entropy generation associated with the equilibration process in the wake, the overall flow rates of mass and total enthalpy as well as stream thrust at the wake entrance (plane 'e') must first be determined. The flow rates at station 'e' are the respective sums of the exiting flow-rates from the two distinct flow-fields in the global control volume from '0' to 'e' (the engine and the side-bounding sub-control volumes upstream of 'e'). The side-bounding flow over the cowl outside the engine upstream of plane 'e' is treated as isentropic such that the flow-rates and flow conditions at the exit plane (wake entrance) for that portion of the global control volume are easily determined (for instance for calorically perfect gas) using the isentropic relations in conjunction with the isentropic Mach-Area relation, Eq. (85).

$$\frac{A_s}{A_{0s}} = \frac{M_{0s}}{M_s} \left[\frac{1 + \frac{\gamma - 1}{2} M_s^2}{1 + \frac{\gamma - 1}{2} M_{0s}^2} \right]^{\frac{\gamma+1}{2(\gamma-1)}} \tag{85}$$

Subscript '$0s$' denotes the inlet of the side bounding sub-control volume and subscript 's' denotes the exit of the side bounding sub-control volume.
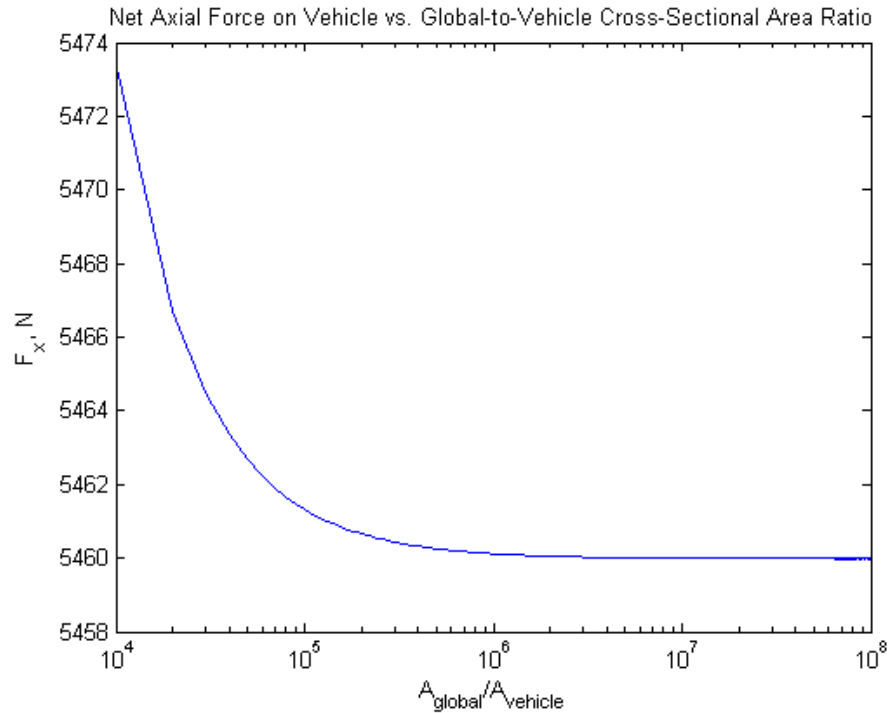
Figure 4.3. Net axial force calculated using different global control volume cross-sectional areas.

The exiting flow rates from the engine sub-control volume at station 'e' are determined based on the engine model used, i.e., cycle analysis as discussed in Section 3. Once the overall wake inlet flow rates are computed, the conservation relations for a constant area control volume extending from 'e' to 'w' (an adiabatic constant-area mixing analog) can be used to solve for the equilibrated (albeit infinitesimally displaced from free-stream) wake exit conditions at station 'w'. Specifically, continuity, momentum (stream thrust equivalence), and energy equation (total enthalpy flow rate equivalence) along with the gas equation of state are used to provide a closed system which allows calculation of wake exit (station 'w') velocity, pressure, temperature, density, etc. These flow-rate

relationships used in the wake analysis are as follows:

Continuity
$$\rho_9 u_9 A_9 + \rho_s u_s A_s = \rho_w u_w A_w \qquad (86)$$

Momentum
$$(\rho_9 u_9^2 + P_9)A_9 + (\rho_s u_s^2 + P_s)A_s = (\rho_w u_w^2 + P_w)A_w \qquad (87)$$

Energy
$$\rho_9 u_9 A_9 \left(h(T_9) + \frac{u_9^2}{2} \right) + \rho_s u_s A_s \left(h(T_s) + \frac{u_s^2}{2} \right)$$
$$= \rho_w u_w A_w \left(h(T_w) + \frac{u_w^2}{2} \right) \qquad (88)$$

Equation of State
$$P_w = \rho_w R T_w \qquad (89)$$

Subscript '9' denotes the engine exit plane and a subscript 's' denotes the side-bounding control volume exit plane. Both planes comprise the overall 'e' plane seen in Figure 4.2. The entropy generation rate in the wake mixing region can then be calculated as follows:

$$\dot{S}_{wake} = \rho_s u_s A_s \left[c_p \ln \left(\frac{T_w}{T_s} \right) - R \ln \left(\frac{P_w}{P_s} \right) \right] + \rho_9 u_9 A_9 \left[c_p \ln \left(\frac{T_w}{T_9} \right) - R \ln \left(\frac{T_w}{T_9} \right) \right] \qquad (90)$$

This analysis of the wake can also be done using mixtures of reacting thermally perfect gases, where parameters like c_p and h are then functions of temperature and species mass fractions. Any reactions that may be present in the wake mixing zone will tend to completion at the wake exit due to equilibration to near ambient conditions (thermal, mechanical, and chemical equilibrium).

Note that the analysis presented here (which is dependent in detail on the level of modeling and detail desired) enables the quantification of lost thrust increments both in terms of loss mechanism or engine mechanism as well as spatial quantification of where individual losses occur. This can be seen by examining the overall engine exergy-force relation in the following form (and can be directly compared to the engine thrust as computed from engine exit fluids; Eq. (60)):

$$Thrust = \frac{1}{u_0} \left[f \dot{m}_{engine} \, h_{fuel} - T_0 \left(\dot{S}_{engine} + \dot{S}_{wake} \right) \right] \qquad (91)$$

In the specific case of a lumped component approach (used to generate results to be shown in the next section) where the flow conditions are known at all engine stations and entropy generation rates have been calculated in each part of the global control volume (as well as through the individual components of the engine themselves), all other engine performance parameters can also directly be calculated, specifically, spillage, thrust specific fuel consumption, exergy loss rate, etc.

5. APPLICATION OF SECOND-LAW ANALYSIS TO A STAND-ALONE TURBOJET IN FLIGHT

This section applies the methodologies developed in Section 3 and Section 4 for describing turbojet on and off-design performance and second-law (exergy) characteristics across all possible ranges of fuel throttle settings, flight Mach numbers, and altitudes. Specifically, a given turbojet configuration is defined and analyzed. The first section of this section includes the description for the on-design requirements for the turbojet and the physical characteristics and performance which result from the on-design analysis. This includes station-wise flow-field information at the on-design point and the subsequent development of the operating line (and associated information) on the compressor map for the given turbojet. Also shown for comparative purposes is flow-field information at a single (chosen) off-design condition. The next section provides selected and representative results for the on-design condition as well as four representative off-design conditions. These results focus on entropic analysis. The last section then describes performance and exergy results in terms of the more general three-space of fuel throttle setting, flight Mach number, and altitude.

5.1. MODEL PROBLEM DESCRIPTION

The gas turbine engine modeled in this study is a fixed-geometry, single-spool turbojet engine with no afterburner. It has fixed cross-sectional areas throughout the engine and a convergent nozzle (i.e., the nozzle does not expand in area downstream of the throat, hence choked flow is maintained at engine exit under almost all operating conditions). The engine layout and the station-wise numbering used are shown in Figure 5.1. The physical scale selected for this engine corresponds to that of a medium scaled operational engine, such as an engine integrated with a small jet trainer aircraft. The axial lengths of the sections and the details of cross-sectional profiles are not necessary for the methodology used in the current study. The current study, as discussed earlier, is based on lumped component analysis (station to station analysis) with compressor losses obtained from a generic compressor map and losses in other components assumed or modeled.
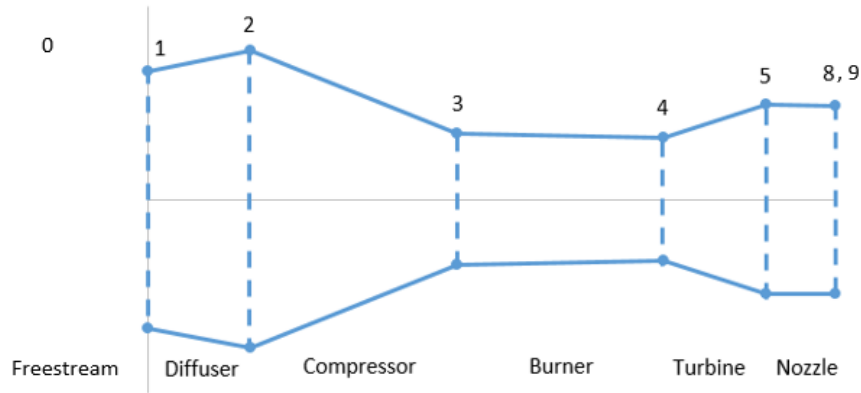
Figure 5.1. Turbojet schematic with station numbering.

A generic inlet/diffuser loss model is used in which the total pressure loss in the inlet is a function of the flight Mach number, i.e., $\pi_d = \pi_d(M_0)$, as shown in Figure 5.2. This model is obtained from [33] and covers subsonic and supersonic flight ranges. For simplicity, the engine is modeled with ideal burner and nozzle (i.e., $\pi_b = \pi_n = 1.0$). Although these quantities are less than unity in operational engines due to losses, they tend to be close to unity for well-designed burners and nozzles across the operating range of an engine.
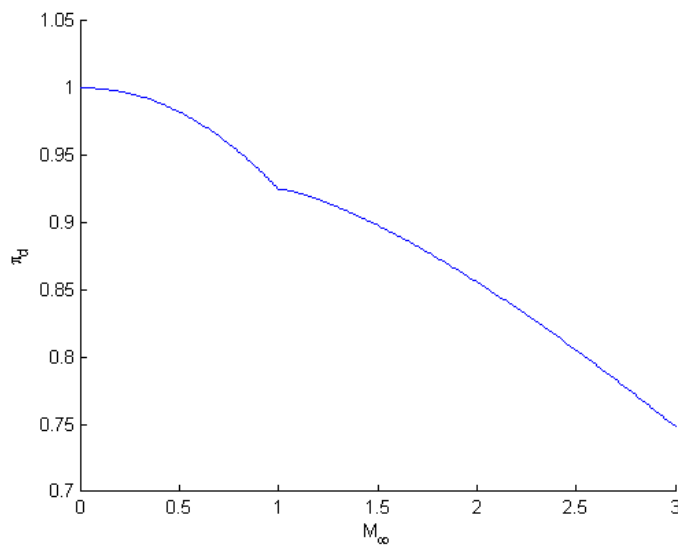
Figure 5.2. Total pressure loss model for inlet/diffuser.

The engine is modeled in terms of operability range and resulting performance with applied limitations on various critical parameters; in an operational engine, the engine control system (ECS) performs this function. A primary ECS limit is the (total) temperature at turbine entrance; for the current study temperatures greater than 1600 K are prohibited. Other parameters are indirectly limited through the physical compressor operation range described by the performance map of the compressor. The limitations on maximum temperature and the range provided on the generic compressor map utilized in this study restricts (provides boundaries) for possible flight Mach numbers, fuel throttle settings, and altitudes at which the given engine can operate.

5.1.1. Definition of On-Design Point for the Engine. The single-point on-design operational condition for the engine was selected to correspond to flight at a standard altitude of 9000 meters, flight Mach number of 0.85 (correlating to a true airspeed of 258.4 m/s or 502 knots), and a fuel mass flow rate of 0.279 kg/s (this on-design value is henceforth designated as 100% throttle setting for presentation of results). The altitude of 9000 m is characterized by an ambient temperature and pressure of 230 K and 30.8 kPa (about 0.3 atm), respectively. A summary of on-design flow conditions at every station in the engine as well as the engine performance is provided in Table 5.1.

The cross-sectional areas at all engine stations (given in Table 5.1) are determined from the application of various requirements at this single on-design flight condition. Specifically, the area at station 1 (inlet/engine face) is found by requiring full mass capture, the cross-sectional area at station 2 is calculated by requiring the compressor face (station 2) Mach number to be 0.5 (a reasonable design target for this parameter), and the areas at station 4 (turbine entrance) and station 8 (nozzle throat and exit of the given engine) are determined from the requirement of choked flow at these stations. Furthermore, the cross-sectional areas at station 3 (compressor exit) and at station 5 (turbine exit) are found by assuming a constant (axial) velocity through the compressor and a 20% velocity reduction through the turbine. These latter two conditions are again representative of design targets for typical compressor and turbine operation at on-design flight conditions. Once these areas have been found for this specified on-design flight condition, they are fixed and remain invariant for all engine operating conditions (off-design).

Table 5.1. Summary of flow condition and performance at on-design conditions (9000 m altitude, 100% throttle, and M = 0.85).

Parameter	Units	Station					
		0	2	3	4	5	8
A	m^2	0.1201	0.1666	0.0327	0.0287	0.0674	0.0666
D	m	0.3910	0.4605	0.2041	0.1911	0.2930	0.2911
T	K	230.0	250.7	538.9	1166.7	962.44	926.5
T_t	K	263.2	263.2	551.5	1400.0	1111.8	1111.8
P	kPa	30.80	39.41	431.34	246.97	108.29	94.78
P_t	kPa	49.40	46.75	467.49	467.49	179.41	179.41
u	m/s	258.4	158.7	158.7	684.7	547.7	610.1
M	$-$	0.85	0.50	0.34	1.00	0.88	1.00
ρ	kg/m^3	0.467	0.548	2.789	0.736	0.392	0.356

Altitude	9000 m	$\dot{m}_{fuel}$	0.279 kg/s
$F_{uninstalled}$	9.36 kN	$\dot{m}_{engine}$	14.478 kg/s
Spillage	0 kg/s	Thrust specific fuel consumption, $TSFC$	0.0298 kg/kN-s
Fuel-to-air ratio, f	0.0193	RPM	15,000
π_d	0.946	T_{t4}/T_{t2}	5.318
π_c	10.0	η_c	0.85
π_t	0.384	η_t	0.86

For comparison, a similar table of data, Table 5.2, is given for a selected off-design case in which altitude, flight Mach number, and fuel throttle setting differ from those for the on-design condition. Specifically, this comparative case is for flight operation at a standard altitude of 4500 meters, flight Mach number of 0.65 (correlating to a true airspeed of 209.7 m/s or 408 knots), and a fuel throttle setting at 125% of on-design (equal to 0.349 kg/s). At this reduced altitude, the ambient temperature and pressure are 258.9 K and 57.82 kPa (about 0.58 atm), respectively.

Table 5.2. Summary of flow conditions and performance at the selected off-design condition (4500 m altitude, 125% throttle, and M = 0.65).

Parameter	Units	Station					
		0	2	3	4	5	8
A	m^2	0.1240	0.1666	0.0327	0.0287	0.0674	0.0666
D	m	0.3974	0.4605	0.2041	0.1911	0.2930	0.2911
T	K	258.9	270.4	540.0	1091.2	900.2	866.6
T_t	K	280.8	280.8	550.4	1309.5	1039.9	1039.9
P	kPa	57.82	65.24	591.00	333.75	146.34	128.08
P_t	kPa	76.81	74.45	631.77	631.77	242.45	242.45
u	m/s	209.7	144.5	144.5	662.2	529.7	590.1
M	$-$	0.65	0.44	0.31	1.00	0.88	1.00
ρ	kg/m^3	0.778	0.841	3.813	1.066	0.566	0.515

Altitude	4500 m	$\dot{m}_{fuel}$	0.349 kg/s
$F_{uninstalled}$	12.37 kN	$\dot{m}_{engine}$	20.23 kg/s
Spillage	-0.641 kg/s	Thrust specific fuel consumption, $TSFC$	0.0282 kg/kN-s
Fuel-to-air ratio, f	0.0173	RPM	14,456
π_d	0.969	T_{t4}/T_{t2}	4.663
π_c	8.486	η_c	0.877
π_t	0.384	η_t	0.86

5.1.2. The Operating Line of the Engine. As described in detail previously in Section 3 of this document, in order to provide component performance for all engine operating conditions, steady-state (integrated engine) operating lines are developed for individual components (overlaid on performance maps). With the approximations used in the current study, the compressor operating line is the dominant feature in component performance description. Shown below in Figures 5.3, 5.4, and 5.5, are the relevant parameters of compressor pressure ratio, scaled RPM, and efficiency versus corrected mass flow rate at station 2 for the operating line on the compressor map for the engine modeled

in this study. These distributions allow the calculation of engine (and component) performance across the operational range of the turbojet as discussed previously.
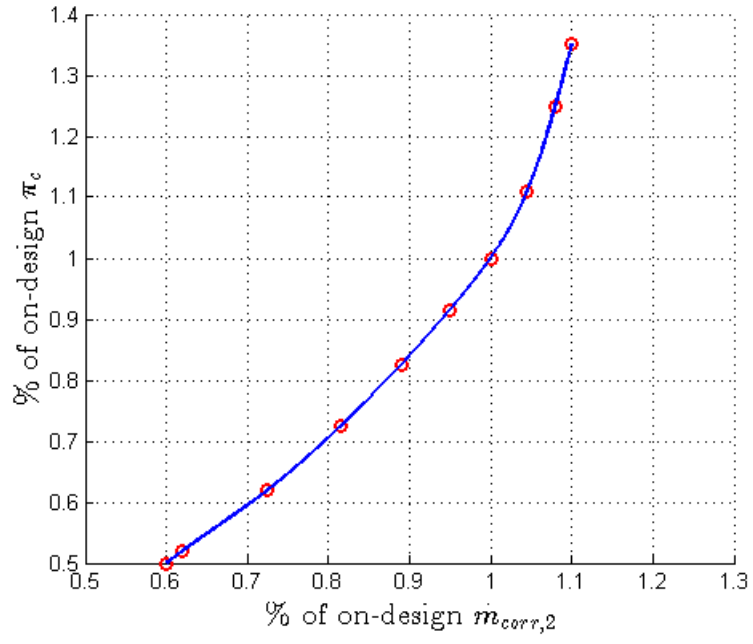
Figure 5.3. Compressor pressure ratio operating line.
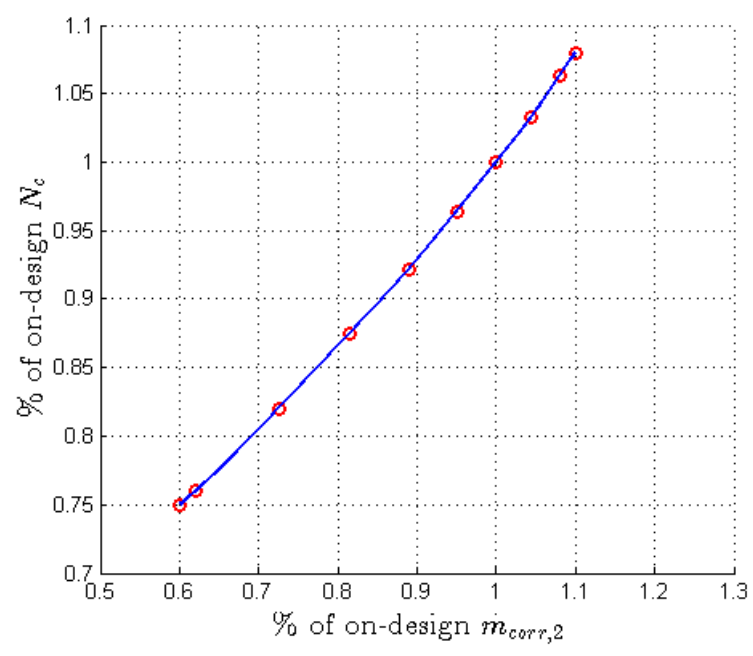
Figure 5.4. Compressor speed (RPM) operating line.
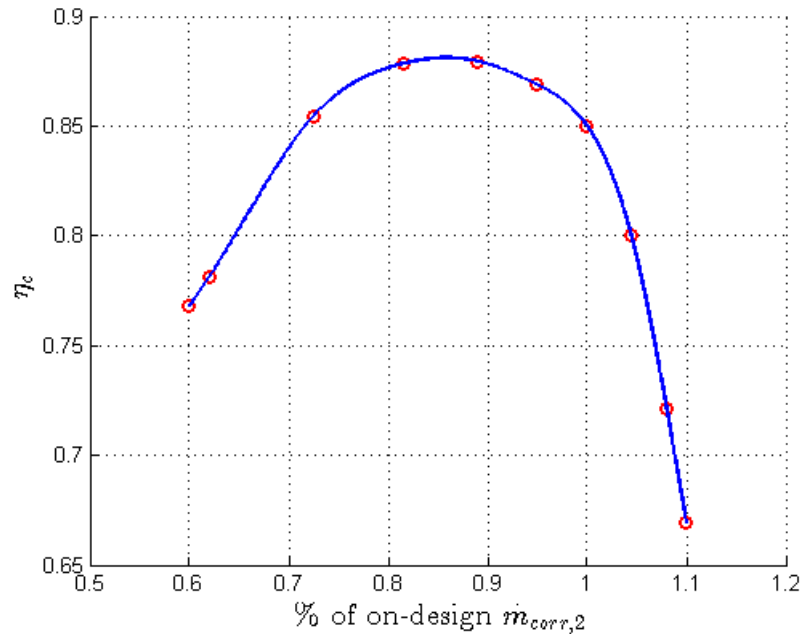
Figure 5.5. Compressor efficiency operating line.

5.2. PERFORMANCE ANALYSIS RESULTS FOR REPRESENTATIVE DISCRETE OPERATING CONDITIONS

The central objective of this work is to develop and apply the methodology for studying the performance of a generic single-spool turbojet engine from an entropic (2nd law) perspective as it operates in the three dimensional engine operational 'space' of allowable flight Mach numbers, altitudes, and throttle settings. This is done by developing and incorporating the operating line on the compressor map in order to track the correlation between entropy change/generation in the components and the wake, along with resultant changes in the engine performance. Component matching is performed for the engine and an operating line on the compressor performance map is developed such that as the off-design point is varied (i.e. as the altitude, flight Mach number, and throttle setting are changed), the component efficiencies and parameters are determined for the selected operating condition. Also, a generic model for the losses in the inlet/diffuser is incorporated in order to add more realistic variability in the overall model. The entropy change/generation through all components, the overall engine, and in the engine wake can then be evaluated using the analysis discussed in Section 4.

5.2.1. On-Design Results. Results are first obtained by applying the methodology described in previous sections to the base-line on-design flight condition for the modeled turbojet. As noted earlier, the engine on-design operation corresponds to an operating altitude of 9000 meters, flight Mach number of 0.85, and fuel throttle setting at 100% (corresponding to a fuel mass flow rate of 0.279 kg/s). Engine thrust obtained using the entropy method is compared to the thrust obtained using the conventional momentum definition. The engine thrust values obtained using the two different (i.e., momentum based and entropy based approaches) are numerically identical (with less than a $3.0\text{x}10^{-4}$% difference between the two values). This top-level check is a verification of the exergy methodology as developed as well as a validation that the method is correctly applied to the turbojet engine configuration.

Figure 5.6 shows the exergy-based decomposition of available (provided) energy rate for the on-design condition (i.e., the total heat input associated with the fuel is represented by the entire circle). This total energy rate input is resolved into two main contributions corresponding to 1) exergy loss (proportional to entropy generated) within the various engine components and within the wake, and 2) the thrust power for the on-design condition. It is seen that the wake mixing (equilibration) process is dominant in terms of entropy generation (losses), representing approximately 64% of the total exergy destroyed. The various engine component exergy losses are also shown in this figure and indicate that, after the wake, the burner represents the next largest loss, and contributes around 31% of total exergy lost. Note that the burner in this study is considered 'ideal'; meaning it has no modeled total pressure drop, hence the availability loss is entirely due to ideal heat addition occurring in this component (i.e., heat interaction at low Mach number and without irreversibility). The inlet and the turbomachinery share the remaining 5% of the total exergy destroyed (i.e., entropy generated). The compressor loss is seen to be larger than the turbine loss.

5.2.2. Representative Off-Design Cases. In order to illustrate the impact of specific changes in the three operational parameters defining the engine operational envelope (namely flight altitude, flight Mach number, and fuel throttle setting), specific results for four different off-design cases are now shown. These four off-design cases are defined by varying one operational parameter (such as altitude) while holding the other

two fixed (i.e., fixing fuel throttle and flight Mach). Table 5.3 describes the (nominal) on-design operational values along with the operational values for the four off-design cases studied.
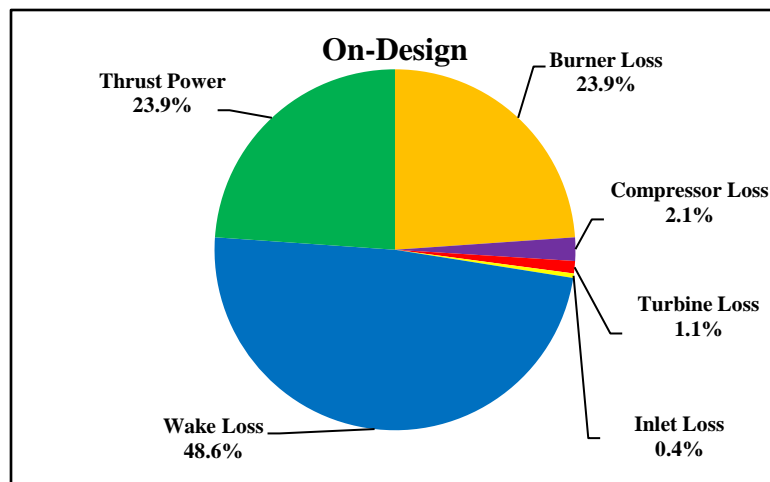
Figure 5.6. On-design power allocation.

Table 5.3. Operating conditions of the on-design case and the four off-design cases studied.

Conditions		Altitude	Flight Mach No.	Fuel Throttle
On-Design		9000 m	0.85	100%
Off-Design Case 1	Altitude Change	4500 m	0.85	100%
Off-Design Case 2	Flight Mach No. Reduction	9000 m	0.60	100%
Off-Design Case 3	Fuel Throttle Change	9000 m	0.85	50%
Off-Design Case 4	Flight Mach No. Increase	9000 m	1.25	100%

5.2.2.1 Off-design case 1. The first off-design case corresponds to a lower operational flight altitude of 4500 m (as compared to 9000m for the on-design case) while holding the on-design values of fuel throttle and flight Mach number fixed. Figure 5.7 provides a breakdown of the overall energy (heat) input rate (representing the entire circle) for this case in terms of the thrust power delivered, wake exergy losses, and the various engine component exergy losses. The most notable changes from on-design loss magnitudes occur in the wake and in the burner. At this lower altitude, the wake exergy loss is reduced from the on-design such that it represents slightly more than one half of the

total exergy losses while the burner loss increases to around 40% of the total losses. The remaining three components (inlet/compressor/turbine) do not change significantly in terms of their collective contribution to losses. However, within the inlet and turbomachinery share of losses, the turbine loss is increased noticeably. For this case, one fourth of the overall power (heat rate) input (or initial exergy available) is converted to useful thrust power.
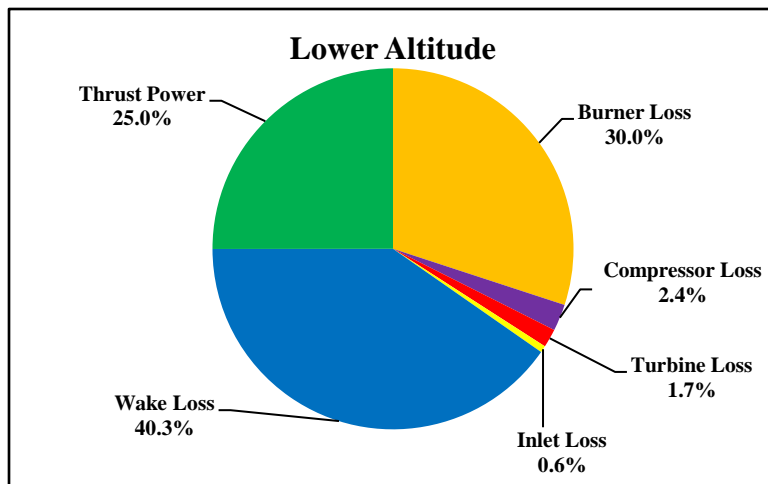
Figure 5.7. Off-design Case 1 power allocation.

5.2.2.2 Off-design case 2. The second off-design case shown is for a lower flight Mach number of 0.6 (as compared to 0.85 for the on-design case). The on-design values of fuel throttle and altitude are held constant. Figure 5.8 provides results for this case; from this figure, it can be seen that the percentages for the inlet and turbine remain roughly the same as for the on-design case. However, the wake and compressor contributions show a slight increase in losses while the burner losses drop (marginally). Also, the thrust power portion is reduced from that of the on-design case; for this reduced flight Mach number it is less than a fifth of the total power input.

5.2.2.3 Off-design case 3. The third off-design case corresponds to a reduction in fuel throttle setting to 50% of the on-design value while maintaining the on-design altitude and flight Mach number (9000 m and 0.85, respectively). The decomposition of the overall power (heat rate) input for this case is shown in Figure 5.9. It is notable that this figure shows very little difference in terms of exergy loss contributions, etc., from that observed for Case 1 (lower altitude); the breakdown of contributions is almost identical. Based on

the trends observed here, it is indicated that varying the altitude and the throttle setting have about the same effect in terms of the variance of availability loss contributions for the different loss components. In line with this observation, for Case 3, the thrust power achieved again represents one fourth of the heat rate input or power input.

Lower Mach Number

Thrust Power 18.8%
Burner Loss 22.7%
Compressor Loss 2.8%
Turbine Loss 1.0%
Inlet Loss 0.2%
Wake Loss 54.5%
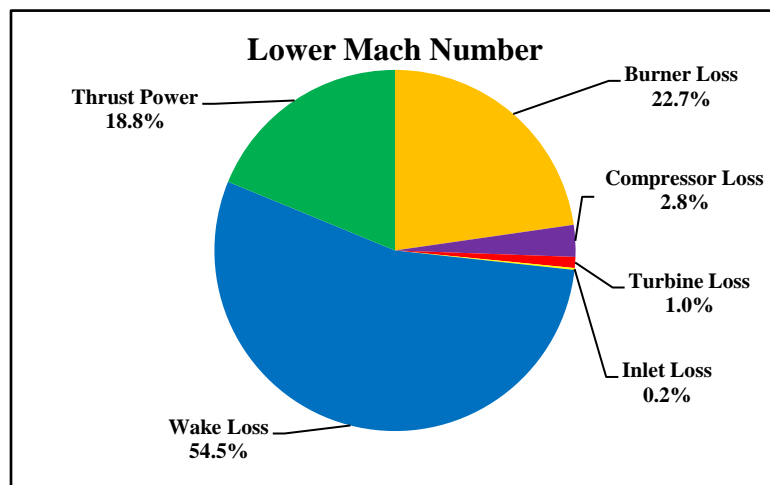
Figure 5.8. Off-design Case 2 power allocation.

Lower Throttle

Thrust Power 25.0%
Burner Loss 30.1%
Compressor Loss 2.4%
Turbine Loss 1.7%
Inlet Loss 0.6%
Wake Loss 40.3%
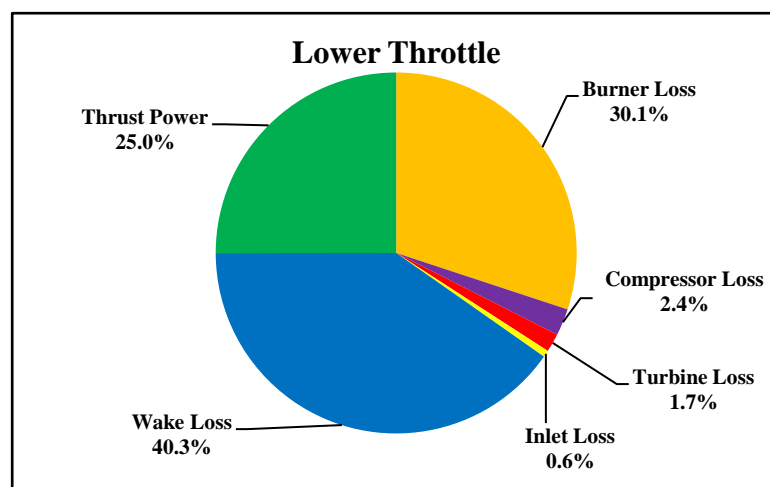
Figure 5.9. Off-design Case 3 power allocation.

5.2.2.4 Off-design case 4. The fourth off-design case is for engine operation at a (higher) Mach number of 1.25 and with altitude and fuel throttle setting held at on-design values. Results are shown in Figure 5.10. The wake loss percentage of the total loss is reduced to about 58%. The burner losses contribution is increased to about 36% of overall losses. The rest of the components combined continue to have approximately a 5% share

of the overall losses; however the loss contribution of the inlet is measurably higher. This is, of course, expected for supersonic flow; especially with the inlet model used in this study. For this supersonic flight Mach number case, there is an increase in the portion of thrust power realized from the energy rate input. Thrust power represents almost a third of the input power, and with the results from the lower Mach number case in mind, is demonstrative of the fact that a turbojet operates more efficiently at higher Mach numbers (in terms of percentage of supplied power realized as useful power).
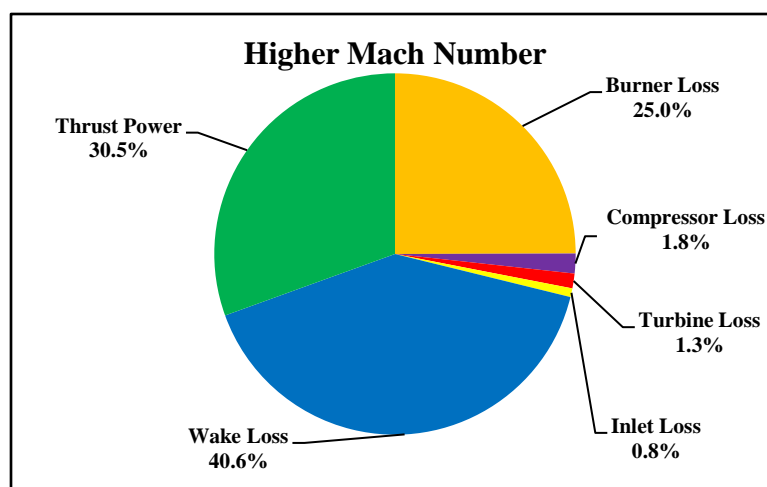
Figure 5.10. Off-design Case 4 power allocation.

5.2.3. Overview. Figure 5.11 illustrates these same results in terms of bar charts utilizing actual values of losses, etc., for this engine (as opposed to presenting the data in terms of percentages as used in Figures 5.6 through 5.10). In this figure, the far left hand bar (in orange) represents the overall energy rate (heat rate or power) input in units of MW for the on-design case as well as for off-design cases 1, 2, and 4 (all at the nominal fuel flow rate, hence have the same value). The on-design case, Case 1, Case 2, and Case 4 are then shown in terms of the decomposition of this energy rate input into contributions associated with the various losses and the productive thrust power realized. A similar distribution is shown on the right side of Figure 5.11 for off-design Case 3 with its lower heat power input bar (in orange). The first-law efficiency (the overall efficiency) of the engine can easily be calculated as well for each operating case here. This efficiency is defined as the ratio of the thrust power delivered to the total heat input rate. Table 5.4 again

provides results for these cases (on-design along with the four off-design cases); emphasis in this table is on actual entropy generation increments.
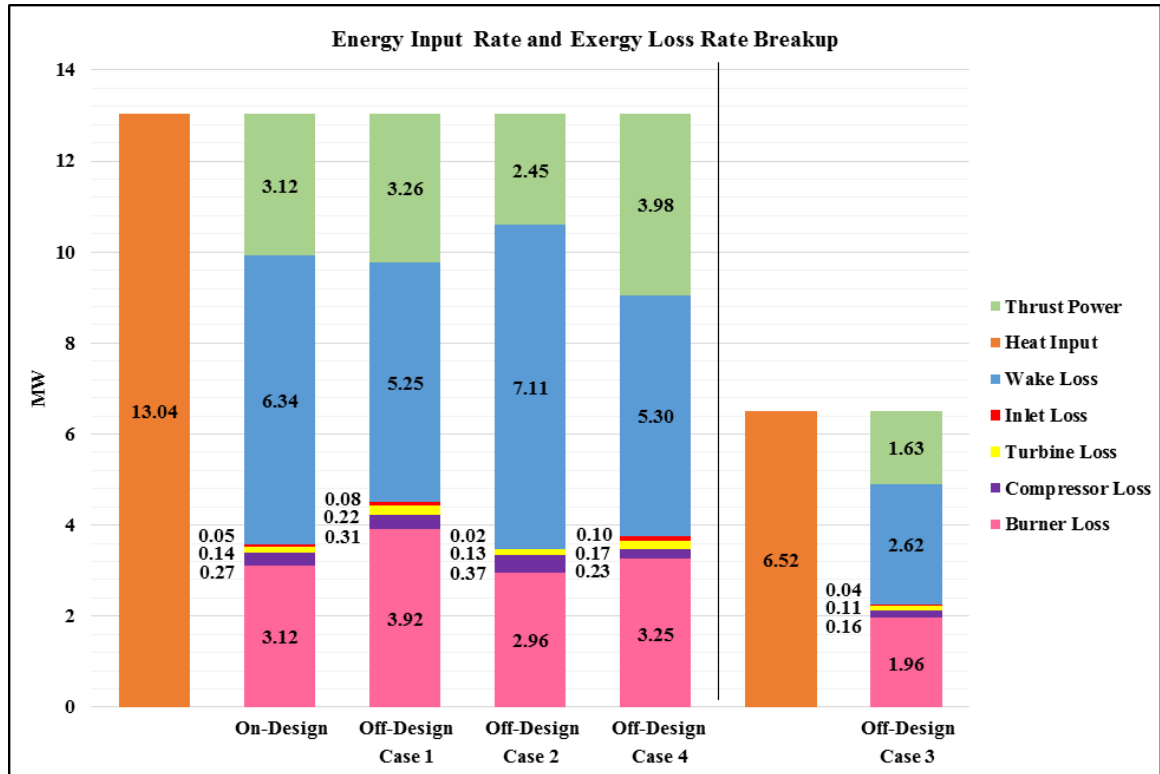
Figure 5.11. Comparative total power allocation for the on-design case and the four off-design cases studied.

Table 5.4. Comparative parameter values for the on-design case and the four off-design cases.

		On-Design Alt = 9000m, M = 0.85, mf = 100%	Case 1 Alt = 4500m, M = 0.85, mf = 100%	Case 2 Alt = 9000m, M = 0.60, mf = 100%	Case 3 Alt = 9000m, M = 0.85, mf = 50%	Case 4 Alt = 9000m, M = 1.25, mf = 100%
Thrust	(kN)	9.36	9.34	9.59	4.96	8.64
Total Exergy Loss Rate	(MW)	9.924	9.778	10.591	4.889	9.060
$\dot{S}_{wake}/\dot{S}_{engine}$		1.77	1.16	2.04	1.16	1.41
$T_0\dot{S}_{total}/\dot{Q}$		0.80	0.79	0.86	0.79	0.73
$\eta_{1st\ law}$		0.20	0.21	0.14	0.21	0.27

Table 5.4. (cont.) Comparative parameter values for the on-design case and the four off-design cases.

		On-Design Alt = 9000m, M = 0.85, mf = 100%	Case 1 Alt = 4500m, M = 0.85, mf = 100%	Case 2 Alt = 9000m, M = 0.60, mf = 100%	Case 3 Alt = 9000m, M = 0.85, mf = 50%	Case 4 Alt = 9000m, M = 1.25 mf = 100%
TSFC	(kg/kN-s)	0.0298	0.0299	0.0291	0.0282	0.0323
RPM		15,000	13,320	15,051	12,530	14,084
$\dot{S}_{inlet/diffuserr}$	(W/K)	229.3	305.0	97.5	172.3	444.3
$\dot{S}_{compressor}$	(W/K)	1,188.4	1,203.4	1,612.6	682.1	1,007.5
$\dot{S}_{burner}$	(W/K)	13,566.5	15,125.5	12,901.2	8,533.2	14,165.4
$\dot{S}_{turbine}$	(W/K)	627.9	835.2	557.7	471.7	749.3
$\dot{S}_{wake}$	(W/K)	27,584.9	20,294.3	30,930.9	11,424.4	23,069.5

5.3. OPERATING ENVELOPE AND OVERALL TRENDS

Although the previous results (summarized numerically in Table 5.4) give significant insight in terms of understanding basic performance and corresponding loss trends for this engine at on-design and at four different (discrete) off-design operational conditions, it is, of course, not comprehensive. The actual engine operational performance envelopes (i.e. thrust, RPM, mass capture, losses, and details of loss breakdowns) are complex four-dimensional constructs within the three-space operational envelope domain of fuel throttle setting, flight Mach number, and altitude. This envelope can be graphically represented to some degree by showing slices of the contours of the various performance results (including the loss results) in this operational envelope. Specifically, it can be represented by generating color-coded contour maps of each performance and loss parameter as a function of two of the three-space operational parameters while holding the third operational parameter constant (i.e., for example viewing the contours of a given performance or loss for a fixed fuel throttle setting but across the flight Mach number and altitude space). This, however, necessarily results in a very large number of contour plots in order to adequately describe the entire operational envelope; therefore, in this paper,

only a few representative plots are shown in this section for illustrative purposes. More results are included in Appendix A.

Figures 5.12 to 5.14 depict contours of engine thrust for various fuel throttle settings and flight Mach numbers for three different altitudes of 0, 4500, and 9000 meters, respectively. All three plots use the same scales for a straightforward comparison. It should be noted that the colored region corresponding to calculated performance on each of these plots has a defined shape (i.e., an envelope with distinct boundaries). Specifically, this means that the engine can only operate (in steady state) for some - but not all - combinations of fuel throttle settings and flight Mach numbers at that given altitude. These combinations and hence the defined shape of the plot are dictated by the engine limitations discussed earlier (for this study, it is determined by maximum allowable turbine inlet temperature and compressor operating range as provided on the compressor map). It is also noted that this performance envelope shape (defining the allowable independent variable set) shifts as the third independent variable is changed, thus defining the 3-D surface of altitude, Mach number, and throttle sets where the engine can operate. From the results given, and as expected, the engine produces, in general, more thrust at lower altitudes. Also, the operational range or envelope is broader at lower altitudes. For a given flight Mach number, the permissible range of throttle settings is shifted down as the altitude is increased, indicating lower fuel consumption, generally, at higher altitudes.
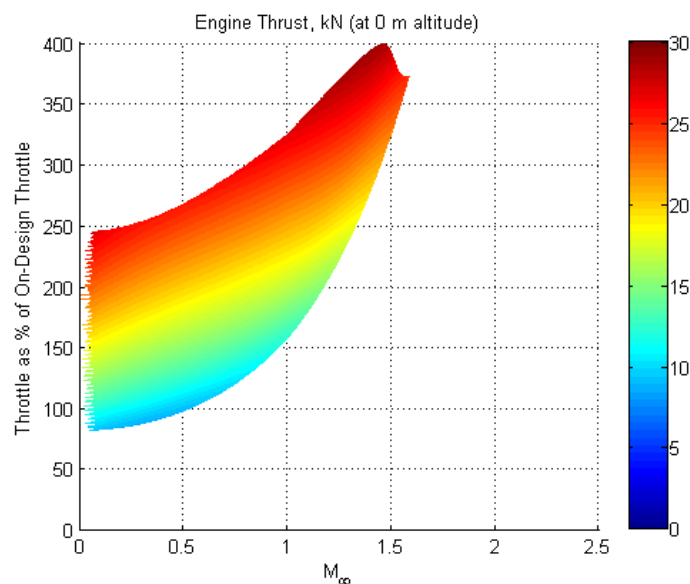
Figure 5.12. Thrust distribution at 0m altitude (standard sea level).
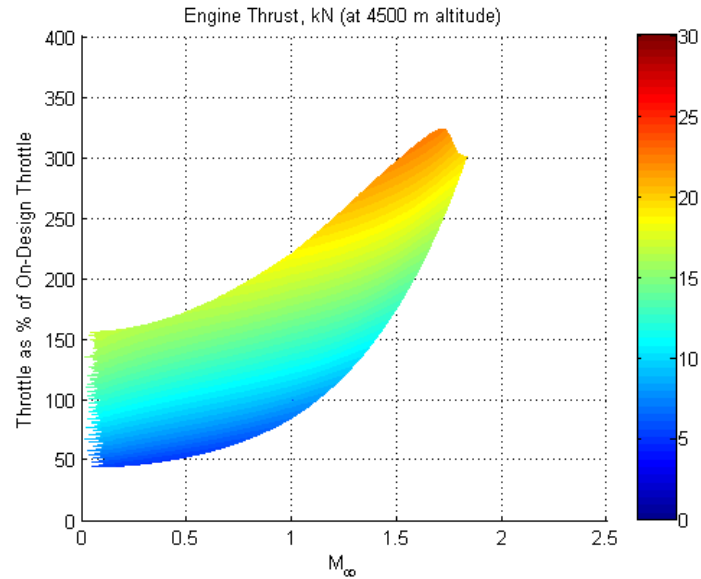
Figure 5.13. Thrust distribution at 4500m altitude.
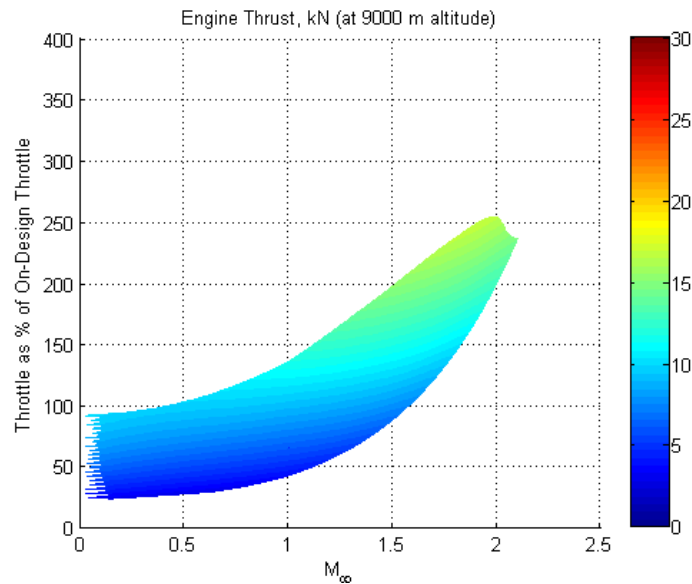
Figure 5.14. Thrust distribution at 9000m altitude.

Figures 5.15 to 5.17 depict contours of engine thrust for various altitudes and flight Mach numbers for three fuel throttle settings corresponding to 50%, 100%, and 200% on-design fuel throttle setting. Again, there is a defined envelope and shape for the allowable operational range; the envelope shifts in extent and coverage as the third parameter (throttle setting for these particular plots) is varied.
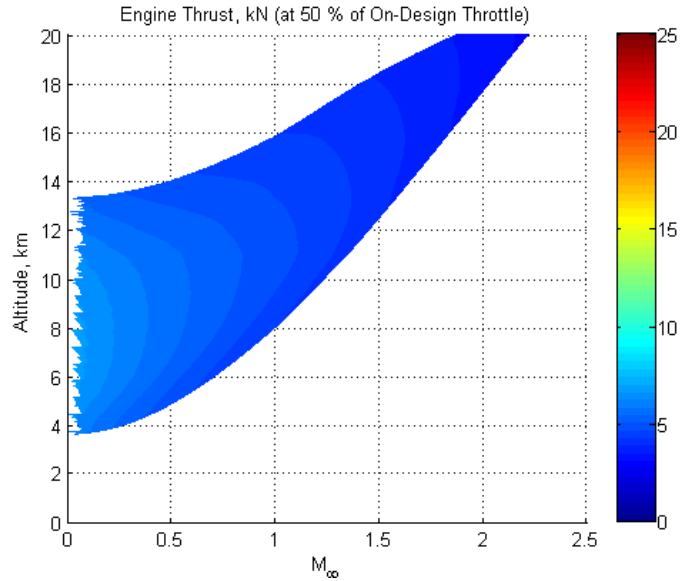
Figure 5.15. Thrust distribution at 50% throttle setting.
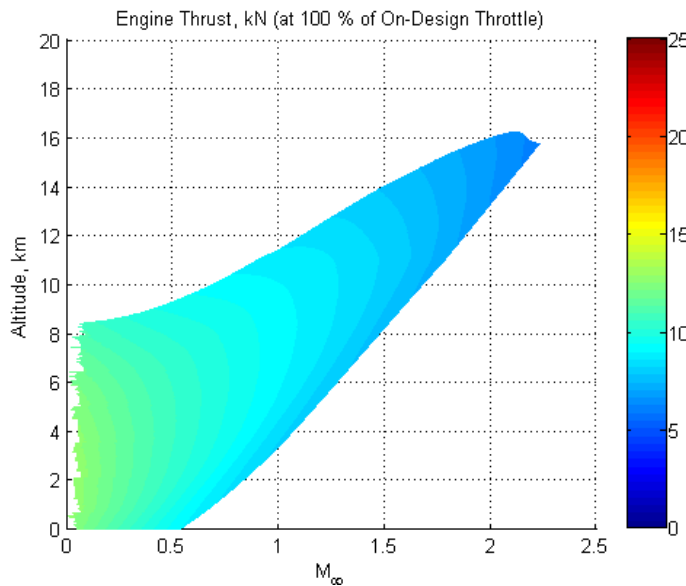
Figure 5.16. Thrust distribution at 100% throttle setting.

Table 5.5 provides a compendium of the general trends that result from a comprehensive examination of the performance/losses across the (allowable) operational envelope of fuel throttle settings, flight Mach numbers, and altitudes. In this table, the trends are shown in terms of colored arrows, i.e. an upward green arrow indicates that the parameter tends to increase; conversely a downward red arrow indicates that the parameter tends to decrease.
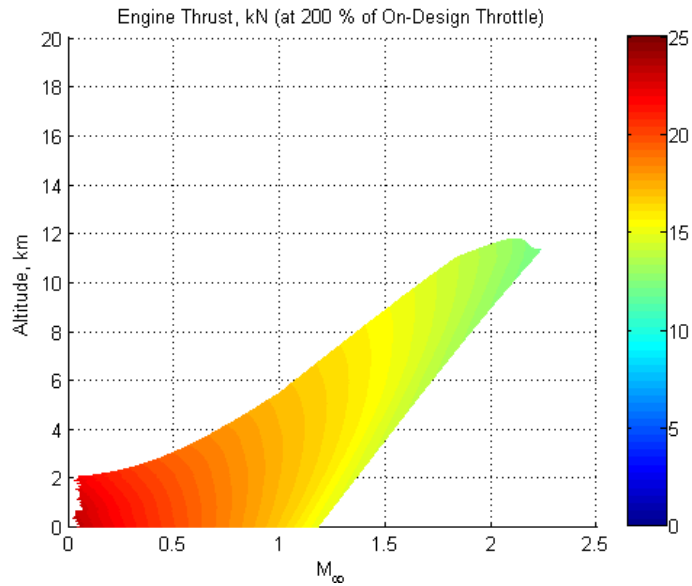
Figure 5.17. Thrust distribution at 200% throttle setting.

Table 5.5. General trends for some engine performance parameters with respect to the three-space parameters.

	↑ throttle	↑ M$_\infty$	↑ altitude
Thrust	↑	↓	↑ then ↓
Total Exergy Loss Rate	↑	↓	weak dependence
$\dot{S}_{wake}/\dot{S}_{engine}$	↑(weaker as M$_\infty$ ↑)	↓	↑
$T_0\dot{S}_{total}/\dot{Q}$	weak dependence	↓	weak dependence
TSFC	trend varies with M$_\infty$	↑	trend varies with M$_\infty$
RPM	↑(weaker as M$_\infty$ ↑)	↓(weak)	↑
$\dot{S}_{inlet/diffuserr}$	weak dependence	↑	↓(stronger as altitude ↑)
$\dot{S}_{compressor}$	↓ then ↑ (over entire range)	↓ then ↑ (over entire range)	↓ then ↑ (over entire range)
$\dot{S}_{burner}$	↑(weak)	weak dependence	↓
$\dot{S}_{turbine}$	↑(weak)	↑	↓
$\dot{S}_{wake}$	↑	↓(weak)	↑

Figures 5.12 to 5.14 (and therefore the associated trends indicated in Table 5.5) show, unsurprisingly, the obvious increase in thrust with increasing fuel throttle setting (since energy input is increasing). Thrust also decreases as expected with increasing flight Mach number due to the lower velocity differential across the engine as well as (to some

degree) increased inlet losses. The thrust trend with increasing flight altitude is not as monotonic across the entire range of altitude (for a given throttle setting and Mach number). Specifically, the thrust first increases for increasing altitude and reaches a maximum, then decreases for further increases in altitude.

Table 5.5, therefore, represents a summary of the trends for all performance parameters and losses of interest in this investigation. As explained, it is developed by examining and analyzing results across the operational three-space of fuel throttle setting, flight Mach number, and altitude. Besides the engine thrust as discussed above, trends for other (classic) performance parameters such as thrust specific fuel consumption and engine RPM are also shown in Table 5.5. However, of particular interest in the current investigation are the exergy losses (or entropy generation) and associated trends and magnitudes.

Table 5.5 indicates that the total exergy loss rate monotonically increases with increasing throttle, which is expected since the amount of energy rate input is increasing. The opposite trend is found for increasing flight Mach number; the total exergy destruction rate decreases monotonically. There is little to no altitude dependence on total exergy loss rate. The trend and magnitudes of the ratio of wake entropy generation rate to engine entropy generation rate as shown in Table 5.5, and in Figures 5.18 to 5.23 are instructive as these values are directly indicative of the balance of exergy destruction between the
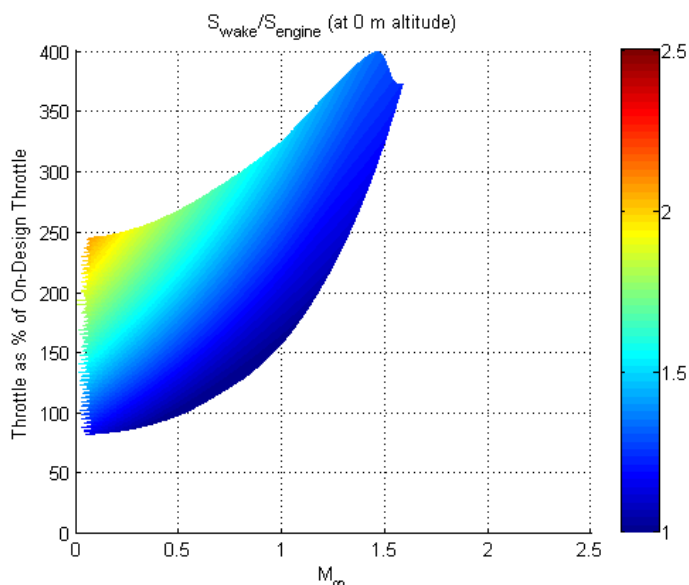
Figure 5.18. Ratio of wake losses to engine losses at 0m altitude.
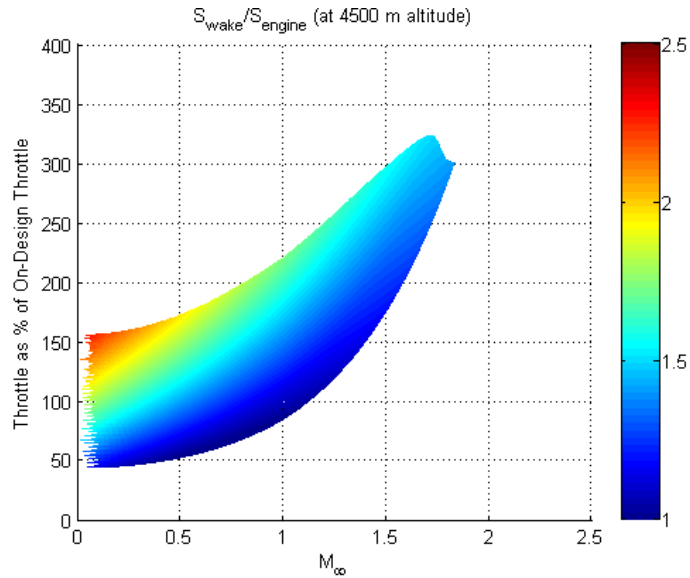
Figure 5.19. Ratio of wake losses to engine losses at 4500m altitude.
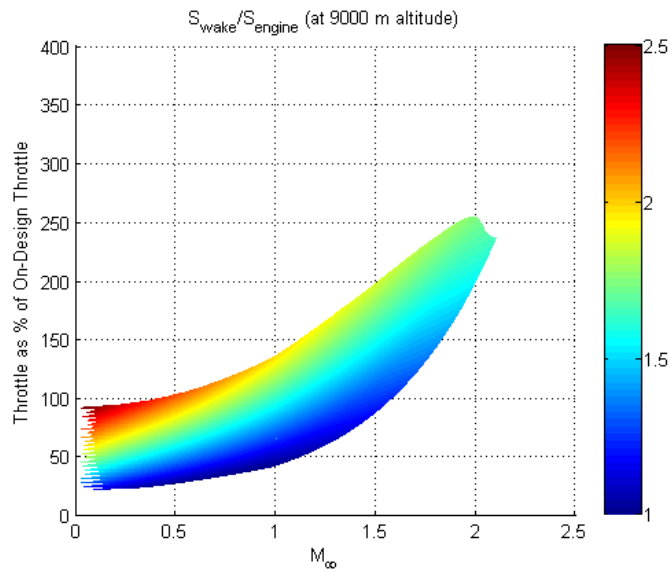
Figure 5.20. Ratio of wake losses to engine losses at 9000m altitude.

engine flow-field and the downstream wake. Specifically, this ratio monotonically grows with increasing throttle and altitude while it decreases with increasing flight Mach number. Across the entire engine operational space, this ratio has a minimum that is close to unity (i.e. the wake to engine loss is evenly distributed) and reaches a maximum of around 2.5, indicating that the wake is by far the dominant loss construct for the turbojet engine. The trends in this parameter can be readily understood by observing that the entropy generation

in the wake increases with larger fluid/thermodynamic gradients between engine exhaust flow and the ambient (hence resulting in more entropy generation as the wake region is equilibrated).
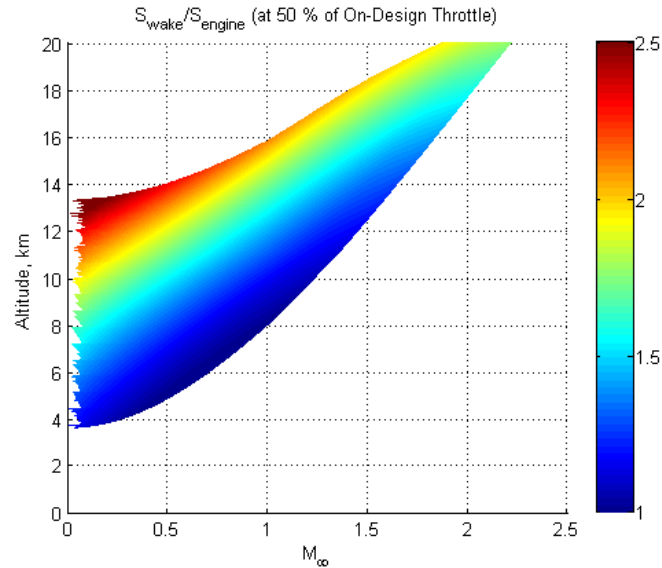
Figure 5.21. Ratio of wake losses to engine losses at 50% throttle setting.
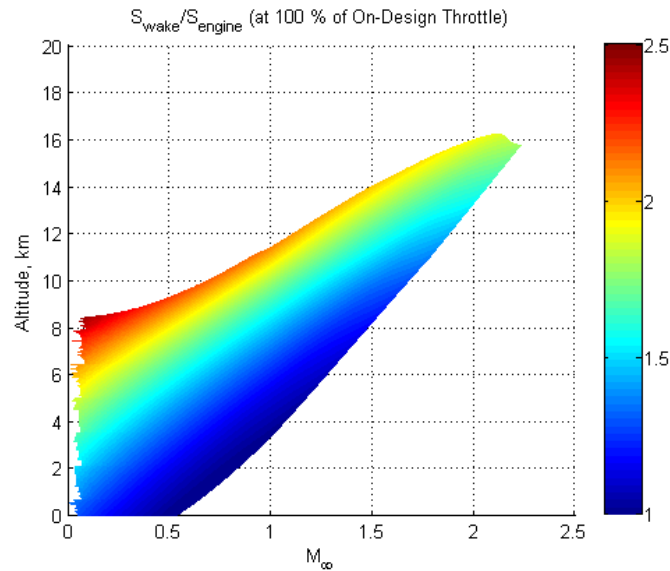
Figure 5.22. Ratio of wake losses to engine losses at 100% throttle setting.

Another important ratio of interest (from Table 5.5) is the total exergy loss rate to the total heat (energy) input rate, also presented below for different altitudes and fuel throttle settings in Figures 5.24 to 5.29. This ratio can be directly related to the engine first
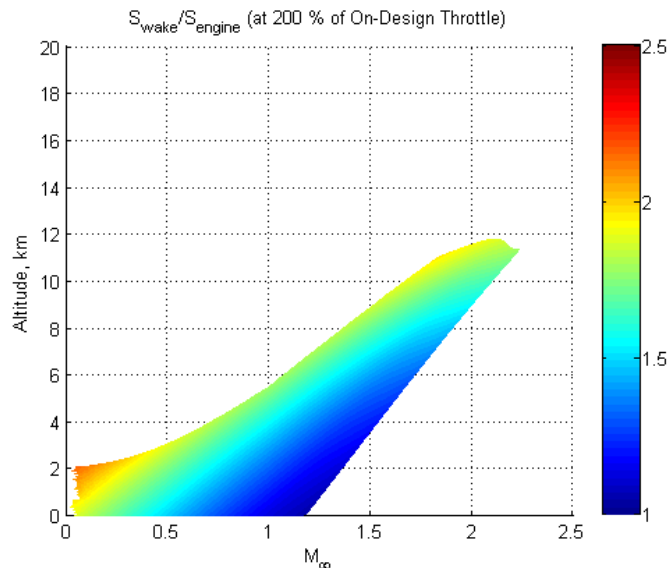
Figure 5.23. Ratio of wake losses to engine losses at 200% throttle setting.

law efficiency. This ratio (hence the engine efficiency) has a weak dependence on both the throttle setting and the flight altitude (it slightly increases as these operational parameters are increased). Conversely, its dependence on the flight Mach number is much more prominent. The ratio decreases monotonically, ranging from unity (all input exergy destroyed) at zero flight Mach number to a minimum of about 0.65 at a maximum flight Mach number of around 2.25. This is interesting as it shows that at zero velocity (stationary or static operation), all energy supplied by the engine is by definition lost to entropy
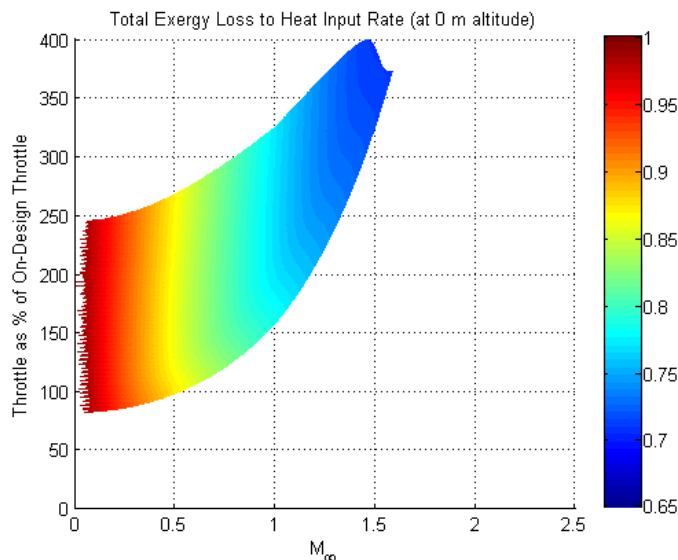
Figure 5.24. Total availability loss to energy input rate at 0m altitude.
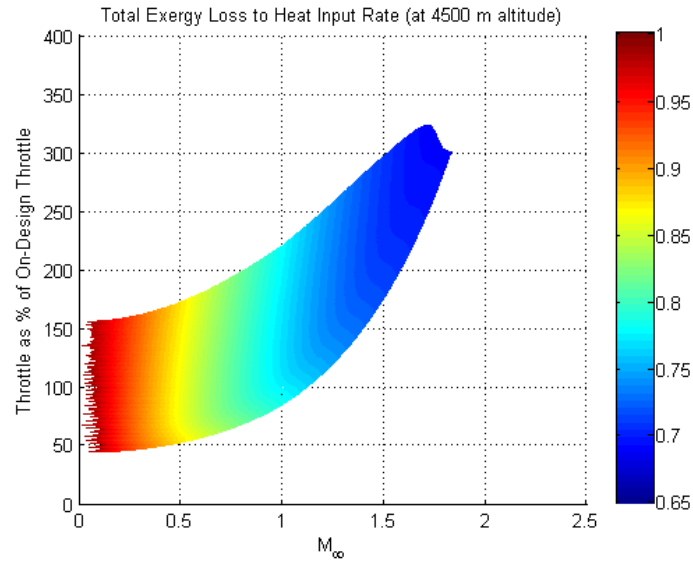
Figure 5.25. Total availability loss to energy input rate at 4500m altitude.
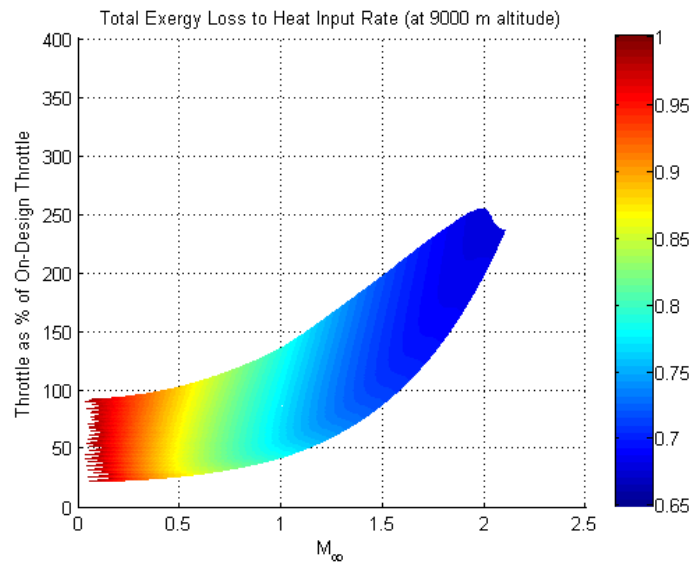
Figure 5.26. Total availability loss to energy input rate at 9000m altitude.

generation (the engine is not developing any force-based propulsive power). At best, at the high (supersonic) range of the allowable flight Mach number, the engine is converting only about 35% of the energy being supplied to it into useful propulsive work. For high subsonic speeds the turbojet converts only (approximately) 20% of the power supplied to it into useful (thrust-based) power.
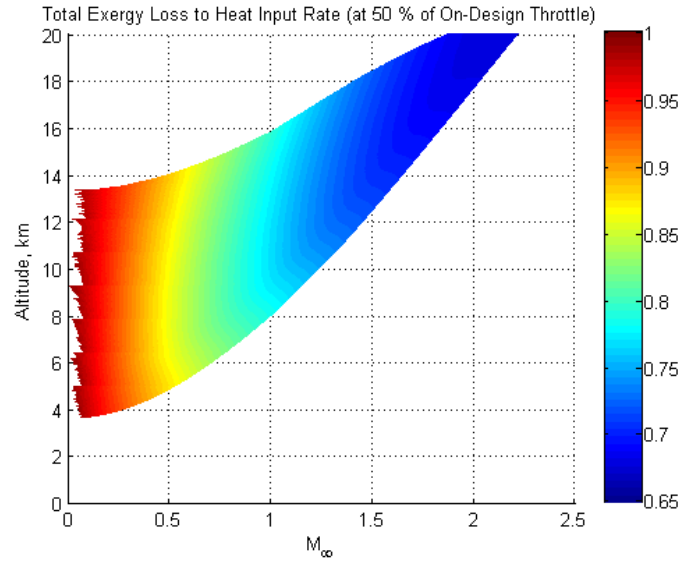
Figure 5.27. Total availability loss to energy input rate at 50% throttle setting.
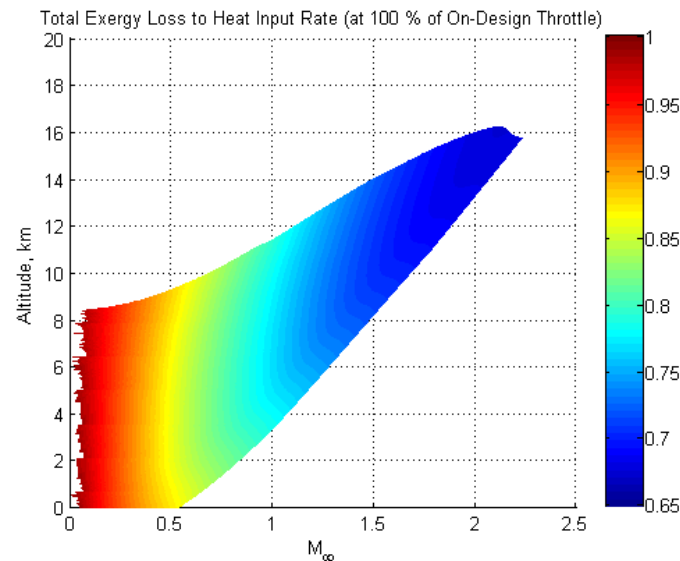
Figure 5.28. Total availability loss to energy input rate at 100% throttle setting.

Table 5.5 also provides the trends (increasing/decreasing) for the exergy losses in the various engine components. The inlet/diffuser exergy losses are larger for higher throttle settings and higher flight Mach numbers but are smaller at lower altitudes. The compressor loss trends are similar for all three operational parameters (fuel throttle, flight Mach, and altitude). As these operational parameters are increased, the compressor losses first decrease, reach a minimum approximately mid-range, and then begin to increase
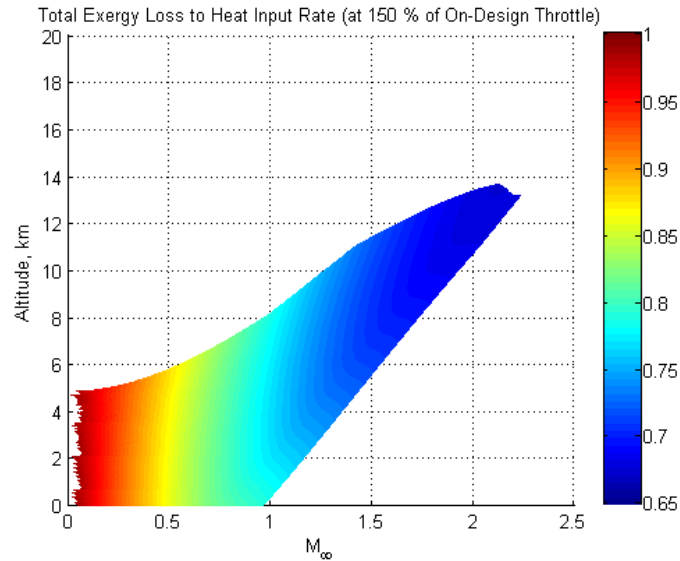
Figure 5.29. Total availability loss to energy input rate at 200% throttle setting.

again. This simply indicates that the compressor is most efficient near its on-design operational point (as can be seen from the compressor's operating line; see, for instance, Figure 5.5). The burner loss increases as fuel throttle is increased, which is obvious from a 2nd law stand point; entropy transfer/generation rate is proportional to the heat input rate. As the flight Mach number increases there is a slight increase (weak dependence) in burner loss for the majority of the range before it begins to decrease near the maximum allowable Mach number. Burner loss is reduced at higher altitudes. The turbine loss increases with increasing throttle and with increasing flight Mach number; turbine loss decreases with increasing altitude. Plots for these parameters are included in Appendix A.

6. SUMMARY, CONCLUSIONS, AND FUTURE WORK

6.1. SUMMARY

In this investigation, recently developed methodology for exergy-based (2nd law) analysis of aerospace vehicles is extended and applied to a simple stand-alone turbojet engine. This approach provides performance-based assessment of all losses both inside and external to the engine (including in the engine wake) in terms of entropy change/generation (or exergy destruction). For enhanced realism in terms of assessing the entire envelope of engine on and off-design behavior (performance and loss distributions and magnitudes), component matching (i.e. a compressor performance map) is incorporated into the analysis along with an empirically-based loss model for the inlet/diffuser. The validity of the method is confirmed by comparing thrust values obtained using this entropy-based approach with the values obtained using the classic momentum based definition. Engine performance and attendant losses (entropy generation or exergy destruction) in the engine and in the wake of the engine are quantified throughout the operational three-space envelope of possible altitudes, flight Mach numbers, and fuel throttle settings. This is accomplished by defining four off-design cases in which one operational parameter is varied from the on-design value while holding the other two operational parameters constant (i.e., examining performance and losses for the case with throttle reduced from on-design but with on-design altitude and flight Mach number, etc.). In addition, the entire operational space is then examined by means of providing trends in terms of performance and losses. This is presented as color-contour plots of the different studied parameters as functions of the three-space parameters of altitude, flight Mach number, and fuel throttle setting. These trends cannot be presented in one plot (for each parameter examined) because of the three dimensional nature of the domain, so 'slices' of the surface are shown (with one of the three-space parameters held constant). The observed trends from the large collection of results obtained in this investigation are summarized in a single table, namely Table 5.5.

6.2. CONCLUSIONS

While this study is primarily focused on the comprehensive second law aspects of the turbojet engine, trends and analysis of the first law efficiency of the engine (ratio of thrust power to heat energy rate, or power input) are also obtained. From an exergetic perspective, the results are seen to mirror classical analysis insomuch as they show that turbojet engines are most efficient at (low) supersonic Mach numbers, which is at the top end of their flight Mach number operation envelope. This simply indicates that for lower flight Mach numbers, more of the input heat rate (or power input associated with fuel) ultimately is associated with exergy destruction, as delivered thrust power decreases with decreasing flight Mach numbers.

For the limiting case of a stationary engine (or vehicle), the thrust power (or net force power) is by definition zero due to the zero flight velocity, meaning that all the power input (available for work) is lost; i.e., processed as destruction of exergy, either in the engine itself or in the wake behind the vehicle. It should be noted that a vehicle operating at 'cruise' (nonaccelerating) conditions, experiences an identical exergy rate balance situation as a stationary engine or vehicle, where all the exergy provided is lost/destroyed in the flow in and around the vehicle (including in the engine) and in the vehicle wake due to entropy generation. In such a case, the flight velocity is finite but the net force developed by the vehicle (engine thrust – vehicle drag) is zero, hence making the force-power zero.

It is instructive to consider the case of an accelerating or decelerating vehicle. For the case of an accelerating vehicle, a portion of the exergy associated with the fuel is lost as entropy generation; the balance is realized as productive (accelerative) force power. In the case where the losses exceed the exergy power provided, a net negative force power is delivered to the vehicle with a resulting deceleration of the vehicle. This indicates that for any case where the vehicle is decelerating, the exergy losses necessarily equal the entirety of the exergy associated with the fuel plus a portion of the kinetic energy associated with the flight of the vehicle itself. The exergy relationships therefore clarify why non-powered bodies immersed in a fluid flow experience drag; with no power input, the net axial force on such an object is necessarily counter to the flight direction (i.e., the object experiences drag); this drag production is directly related to the entropy production associated with friction and the wake equilibration process.

Note that a stand-alone engine analysis (as studied in the present work) generally does not result in a zero net force , i.e., thrust – and realized thrust power - is almost always positive, at least from a practical standpoint of realistic engine operation. This indicates, then, that a stand-alone engine exergy analysis will almost always exhibit a considerable fraction of the exergy associated with on-board fuel being realized as productive force (accelerative) power, unless stationary, as discussed before.

An important aspect often not considered in first-law (and even in some second-law) investigations of jet engines is the inherent and unavoidable loss within the wake equilibration process. The entropy generated in the wake (and hence the penalty in terms of heat rate input converted to realized thrust power) is found to be generally considerably greater than the entropy generated in the engine itself. The ratio of entropy generation in the wake to entropy generation/addition in the engine ranges in this study of a simple turbojet from around unity to close to two and a half, depending on the exact selection of fuel throttle setting, altitude, and flight Mach number. This indicates the importance of this (wake) region and the loss processes that occur within it, especially in terms of their direct impact on performance and efficiency. In essence, the fact that the plume at engine exit is not initially in equilibrium with the ambient (i.e., it is in a different thermodynamic state than the ambient) means that the fluid at exit plane has the potential to do useful work; it retains some amount of exergy. This is, of course, not utilized in any way in the wake, where the exiting jet stream (exhaust) experiences a highly non-isentropic equilibration process with the surrounding air in which all this work potential (exergy) is destroyed. In general, the greater the thermo/fluid dynamic gradients between exhaust and ambient flow-fields (or the effective flow-field adjacent to engine exhaust), the more exergy the system possesses at that point, which in turn means more entropy generation and exergy destruction occur in the wake since that exergy is inherently lost in an equilibration process that is not utilized to produce work. This then corresponds to a necessary drop in the thrust power that the engine can produce.

This observation clarifies the comparison of the efficiency of a turbojet to the efficiency of a high-bypass turbofan. Specifically, in order to achieve the same thrust as a turbofan, the turbojet accelerates significantly less air to a significantly higher speed than the turbofan. Consequently, in the high subsonic flight regime, the velocity (and thermal)

gradients between the exhaust and the adjacent flow at the aft end of the turbojet are significantly larger than that of a turbofan, resulting in more entropy generated in the wake equilibration process. This in turn leads to a lower energy-based efficiency even for large specific thrust (thrust may be large due to large exit to free-stream velocity ratio). At higher Mach numbers, i.e., in the low supersonic regime, the exhaust conditions of the turbojet are generally likely to be more closely matched to the surrounding flow, hence meaning relatively less entropy generated in the wake as compared to within the engine itself. This can result in higher first-law efficiencies for the turbojet than for the turbofan in this regime.

This investigation clearly indicates the dominance of the wake losses in engine analysis. However, it is important to realize that it is impossible in realistic engine design to completely (or even substantially) reduce wake losses. For instance, in the limit, if the exhaust conditions (pressure, temperature, velocity, etc.) were exactly matched to the free-stream conditions (hence eliminating wake losses altogether), the engine would not be capable of producing thrust – in fact, it could not even exist as a physically plausible construct within the flow. In a very real sense, the generation of thrust (to first order directly proportional to the velocity difference between engine exit and free-stream) mandates entropy generation in the wake; the greater the velocity difference, the larger the thrust and the greater the entropy generation in the wake.

Results of this investigation show that at a given altitude and fuel throttle setting, for increasing flight Mach number, both force power delivered and the first law efficiency of the engine increase even though thrust decreases. In addition, results also demonstrate that higher efficiencies are achieved at higher fuel throttle settings for given altitude and flight Mach number with thrust also increasing. This latter result indicates that increasing fuel flow rates result in larger fractions of exergy associated with the fuel being realized as thrust power. These and similar observations of contrasting thrust trends and efficiency trends highlight the importance of understanding the central exergy-performance relationship as derived in this work; specifically, this relationship completely defines and quantifies the fundamental balance between energy input (exergy associated with fuel), overall losses (losses in exergy), and the realized force power produced by the engine at some flight velocity. The realized efficiency and thrust of the engine are then best viewed as completely derivative from this over-arching relationship. Specifically, their values at a

given flight condition as well as their respective increases and decreases as flight conditions change are entirely determined/driven by the interplay between on-board energy and exergy losses.

This investigation demonstrates that the burner in a gas turbine is by far the largest availability loss component in the engine itself, providing over six times the losses in all other engine components combined. In general, the exergy destruction in the compressor, turbine, and inlet combine to represent less than around 5% of the exergy associated with the fuel (or power equivalent input). While this trend is well known, the ability to quantify this and other losses across the operational envelope in terms of fuel throttle setting, flight Mach number, and altitude can provide critical design and optimization information for such engines.

6.3. FUTURE WORK

The methodology described in this study enables the comprehensive examination of the performance of an engine throughout the operational space of that engine. This is done in terms of the universal and single metric of entropy generation or (equivalently) exergy destruction/loss. This metric is the most fundamental loss measure for all physical processes of any type. By unifying the performance of an aerospace jet engine with this single 'currency' of losses, the true allocation and quantification of losses can be realized. This has significant promise in terms of multi-disciplinary analysis, design, and optimization as it, in principle, reduces the objective function to one parameter. It also provides the true assessment of where to put effort in reducing losses and hence can direct allocation of resources in engine design.

As described in previous sections, this entropy based analysis can readily be extended to higher fidelity/more complex models ranging from differential quasi-1D solvers, to high fidelity, multi-dimensional CFD simulations. The use of such methods provides yet more insight and details in terms of loss mechanism and spatial location of the losses. The methodology described here for a simple single-spooled turbojet can also be readily extended to more complex gas-turbine engines such as turbofans and turboprops, including variable bypass configurations and engines with multiple spools and afterburners. Furthermore, it should be highly beneficial to use this type of operational

analysis for an entire vehicle, hence allowing performance and losses to be studied over the entire operational envelope of the overall vehicle. The entropy-based method can also be applied to other types of aerospace engines and systems such as traditional chemical rockets. A study is currently in progress for a LOX-LH$_2$ rocket in which the performance trends and exergy losses will be investigated for the entire operating envelope of the rocket.

APPENDIX A.

ADDITIONAL RESULTS

Figures A.1 to A.4 show the variation of total exergy destruction rate at two different altitudes and at two different fuel throttle settings.
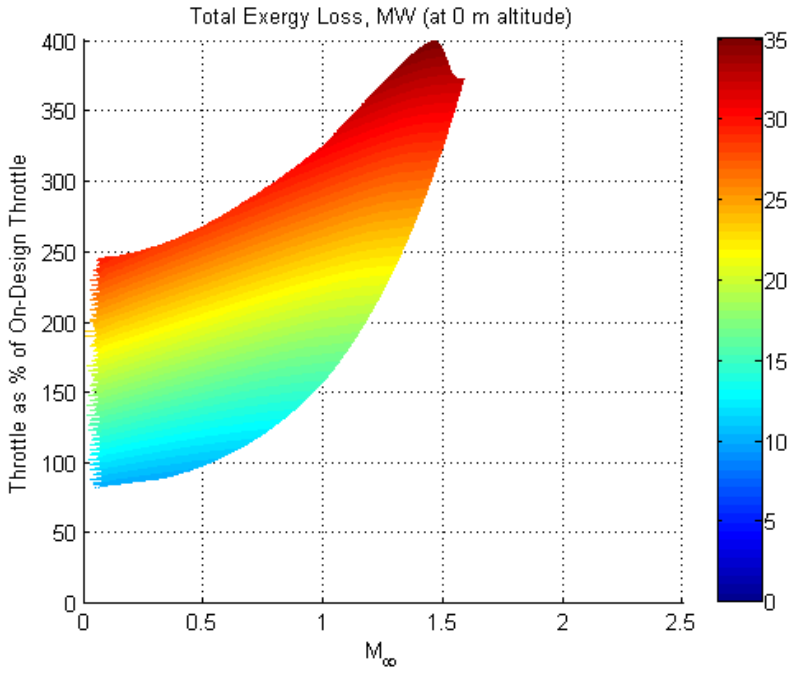
Figure A.1. Total exergy loss rate distribution at 0m altitude.
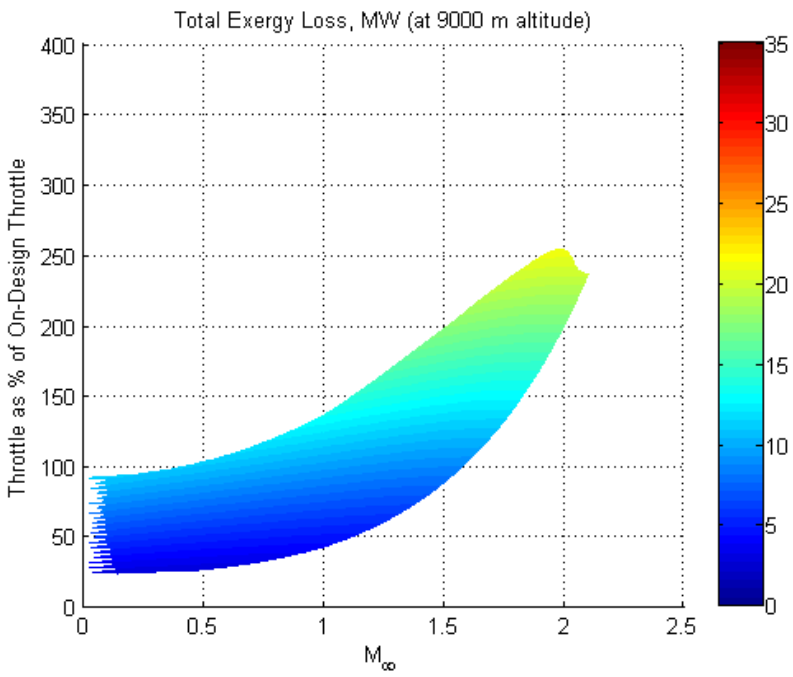
Figure A.2. Total exergy loss rate distribution at 9000m altitude.
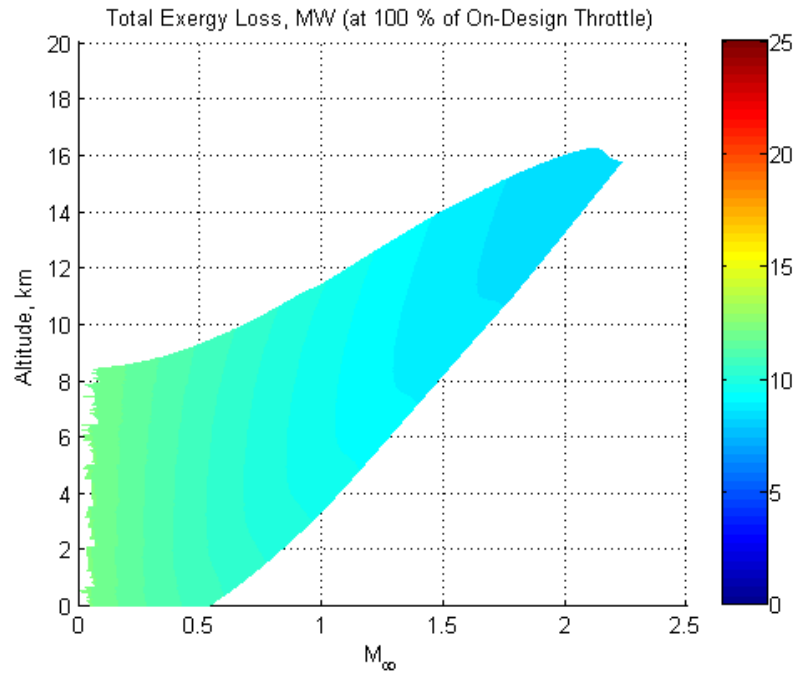
Figure A.3. Total exergy destruction rate distribution at 100% throttle setting.
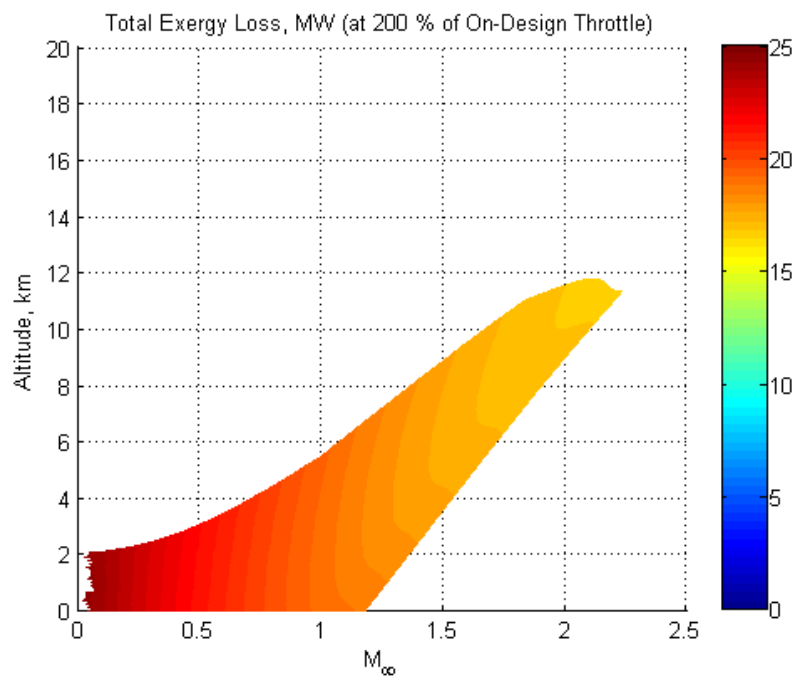
Figure A.4. Total exergy destruction rate at 200% throttle setting.

Figures A.5 through A.8 show the variation of thrust specific fuel consumption at two different altitudes and two different fuel throttle settings.
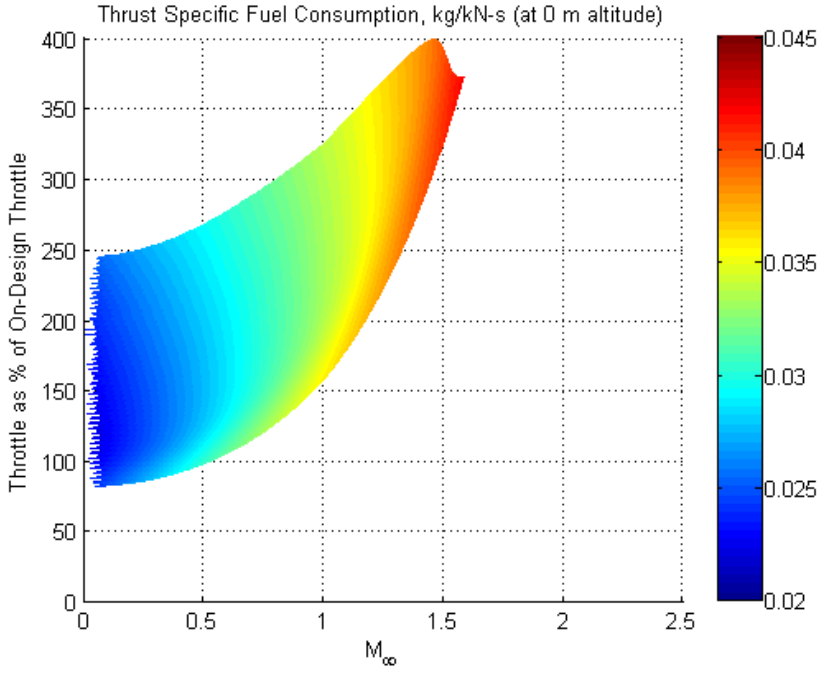

Figure A.5. TSFC distribution at 0m altitude.
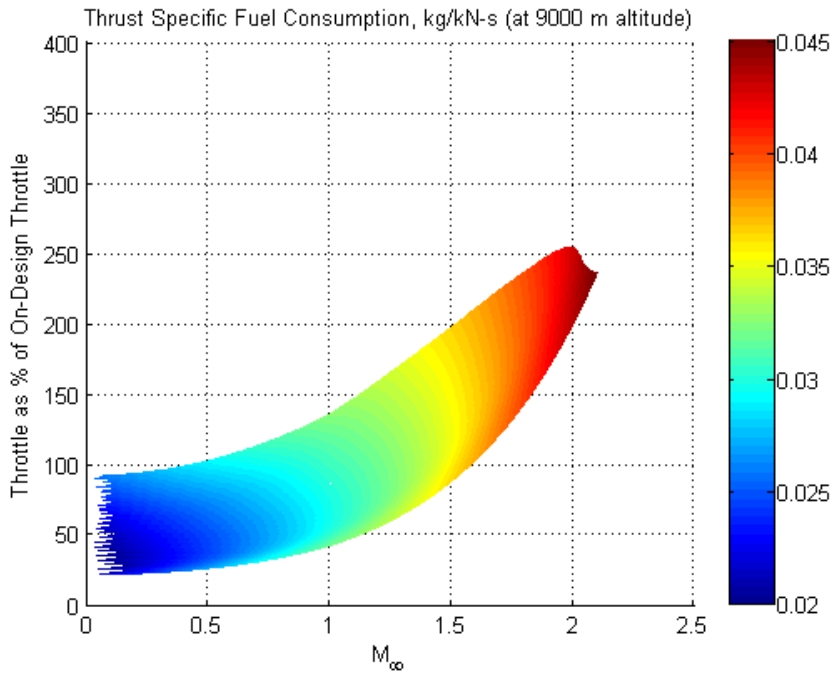
Figure A.6. TSFC distribution at 9000m altitude.

Thrust Specific Fuel Consumption, kg/kN-s (at 100 % of On-Design Throttle)
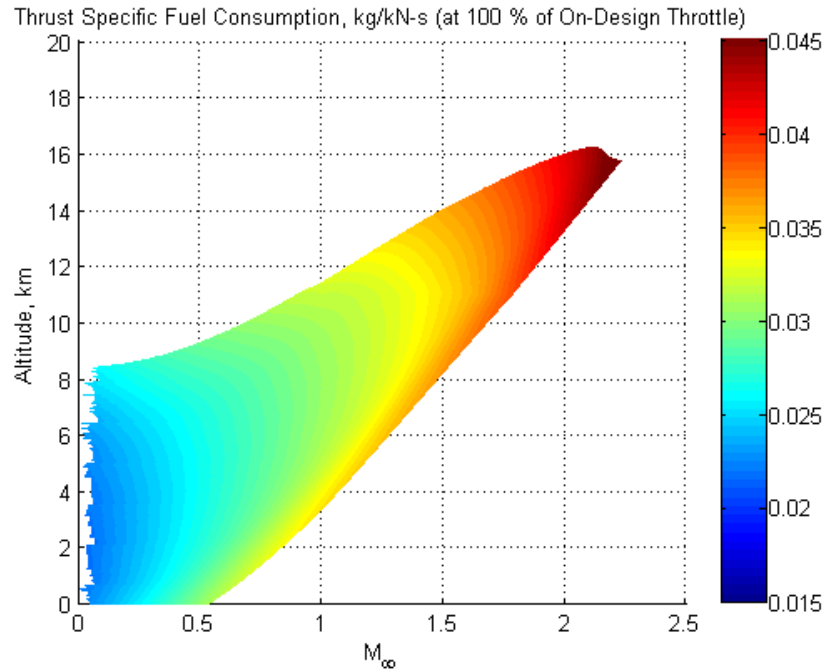
Figure A.7. TSFC distribution at 100% throttle setting.

Thrust Specific Fuel Consumption, kg/kN-s (at 200 % of On-Design Throttle)
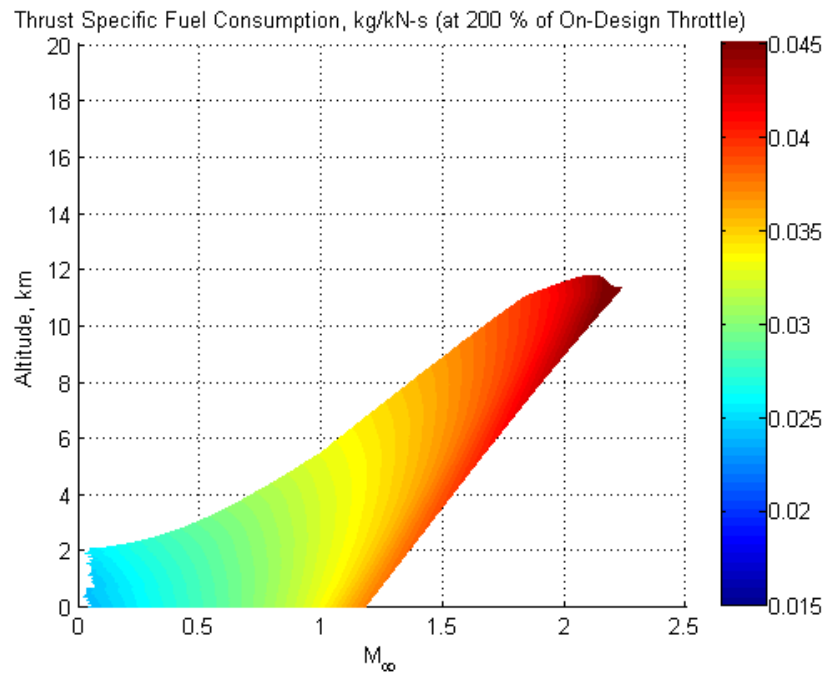
Figure A.8. TSFC distribution at 200% throttle setting.

Figures A.9 through A.12 show the variation of spillage at two different altitudes and two different fuel throttle settings.
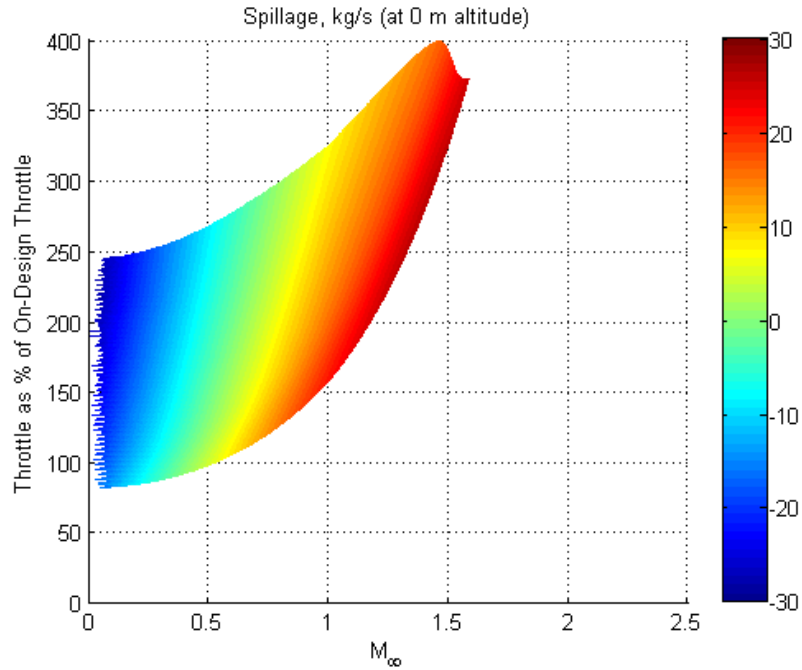
Figure A.9. Spillage distribution at 0m altitude.
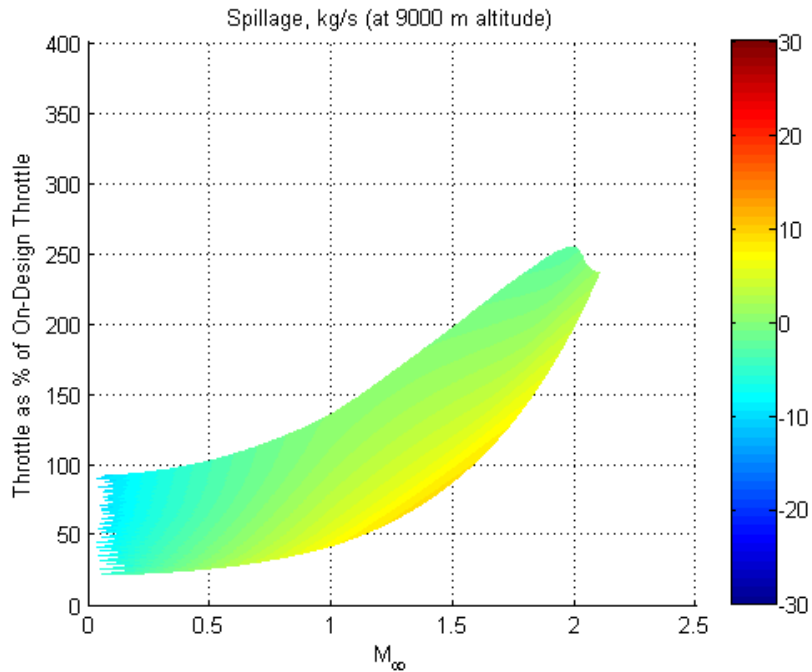
Figure A.10. Spillage distribution at 9000m altitude.
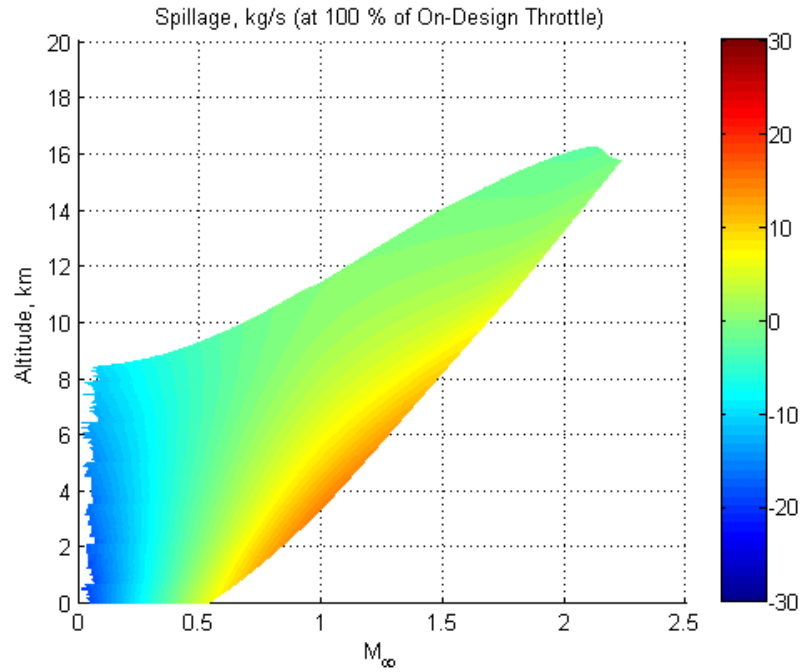
Figure A.11. Spillage distribution at 100% throttle setting.
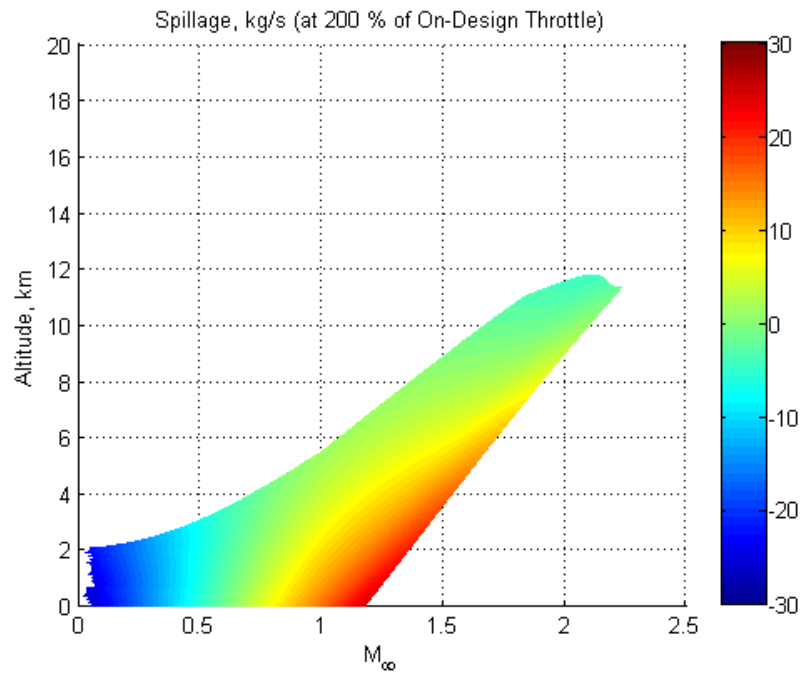
Figure A.12. Spillage distribution at 200% throttle setting.

Figures A.13 through A.16 show the variation of engine spool speed (RPM) at two different altitudes and two different fuel throttle settings.
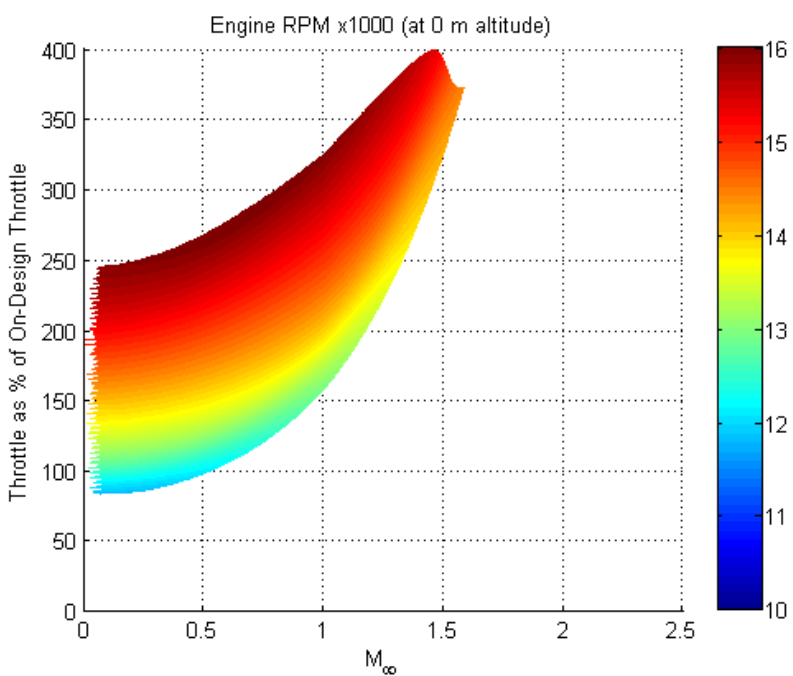
Figure A.13. Engine RPM distribution at 0m altitude.
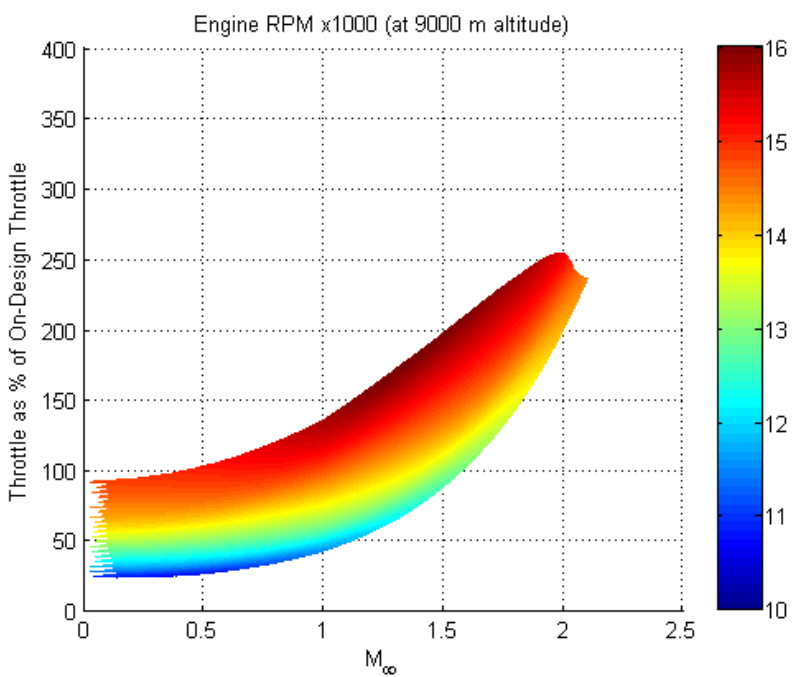
Figure A.14. Engine RPM distribution at 9000m altitude.
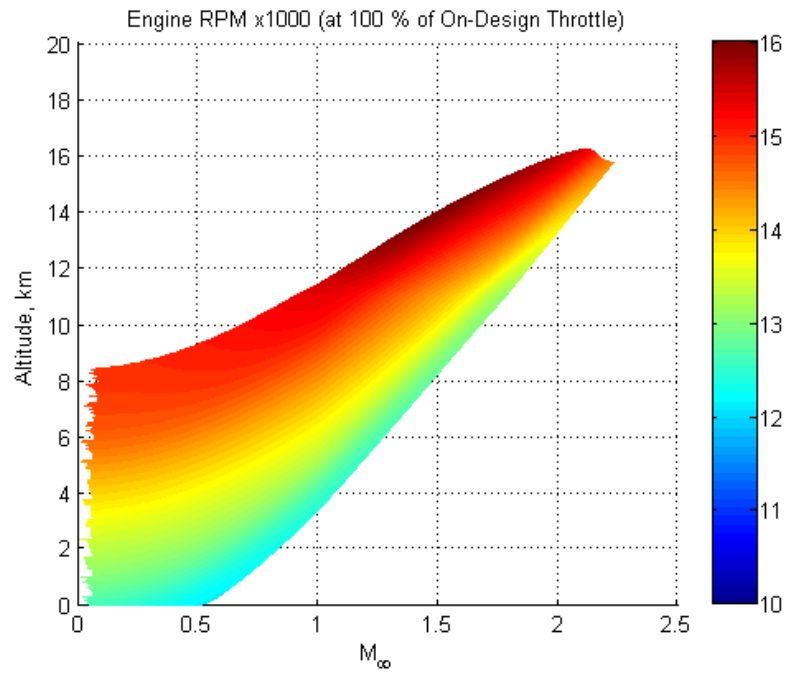
Figure A.15. Engine RPM distribution at 100% throttle setting.
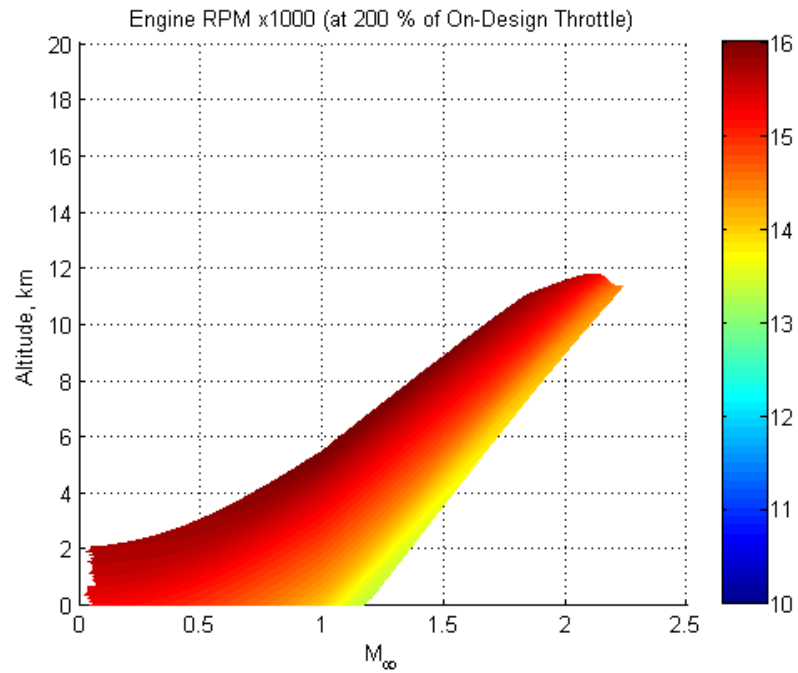
Figure A.16. Engine RPM distribution at 200% throttle setting.

Figures A.17 through A.20 show the variation of the entropy generation rate in the inlet/diffuser at two different altitudes and two different fuel throttle settings.
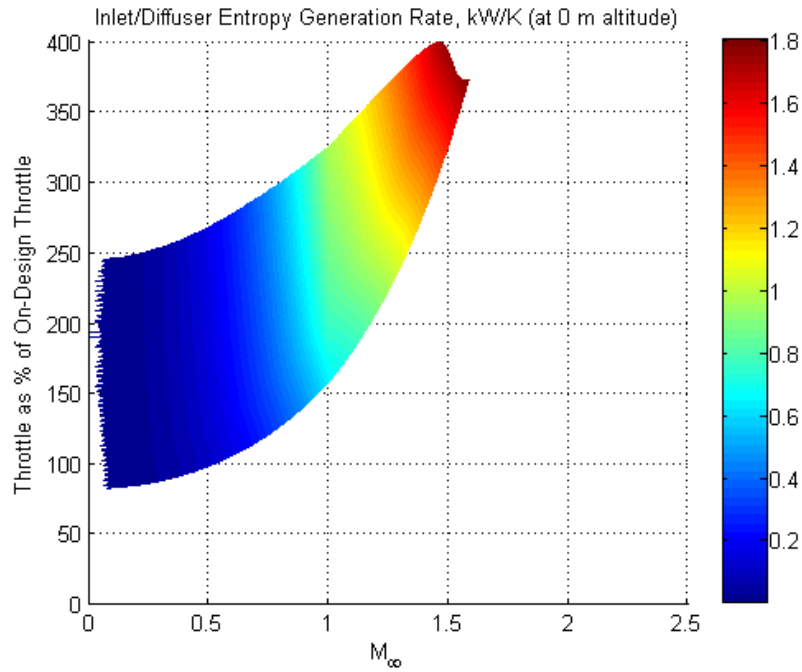
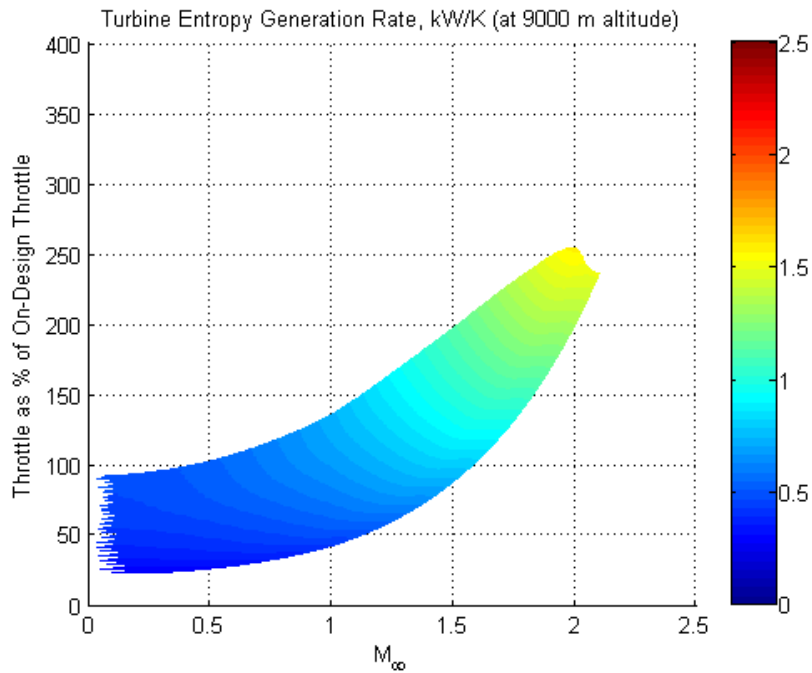Figure A.17. Inlet/diffuser entropy generation rate at 0m altitude.
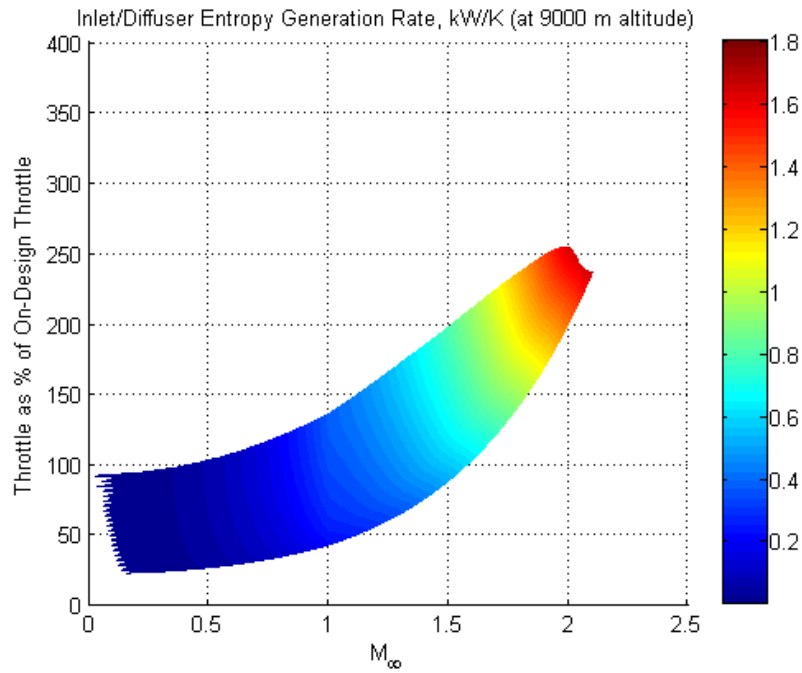
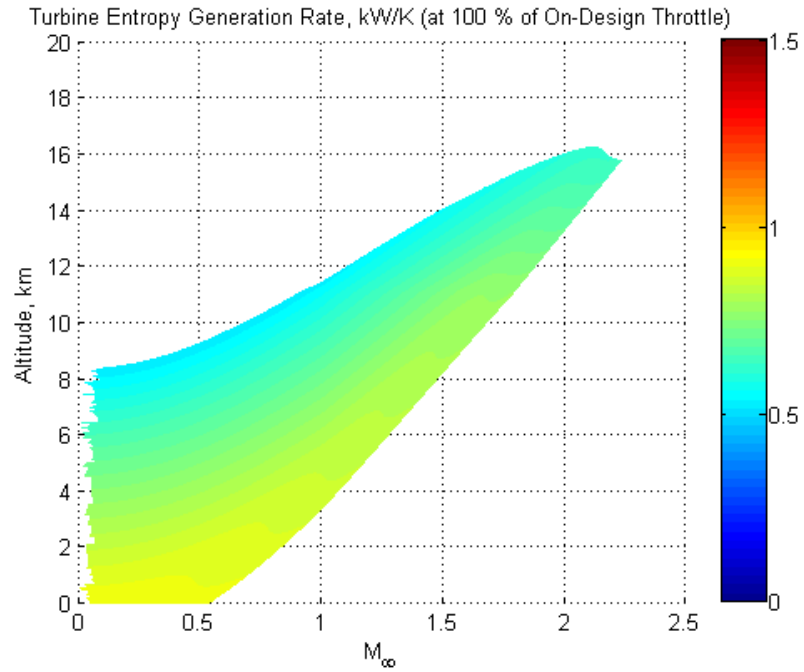Figure A.18. Inlet/diffuser entropy generation rate at 9000m altitude.
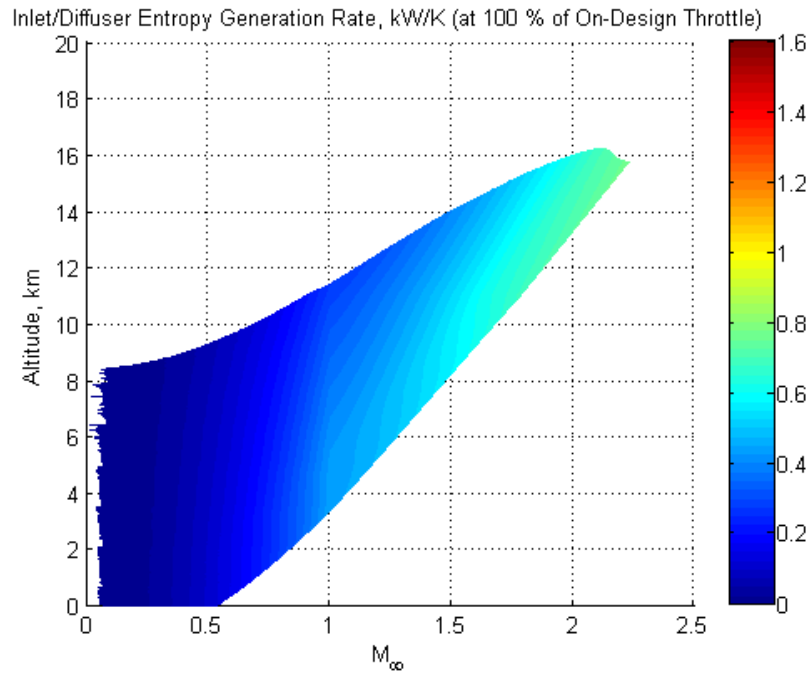
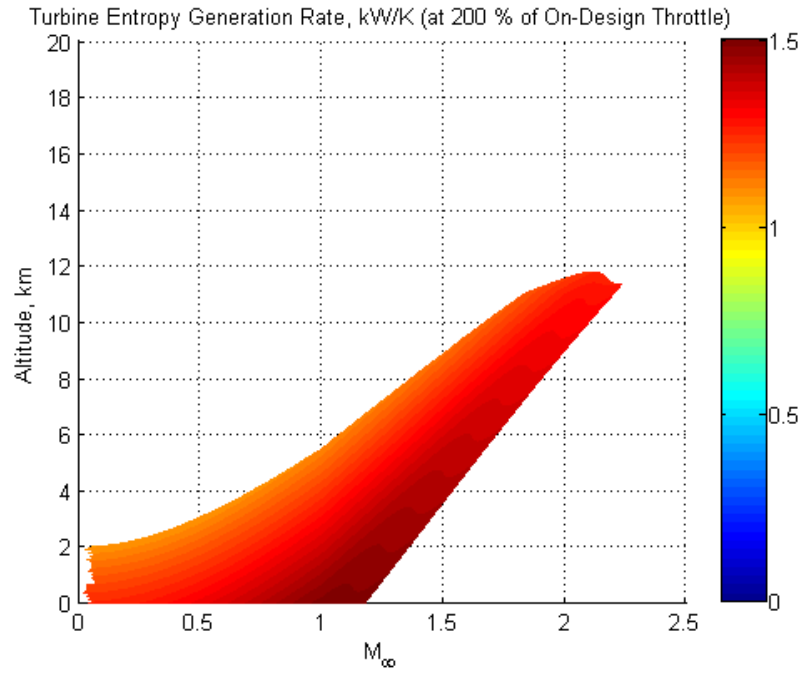Figure A.19. Inlet/diffuser entropy generation rate at 100% throttle setting.
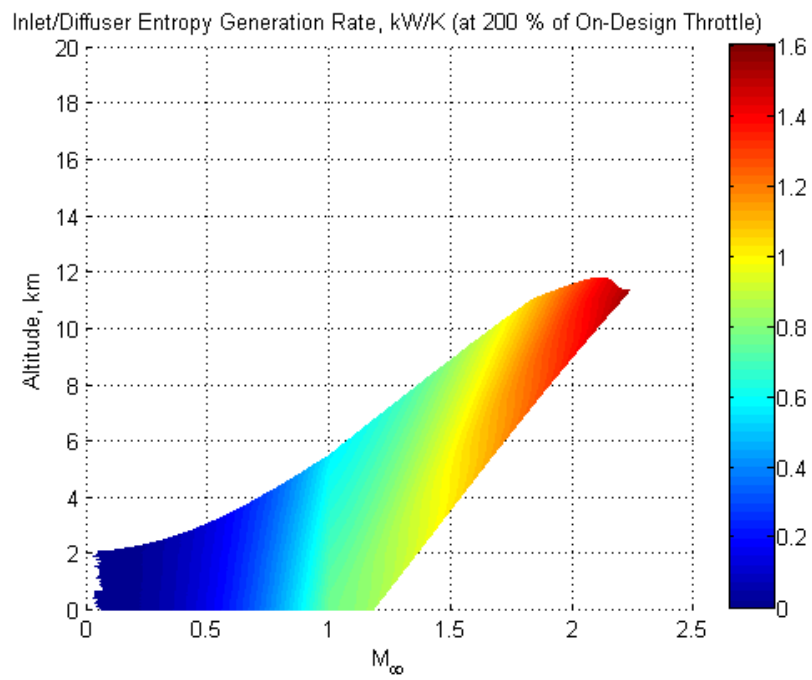
Figure A.20. Inlet/diffuser entropy generation rate at 200% throttle setting.

Figures A.21 through A.24 show the variation of entropy generation in the compressor at two different altitudes and two different fuel throttle settings.
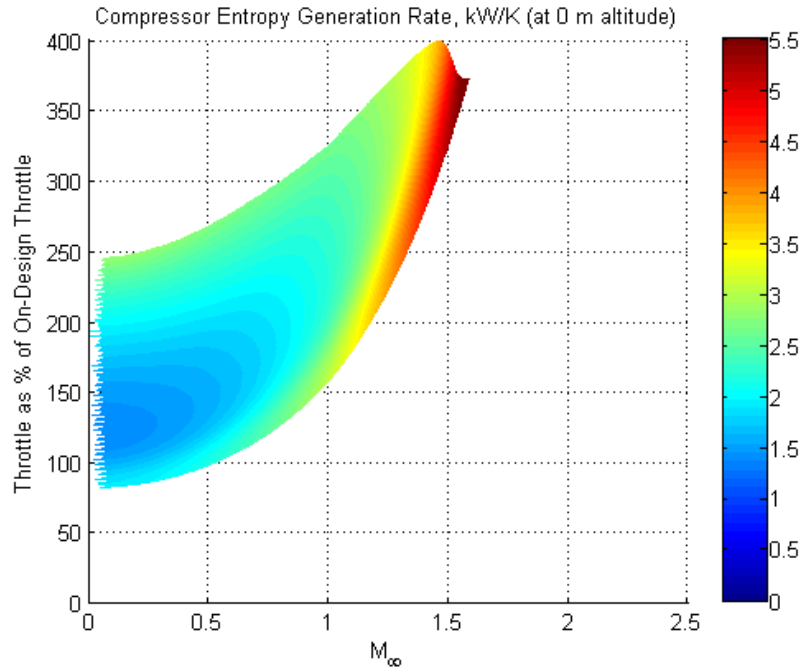

Figure A.21. Compressor entropy generation rate at 0m altitude.
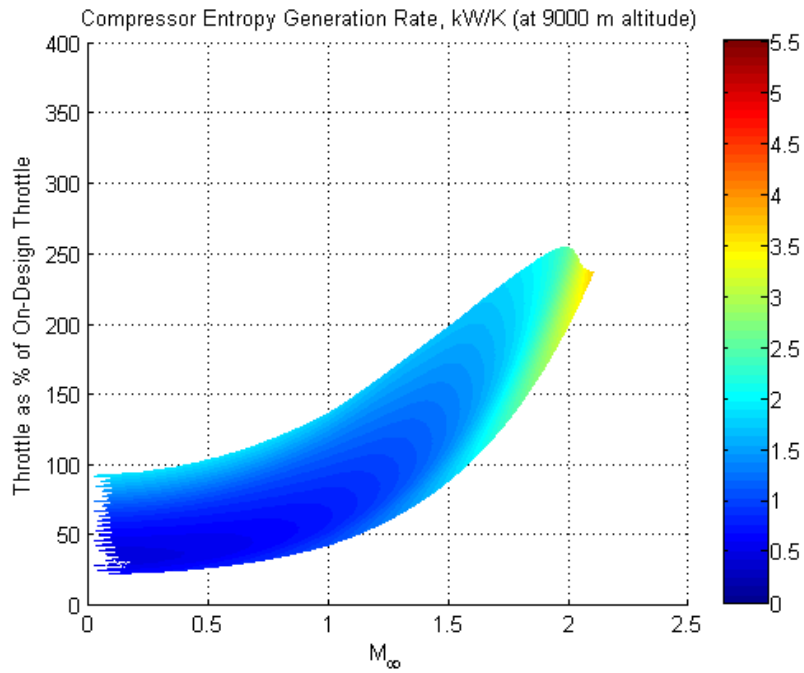
Figure A.22. Compressor entropy generation rate at 9000m altitude.
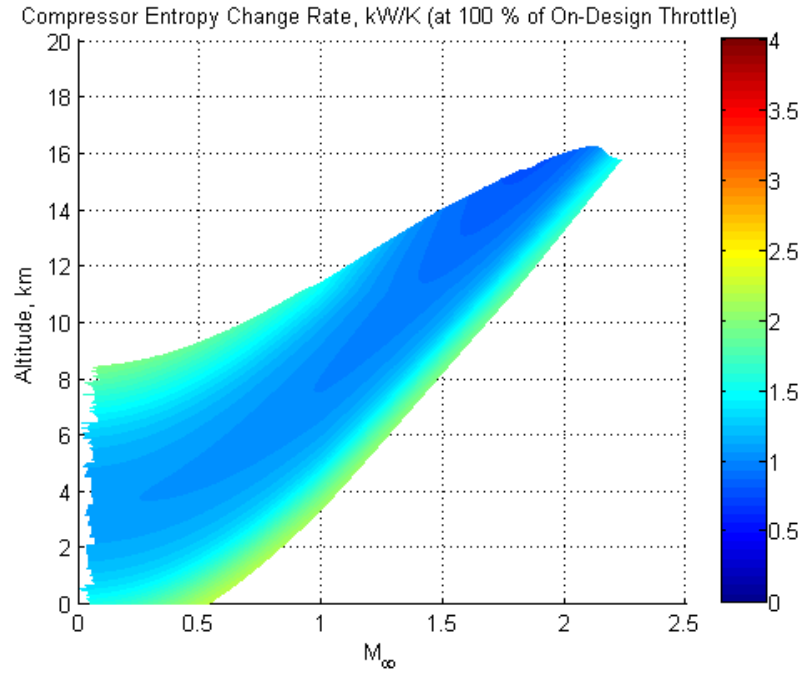
Figure A.23. Compressor entropy generation rate at 100% throttle setting.
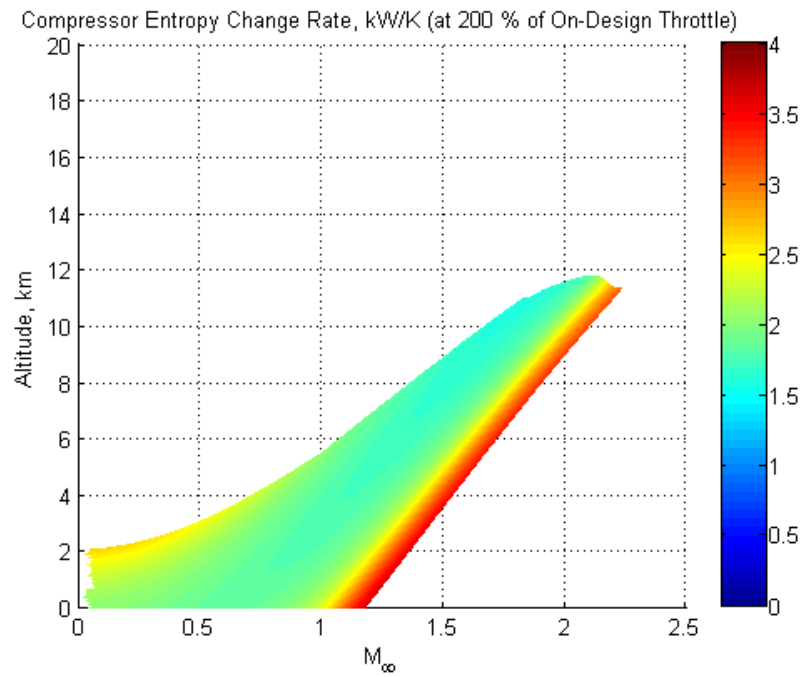
Figure A.24. Compressor entropy generation rate at 200% throttle setting.

Figures A.25 through A.28 show the variation of entropy generation in the burner at two different altitudes and two different fuel throttle settings.
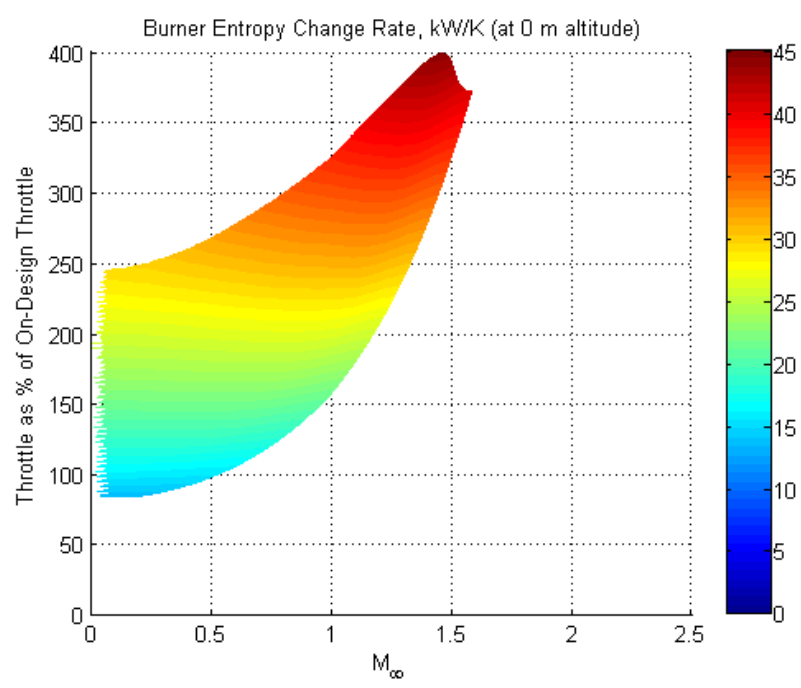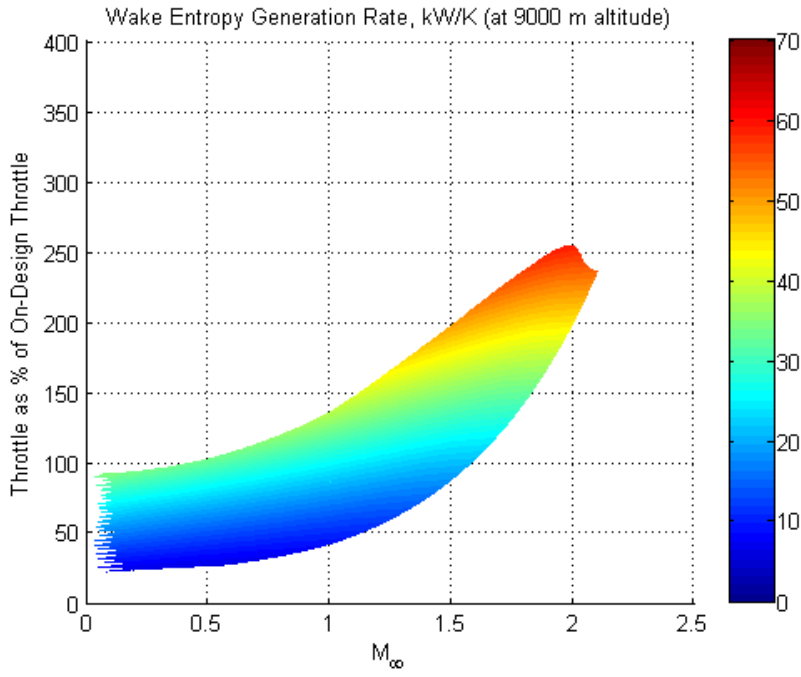

Figure A.25. Burner entropy generation at 0m altitude.
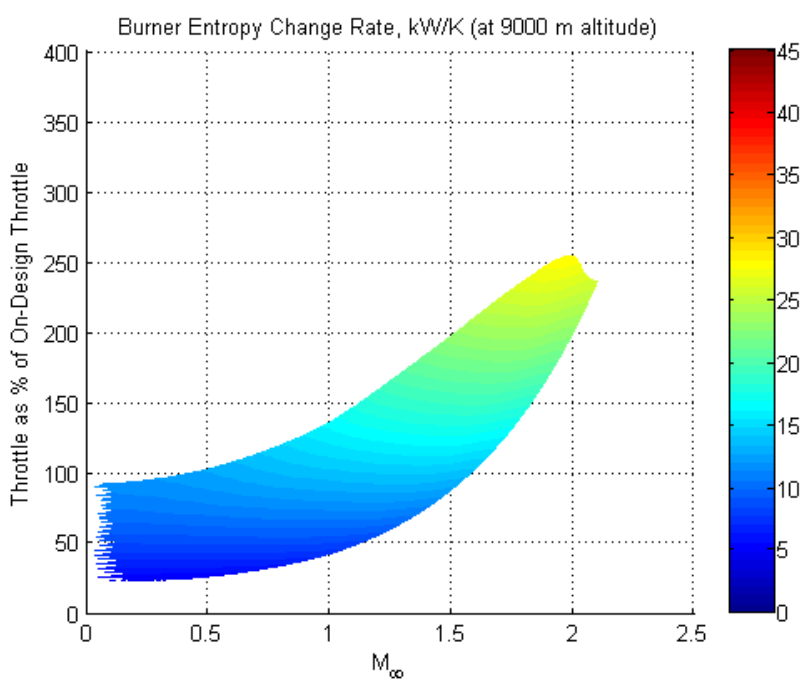
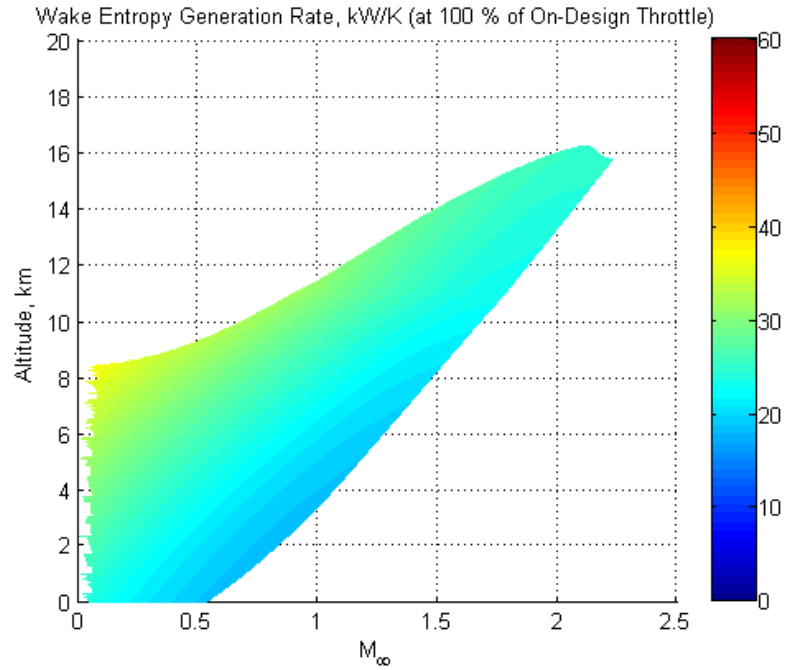Figure A.26. Burner entropy generation at 9000m altitude.
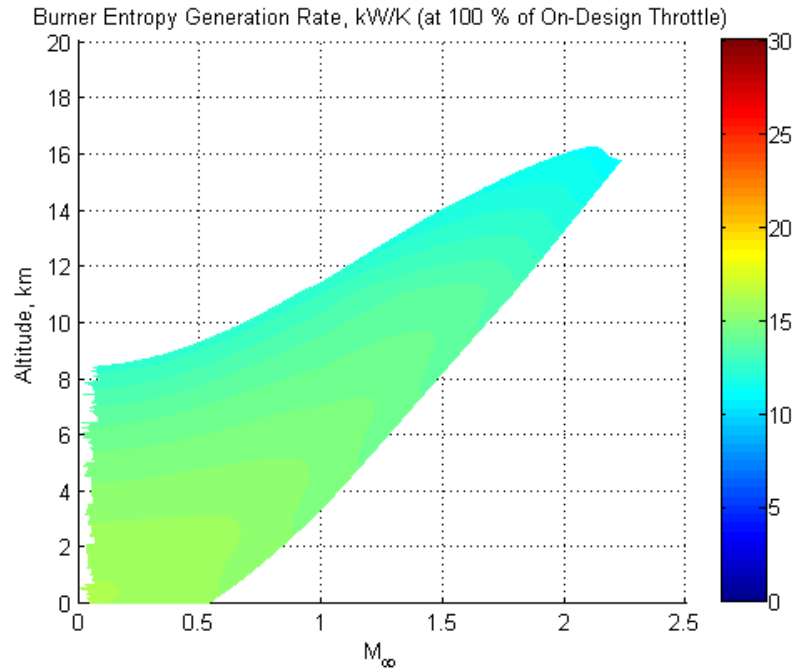
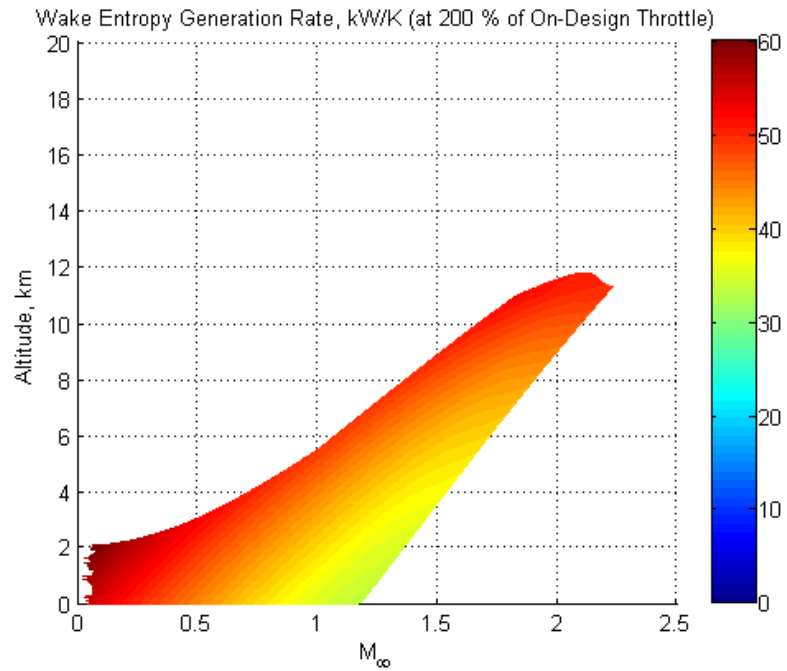Figure A.27. Burner entropy generation at 100% throttle setting.
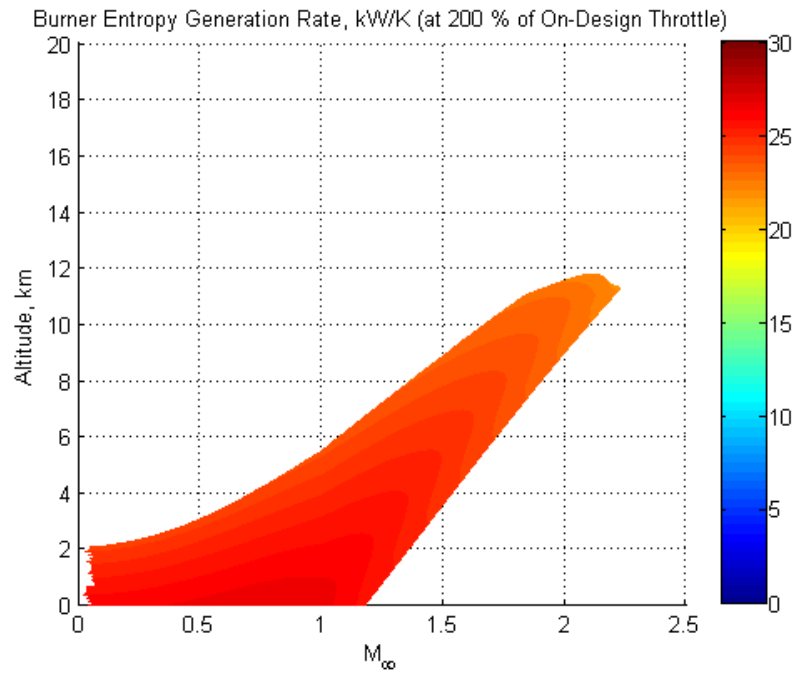
Figure A.28. Burner entropy generation at 200% throttle setting.

Figures A.29 through A.32 show the variation of entropy generation in the turbine at two different altitudes and two different fuel throttle settings.

Turbine Entropy Generation Rate, kW/K (at 0 m altitude)
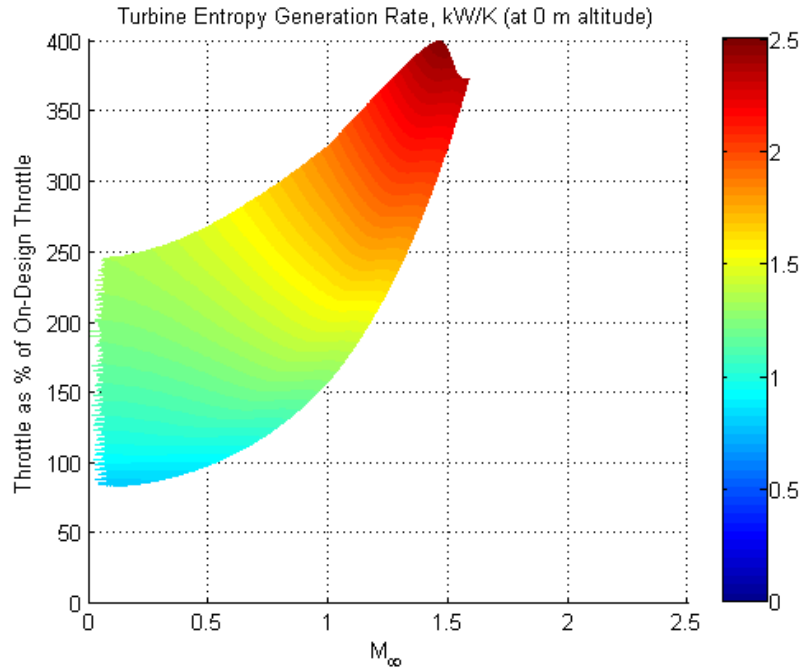
Figure A.29. Turbine entropy generation rate at 0m altitude.

Turbine Entropy Generation Rate, kW/K (at 9000 m altitude)

Figure A.30. Turbine entropy generation rate at 9000m altitude.

Figure A.31. Turbine entropy generation rate at 100% throttle setting.

Figure A.32. Turbine entropy generation rate at 200% throttle setting.

Figures A.33 through A.36 show the variation of entropy generation in the wake mixing zone at two different altitudes and two different fuel throttle settings.
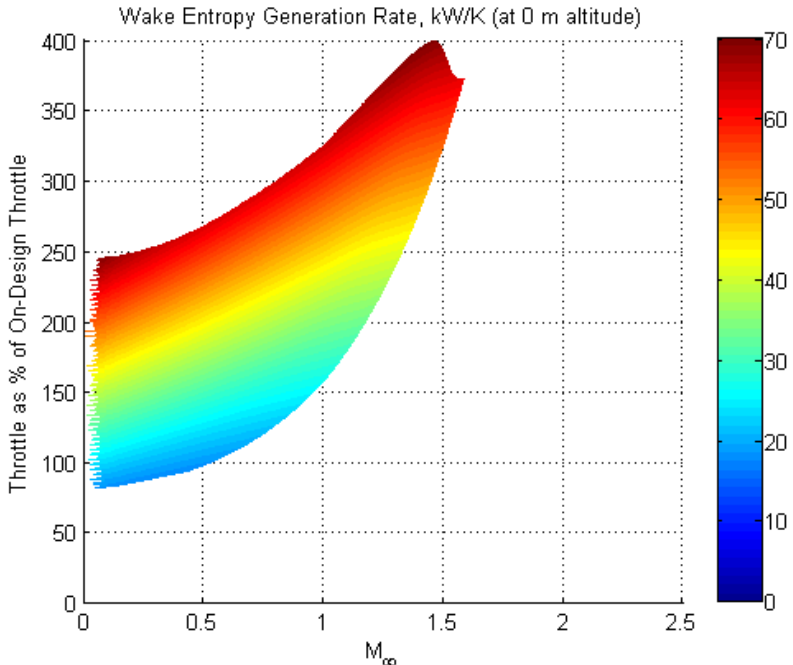
Figure A.33. Wake entropy generation at 0m altitude.

Figure A.34. Wake entropy generation at 9000m altitude.

Figure A.35. Wake entropy generation at 100% throttle setting.

Figure A.36. Wake entropy generation at 200% throttle setting.

Figures A.37 through A.40 show the variation in the propulsive power delivered to the engine (thrust power) at two different altitudes and two different fuel throttle settings.
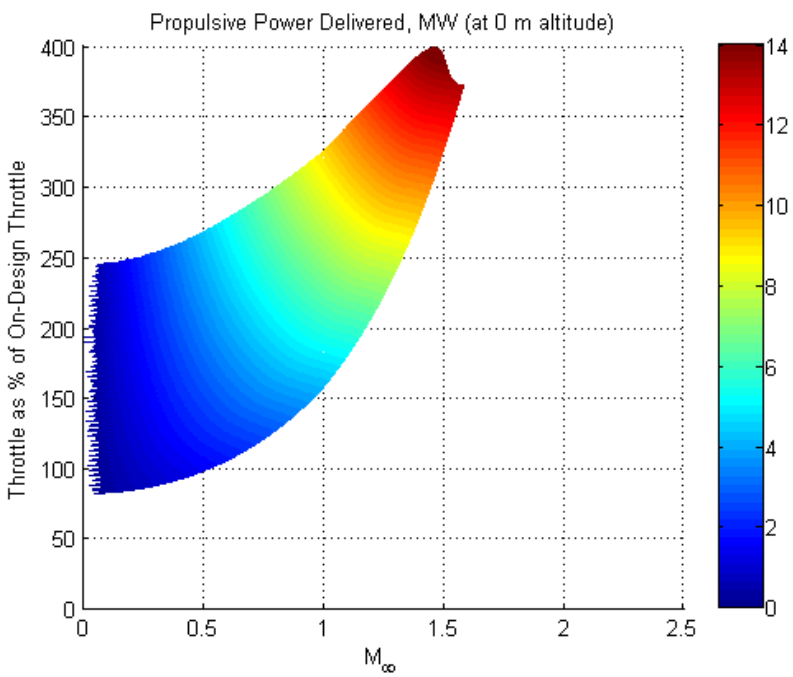
Figure A.37. Thrust power at 0m altitude.
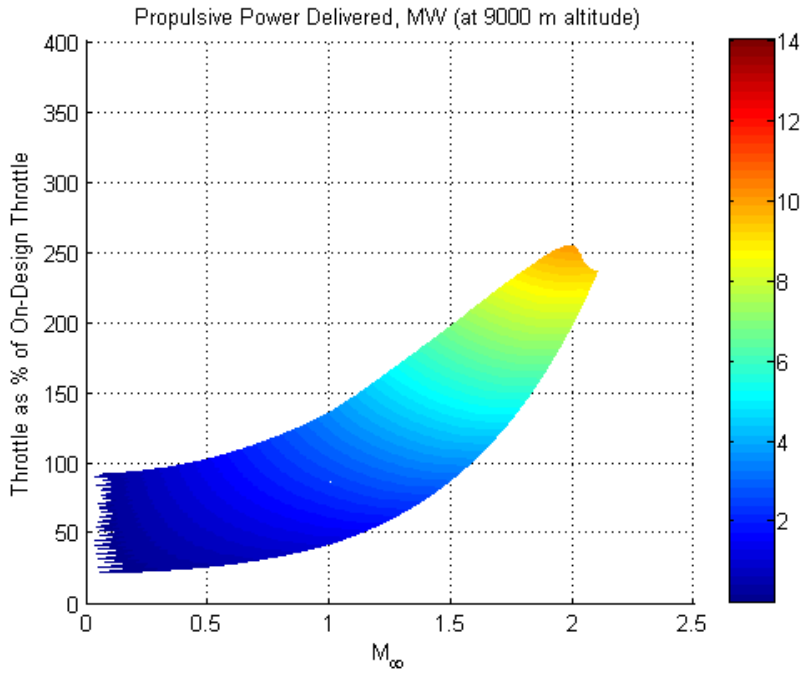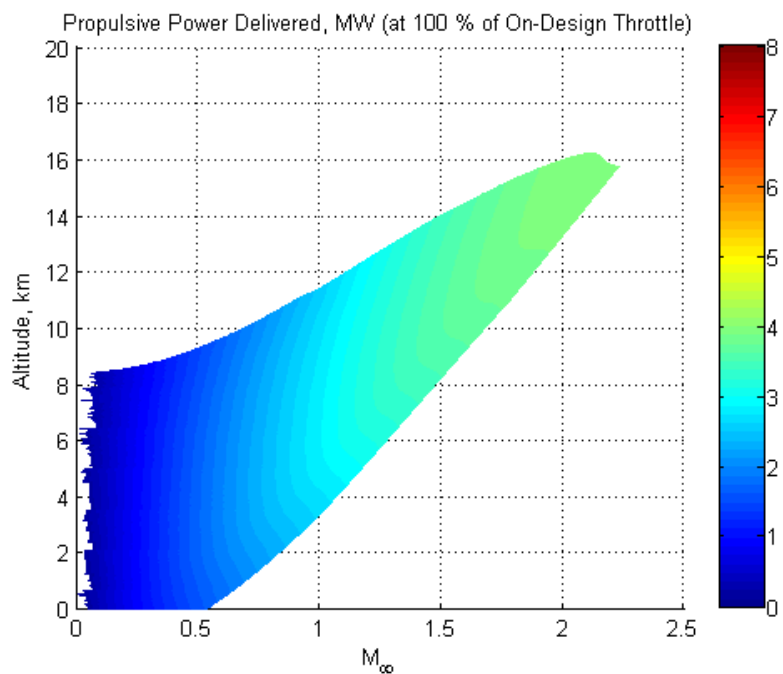

Figure A.38. Thrust power at 9000m altitude.
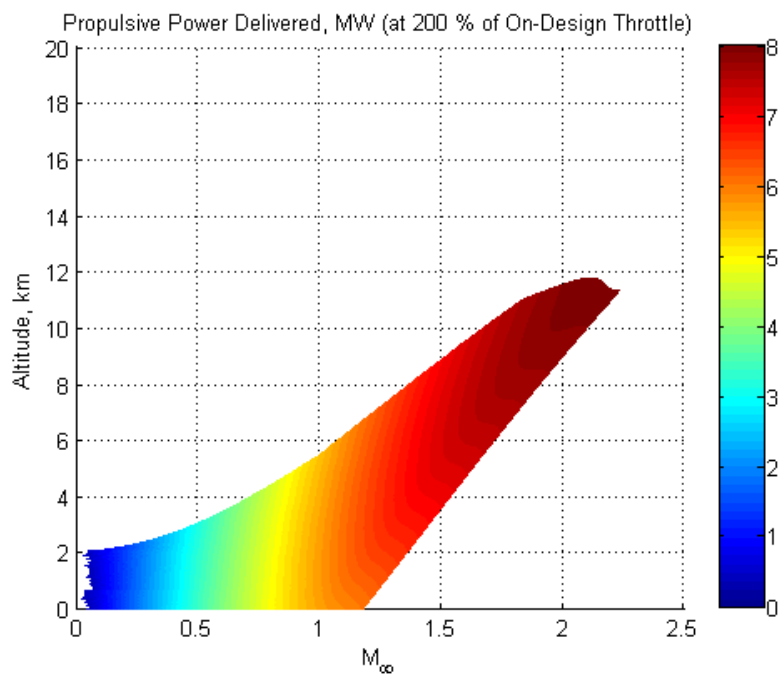
Figure A.39. Thrust power at 100% throttle setting.

Figure A.40. Thrust power at 200% throttle setting.

Figures A.41 through A.44 show the variation in the flow velocity difference between engine exit and freestream at two different altitudes and two different fuel throttle settings.
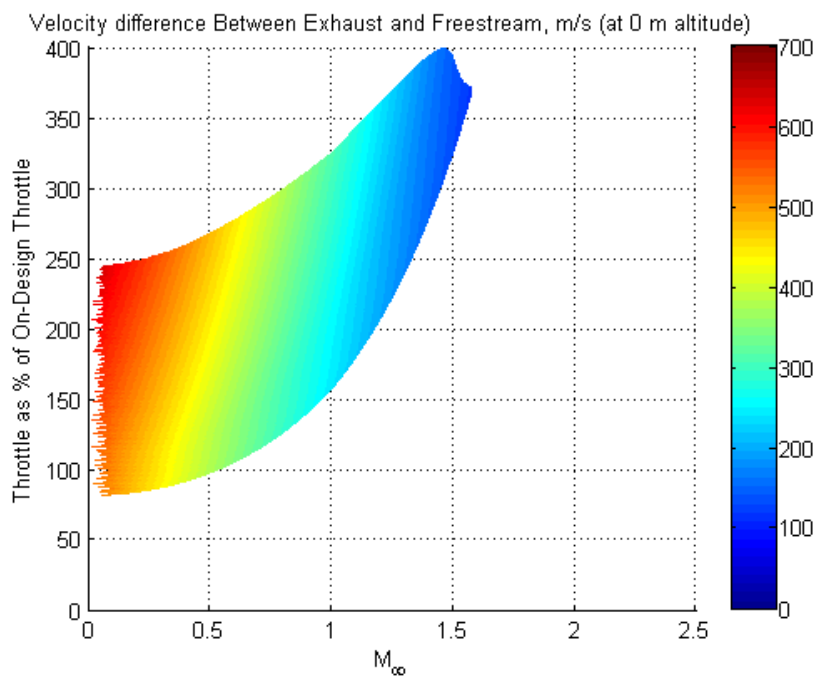

Figure A.41. Velocity difference between exhaust and freestream at 0m altitude.
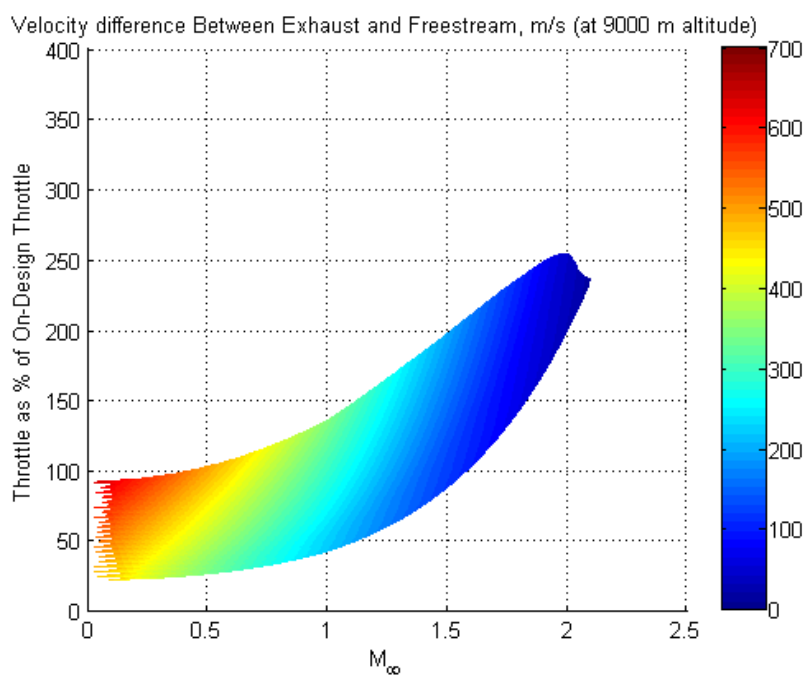

Figure A.42. Velocity difference between exhaust and freestream at 9000m altitude.
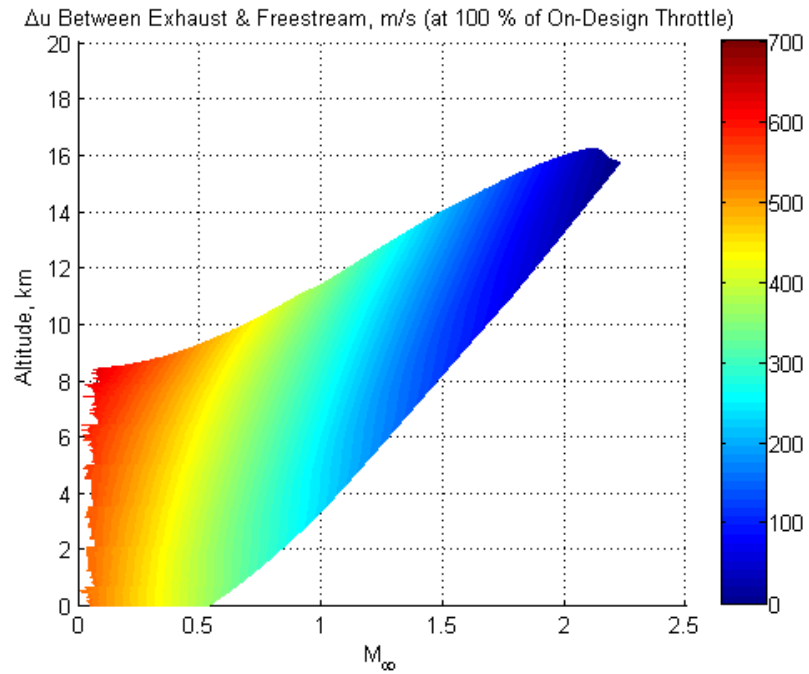
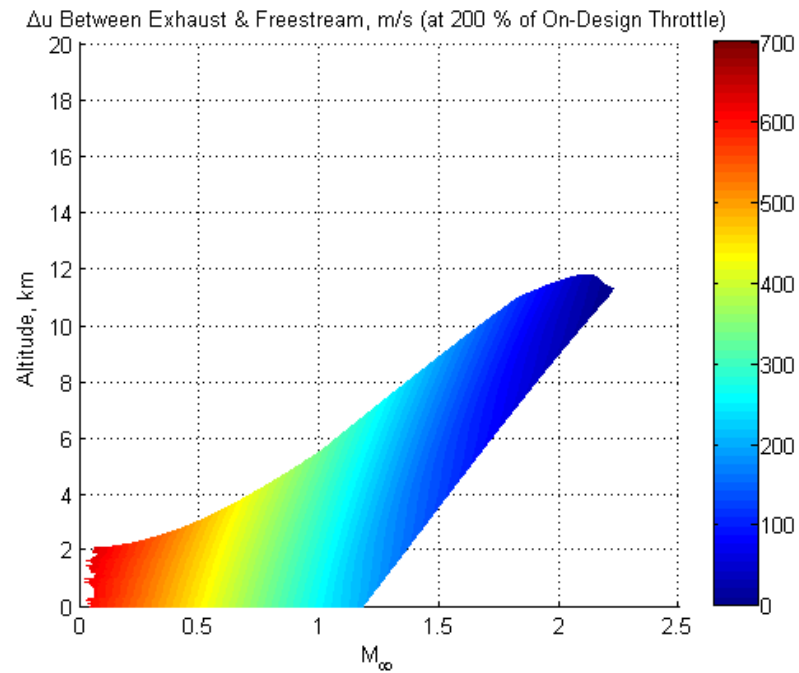Figure A.43. Velocity difference between exhaust and freestream at 100% throttle setting.

Figure A.44. Velocity difference between exhaust and freestream at 200% throttle setting.

APPENDIX B.

SAMPLE RESULTS FROM A QUASI-ONE-DIMENSIONAL ANALYSIS CASE
STUDY

Figure B.1 shows the axial distribution of the magnitude of entropy generation per unit mass, whereas Figure B.2 shows the cumulative amount of entropy generated per unit mass as the flow moves through the engine.
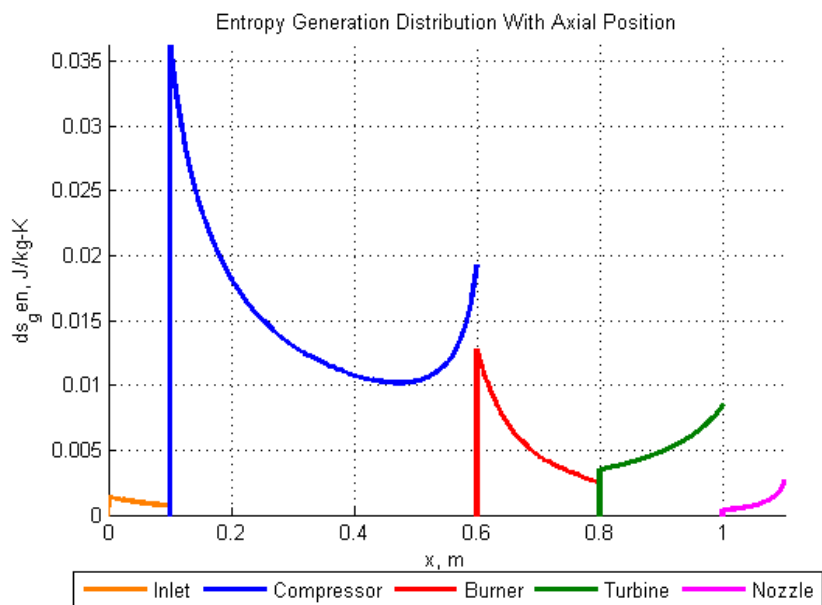

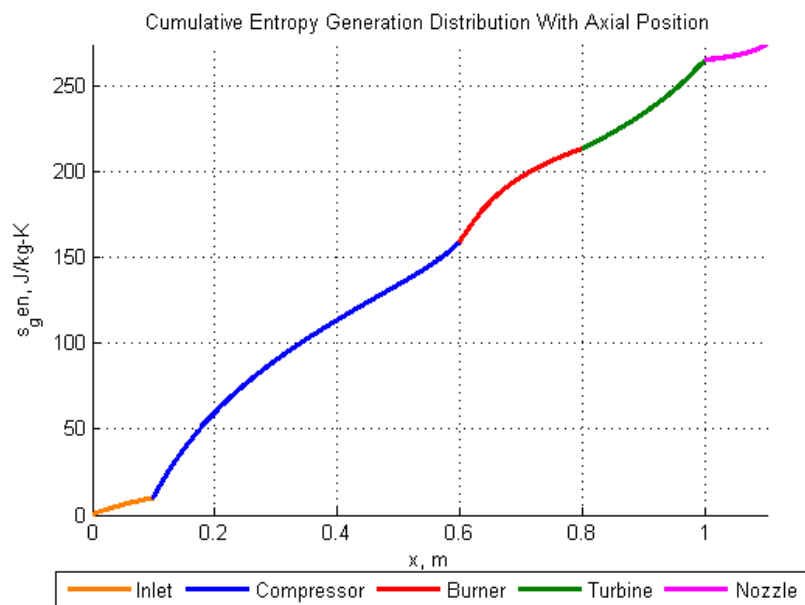Figure B.1. Axial distribution of entropy generation per unit mass.

Figure B.2. Cumulative entropy generation per unit mass.

Figures B.3 and B.4 show the axial distribution of total pressure and total temperature, respectively.
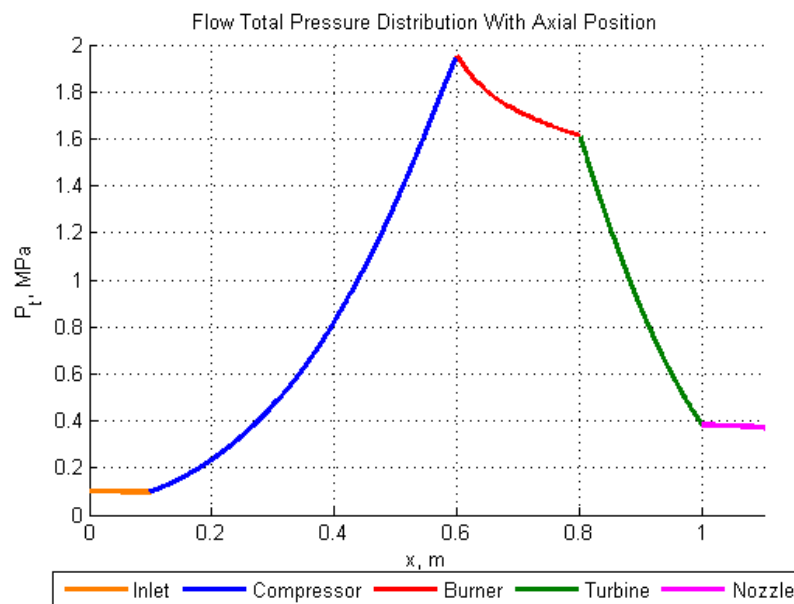

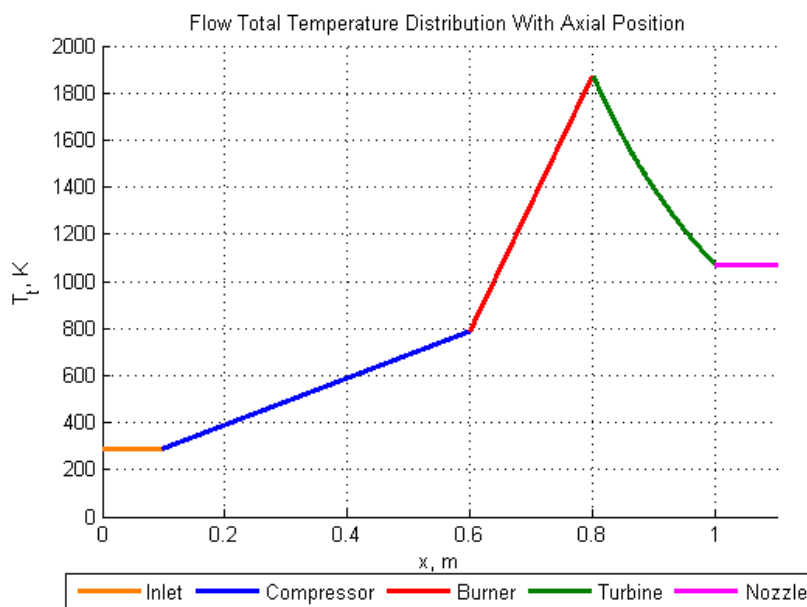Figure B.3. Axial distribution of total pressure.

Figure B.4. Axial distribution of total temperature.

BIBLIOGRAPHY

[1] Riggins, D.W., Camberos, J., Moorhouse, D., "Characterization of Aerospace Vehicle Performance and Mission Analysis Using Exergy", Chapter 8, Volume 238, AIAA Progress in Astronautics and Aeronautics Series, *Exergy Analysis and Design Optimization for Aerospace Vehicles and Systems*, AIAA, 2011, Reston, Virginia, pp. 275-307.

[2] Riggins, D. W., Camberos, J., Wolff, M., Bowcutt, K., "Mission-Integrated Exergy Analysis for Hypersonic Vehicles: Methodology and Application", <u>AIAA Journal of Propulsion and Power</u>, Vol. 29, No. 3, pp. 610-620, May-June 2013.

[3] Abbas, Mohammad, and David W. Riggins. "Exergy-Based Performance Analysis of a Turbojet Engine." *52nd AIAA/SAE/ASEE Joint Propulsion Conference* (2016): n. pag. Web.

[4] Foa, J., "Efficiencies: Propulsive Cycles," Elements of Flight Propulsion, Wiley, New York, 1960, pp. 274–287.

[5] Builder, C. H., "On the Thermodynamic Spectrum of Air-Breathing Propulsion," AIAA Paper 64-243, June 1964.

[6] Lewis, J. H., "Propulsive Efficiency from an Energy Utilization Standpoint," Journal of Aircraft, Vol. 13, No. 4, 1976, pp. 299–302.

[7] Clarke, J., and Horlock, J., "Availability and Propulsion," Journal of Mechanical Engineering Science, Vol. 17, No. 4, 1975, pp. 223–232.

[8] Czysz, P. and Murthy, S. N. B., "Energy Analysis of High-Speed Flight Systems," Chapter 3 in High-Speed Flight Propulsion Systems. Progress in Astronautics and Aeronautics Series, AIAA, Volume 137.

[9] Murthy, S. N. B., "Effectiveness of a Scram Engine," AIAA Paper 94-3087.

[10] Brilliant H. M., "Analysis of Scramjet Engines Using Exergy Methods," AIAA Paper 95-2767.

[11] Curran, E. T. and Craig, R. R., "The Use of Stream Thrust Concepts for the Approximate Evaluation of Hypersonic Ramjet Engine Performance," Air Force Aero Propulsion Laboratory, Technical Report AFAPL-TR-73-38, July 1973.

[12] Riggins, D. W., "The Thermodynamic Continuum of Jet Engine Performance; The Principle of Lost Work due to Irreversibility in Aerospace Systems," International Journal of Thermodynamics, Vol. 6, No. 3, 2003, pp. 107–120.

[13]   Riggins, D., McClinton, C. R., and Vitt, P., "Thrust Losses in Hypersonic Engines Part 1: Methodology," Journal of Propulsion and Power, Vol. 13, No. 2, 1997, pp. 281–287.

[14]   Riggins, D., "Thrust Losses in Hypersonic Engines Part 2: Applications," Journal of Propulsion and Power, Vol. 13, No. 2, 1997, pp. 288–295.

[15]   Roth, B., "Comparison of Thermodynamic Loss Models Suitable for Gas Turbine Propulsion," Journal of Propulsion and Power, Vol. 17, No. 2, 2001, pp. 324–332.

[16]   Roth, B., "A Work Potential Perspective of Engine Component Performance," Journal of Propulsion and Power, Vol. 18, No. 6, 2002, pp. 1183–1190.

[17]   Giles, M. and Cummings, R., "Wake Integration for Three-Dimensional Flowfield Computations: Theoretical Development," Journal of Aircraft, Vol. 36, No. 2, 1999, pp. 357–365.

[18]   Marley C., Riggins, D., "The thermodynamics of Exergy Losses and Thrust Production in Gas Turbine engines," AIAA 2011-6130, 47th AIAA/ASME/SAE/ASEE Joint Propulsion Conference and Exhibits, San Diego, California, July 31-August 3.

[19]   Marley, C., Riggins, D., "Exergy Analysis of a Turbojet Engine Modeled as a Lumped Parameter System," AIAA 2012-1122, 50th AIAA Aerospace Sciences Meeting including the New Horizons Forum and Aerospace Exposition, Nashville, Tennessee, January 9-12.

[20]   Moorhouse, D., "A Proposed System-Level Multidisciplinary Analysis Technique Based on Exergy Methods," *AIAA Journal of Aircraft*, Vol. 40, No. 1, 2003, pp. 10-15.

[21]   Arntz, Aurélien, Olivier Atinault, and Alain Merlen. "Exergy-Based Formulation for Aircraft Aeropropulsive Performance Assessment: Theoretical Development." *AIAA Journal* 53.6 (2015): 1627-639. Web.

[22]   Turan, Onder. "Energy And Entropy Analyses Of An Experimental Turbojet Engine For Target Drone Application." *ANADOLU UNIVERSITY JOURNAL OF SCIENCE AND TECHNOLOGY A - Applied Sciences and Engineering* 17.5 (2016): 936. Web.

[23]   Turan, Onder, Hakan Aydın, T. Hikmet Karakoc, and Adnan Midilli. "Some Exergetic Measures of a JT8D Turbofan Engine." *Journal of Automation and Control Engineering* 2.2 (2014): 110-14. Web.

[24]   Turan, Onder. "Exergetic effects of some design parameters on the small turbojet engine for unmanned air vehicle applications." *Energy* 46.1 (2012): 51-61. Web.

[25]   Ehyaei, M.a., A. Anjiridezfuli, and M.a. Rosen. "Exergetic analysis of an aircraft turbojet engine with an afterburner." *Thermal Science* 17.4 (2013): 1181-194. Web.

[26]   Bastani, Milad, Roya Jafari, and Hojat Ghasemi. "Exergy analysis of an aircraft turbojet engine." *INTERNATIONAL JOURNAL OF ENGINEERING SCIENCES & RESEARCH TECHNOLOGY* 4.4 (2015): 380-86. Web.

[27]   Balli, Ozgur. "Advanced exergy analyses to evaluate the performance of a military aircraft turbojet engine (TJE) with afterburner system: Splitting exergy destruction into unavoidable/avoidable and endogenous/exogenous." *Applied Thermal Engineering* 111 (2017): 152-69. Web.

[28]   Balogun, Olaniyi, Changki Mo, and A. K. Mazher. "Exergy Analysis Of Gas Turbine - Burner Engine." *INTERNATIONAL JOURNAL OF SCIENTIFIC & TECHNOLOGY RESEARCH* 3.1 (January 2014): 62-67. Web.

[29]   Berg, Frederick T. N., Martin J. Balchin, and Patrick S. Keogh. "New Principles for Dynamic Aircraft Exergy Mapping." *Journal of Aircraft* 50.4 (2013): 1088-098. Web.

[30]   Tai, Vin Cent, Phen Chiak See, and Cristinel Mares. "Optimisation of energy and exergy of turbofan engines using genetic algorithms." *International Journal of Sustainable Aviation* 1.1 (2014): 25. Web.

[31]   Ekici, Selcuk, Yasin Sohret, Kahraman Coban, Onder Altuntas, and T. Hikmet Karakoc. "Sustainability Metrics of a Small Scale Turbojet Engine." *International Journal of Turbo & Jet-Engines* 0.0 (2016): n. pag. Web.

[32]   Coban, Kahraman, Yasin Sohret, T.hikmet Karakoc, and Can Ozgur Colpan. "Environmental Assessment of a Micro Turbojet Engine with the Aid of Exergy." *52nd AIAA/SAE/ASEE Joint Propulsion Conference* (2016): n. pag. Web.

[33]   Mattingly, Jack D. *Elements of Propulsion: Gas Turbines and Rockets*. Reston, VA: American Institute of Aeronautics and Astronautics, 2006. Print.

[34]   Oates, Gordon C. *Aerothermodynamics of Gas Turbine and Rocket Propulsion (3rd Edition)*. N.p.: American Institute of Aeronautics and Astronautics, 1997. Print.

[35]   "Earth Atmosphere Model - Metric Units." Ed. Nancy Hall. N.p., n.d. Web. 20 Mar. 2017. <https://www.grc.nasa.gov/www/k-12/airplane/atmosmet.html>. NASA.

[36]   Scott, Thomas, and David W. Riggins. "Work Interaction in Quasi-One-Dimensional Flows." *Journal of Propulsion and Power* 16.6 (2000): 1053-059. Web.

[37]   David W. Riggins. "Analysis of the Magnetohydrodynamic Energy Bypass Engine for High-Speed Airbreathing Propulsion", *Journal of Propulsion and Power*, Vol. 20, No. 5 (2004), pp. 779-792.

VITA

Mohammad Abbas was born in Kuwait City, Kuwait, on January 27, 1992. In May 2015, he received his Bachelor's degree, summa cum laude, in Mechanical Engineering from the Missouri University of Science and Technology. In May, 2017, he received his Master of Science degree in Aerospace Engineering from the Missouri University of Science and Technology. He published a conference paper, which is listed with the references, and attended the AIAA Propulsion and Energy forum in July, 2016. He was a peer learning assistant in the university's LEAD program at the Physics Learning Center between the fall of 2012, and the spring of 2015, helping freshmen learn physics. He continued as a volunteer in the Physics Learning Center between the fall of 2015, and the spring of 2017.